Title
Quantitative Analysis of Biological Effects on 18F-FDG Uptake in Tumors: from In-vitro to In-vivo Studies

Author
Sha, Wei

Publication Date
2012

Peer reviewed|Thesis/dissertation

UNIVERSITY OF CALIFORNIA

Los Angeles

Quantitative Analysis of Biological Effects on ^{18}F-FDG Uptake in Tumors: from In-vitro to In-vivo Studies

A dissertation submitted in partial satisfaction of the

requirements for the degree Doctor of Philosophy

in Biomedical Physics

by

Wei Sha

2012

ABSTRACT OF THE DISSERTATION

Quantitative Analysis of Biological Effects on ^{18}F-FDG Uptake in Tumors: from In-vitro to In-vivo Studies

by

Wei Sha

Doctor of Philosophy in Biomedical Physics

University of California, Los Angeles, 2012

Professor Sung-Cheng (Henry) Huang, Chair

Many factors, including tumor size, plasma glucose level, and the time course of 2-[^{18}F]fluoro-2-deoxy-D-glucose (FDG) in plasma can affect ^{18}F-FDG uptake in tumors. The objective of this research work was to systematically investigate the effects of these biological factors on FDG uptake in tumors and to develop methodologies both to overcome measurement problems encountered and to account for the discovered effects to improve the value of FDG PET imaging.

In vitro tumor cell line studies were first performed using a PSAPD-coupled microfluidic cell culture chip (microfluidic beta camera). A novel medium infusion strategy—a switching strategy was used to extract the kinetic parameters of FDG uptake in tumor cells. Results showed

that the switching strategy could provide reliable estimates of cellular FDG transport and uptake constants and the reliability of the model parameters can be further improved with an optimal design of fewer switching cycles. The experimental results also indicated that K_1 (FDG transport constant into cells) and K_i (FDG uptake constant in cells) estimates of glioma cell line U87 and prostate cancer cell line CaP8 were inversely proportional to the glucose concentration in the medium, while the values of k_2 (FDG transport constant out of cells), k_3 (FDG phosphorylation rate constant in cells) and cellular glycolytic rate were not affected by the medium glucose level.

Cellular FDG uptake studies were also performed on multi-well cell culture plates to investigate the effects of medium glucose levels and free fatty acid levels on FDG uptake in cell lines of three different tumor types. It was found that FDG uptake in the tumor cell lines all decreased with increased medium glucose levels, but no effect was seen due to free fatty acid level changes. However, the relationships between FDG uptake and medium glucose level are different among different tumor types, i.e. the FDG uptake in mammary cell line MDA-MB-231 is not affected as much by medium glucose level over the normal physiological glucose range as those of U87 and PC3.

Based on the results from in vitro studies, a set of longitudinal quantitative mouse FDG-PET studies in tumor-bearing mice were launched to investigate whether the in-vitro findings are translatable to in vivo settings. Two tumor types, U87 and MDA-MB-231, were implanted in SCID mice. FDG time activity curves in plasma were derived from dynamic PET images and were used to estimate the tumor FDG kinetic parameters. A multivariate analysis was used to account for multiple factors (plasma glucose level, tumor size, tumor age) at the same time. The

results show that the plasma glucose level affected tumor FDG uptake in ways consistent with the findings obtained in in-vitro experiments. Furthermore, the tumor FDG uptake constant was found to be stable for the two tumor types studied as tumor grew in size (before tumor necrotic core appeared). The study also demonstrated that quantitative longitudinal mouse FDG PET studies can be done in cancer research to provide valuable biological information.

In summary, new kinetic methods have been developed in this study to improve the quantitation of FDG uptake kinetics in tumors, both in-vitro and in-vivo. Findings from the quantitative studies have added new understandings of FDG uptake in tumors that have direct implication on improving the reliability of FDG PET studies in clinical settings.

The dissertation of Wei Sha is approved.

Arion-Xenofon Hadjioannou

William H. McBride

Ren Sun

Sung-Cheng (Henry) Huang, Committee Chair

University of California, Los Angeles

2012

I dedicate this dissertation to my husband Di Zhang, my son Oscar Zhang, my father Defang Sha and my mother Zhenhua Wang

You are all the reason I smile

Table of Contents

Acknowledgements

First and foremost I would like to give special thanks to my advisor Dr. Sung-Cheng Huang for everything in the past five years. Throughout my graduate studies in UCLA, Dr. Huang provided tremendous support and encouragement. Dr. Huang's solid knowledge background and rigorous attitude set an example for being a perfect scientist. Dr. Huang was not only my academic advisor; he also gave me endless support on my career and my family. His vision, breadth of mind and kindness influenced me in many ways and will benefit me throughout the future days of my life.

I am also extremely grateful for the advices and effort devoted to this work from my collaborators. I deeply appreciated Dr. Arion Hadjioannou's and Dr. Hsian-Rong Tseng's work which established the microfluidic beta camera system. I was fortunate to be able to work closely with their previous graduate students Dr. Nam Vu and Dr. Zeta Yu. Without Nam and Zeta's dedication to all the FDG kinetics experiments, my research would have not gotten to this point. I am very grateful for Dr. Kei S. Iwamoto's willingness to give me guidance for performing in vitro cellular studies. Kei provided insightful suggestions from a biological perspective. I enjoyed every refreshing conversation with him. I would like to thank Dr. Chann Lagadec, Robin Saxon and Gilmer Valdes for providing me various types of tumor cells. Waldemar Ladno helped with all the animal studies, without his precise tracer injection, we cannot get those beautiful images.

I would like to take this opportunity to express my gratitude to my lab members, Dr. Gregory Ferl, Dr. James Yu, Dr. Koon-Pong Wong, Dr. Amy Yu, Mirwais Wardak, Hu Ye, Moses Wilks. It has been a pleasure to work with all of you in the past years.

I would also like to thank all of the professors and students in the Biomedical Physics (BMP) program. Specifically, I appreciate the help from Dr. Michael McNitt-Gray, the director of the program. Michael has done wonderful job to make the program run successfully and is like a family member to me and my husband. I enjoyed the friendship with all the BMP students and all the fun activities we had together. I would like to thank Terry Moore and Reth Thach for all the assistance as I progressed in the BMP program toward the doctoral degree.

Time flies. As I grow up, I learned how to stay positive, how to understand other people, how to love the one you cares. I am fortunate to have my husband stand by me all the time. We knew each other since we were 18 years old. We got married in 2007 after we were both admitted to UCLA. We just had a baby boy in May, 2012, right before we graduated. I am proud of what we have been through in the last 12 years. We now know many of life's joys, sufferings, secrets and we are still together. Thank you for your never stopping love. I am looking forward to the next 12 years.

VITA

2004	B.S. Engineering Physics
	Tsinghua University
	Beijing, China
2006	M.S. Engineering Physics
	Tsinghua University
	Beijing, China
2006-2007	M.S. Physics
	University of California, Irvine
	Irvine, California, USA
2007-2012	Graduate Student Researcher Biomedical Physics
	University of California, Los Angeles
	Los Angeles, California, USA
2011-2012	UCLA Dissertation Year Fellowship
	University of California, Los Angeles
	Los Angeles, California, USA

Chapter 1 BACKGROUND AND MOTIVATION

Cancer is a systemic disease resulting from alternations in the interactions between oncogenes and tumor suppressor genes, which under physiological conditions control cell maturation, division and migration. Traditional diagnostic imaging techniques such as computed tomography (CT), magnetic resonance imaging (MRI) and ultrasound (US) only provide anatomic information and cannot reliably discriminate between benign and malignant tumors. The positron emission tomography (PET) has resulted in the emergence of molecular, whole-body functional imaging of disease with PET and glucose 2-deoxy-2-[F-18] fluoro-D-glucose (FDG). PET is a nuclear imaging technique that uses the unique decay characteristics of radionuclides that decay by positron emission. These radionuclides are produced in a cyclotron and are then used to label compounds of biological interest. When the radioactive atom on a particular molecule decays, a positron is ejected from nucleus, ultimately leading to the emission of high-energy photons. In in-vitro studies, these emitted photons from inside the cells could be detected by a gamma counter. FDG is one of the most used tracers in PET imaging. FDG is taken up by tumor cells and phosphorylated by hexokinase to FDG-6-PO_4, which is not metabolized further in the glycolytic pathway. It remains trapped intracellularly because tumor cells do not contain significant amounts of glucose-6-phosphatase to reverse this reaction during the time of the procedure. Compared to normal cells, higher glucose metabolism (high glycolitic rates, glucose transporters in tumor cell membranes and expression of hexokinase) is common to a wide variety of neoplastic cells. Therefore, the whole body distribution of FDG-6-PO_4 in normal and abnormal tissue can be imaged with PET (Figure 1.1). Because of its high diagnostic accuracy and cost-effectiveness, FDG-PET allows for the utilization of these well-defined metabolic abnormalities of malignant tumors for clinical diagnosis.

For tumor staging, qualitative interpretation of FDG-PET studies is generally considered to be sufficient. However, PET imaging also allows quantitative measurements of radioactivity concentrations within the body. Due to the simple metabolic pathway of FDG, this data can be used to estimate the glucose utilization of malignant tumors. Several approaches of varying complexity may be applied for this purpose. The most commonly used techniques are

"standardized uptake values" and simplified tracer kinetic modeling using "Patlak-Gjedde" analysis. More complex modeling approaches that determine individual rate constants for FDG transport and phosphorylation have also been applied. However, these techniques require complex acquisition protocols and arterial blood sampling during data acquisition and cannot be widely applied in clinical or preclinical studies. Furthermore, interpretation of the rate constants is difficult due to tumor heterogeneity.

Several groups have investigated the effects of dietary state and metabolic conditions on FDG uptake of tumors and normal tissues in patients (*1-6*). For these studies, patients were examined after fasting and again following an oral or intravenous glucose challenge. The studies revealed higher tumor FDG uptake in the fasted state than after glucose loading with the use of semiquantitative indices. However, the clinical benefit of intravenous insulin application in patient with PET with elevated serum glucose levels remains controversial. Patients are routinely studied with PET after an overnight fast. Patients with diabetes mellitus are asked to continue their medication. Despite fasting, considerable cardiac glucose metabolic activity is present in up to 50% of all patients. This increased myocardial FDG uptake would be further enhanced after insulin administration. No method has yet been found to consistently reduce the myocardial FDG uptake that potentially compromises the visualization of tumors in close proximity to the heart. Without the intervention to the serum glucose levels, how to account for the effects of blood glucose level and other biological factors (such as insulin, input function variations and tumor size/configuration) on tumor FDG uptake is critical for improvement in the measurement sensitivity of the true biological signals in the tissues.

In the last decade, small animal imaging with PET underwent a major evolution. This has been driven by technical improvements and the development of dedicated PET scanner's for small animals. Studies with small animal PET make the quantification of physiological parameters more practical than clinical human studies. Kinetic modelling of rodent PET data is already well developed and is used to study diseases, to evaluate therapies or new drugs, and to gain insight into molecular processes in-vivo. This has a major impact on the further improvement of the technique. Nevertheless, at this moment there are still several issues which

need further research and evaluation before we can fully employ the possibilities of microPET as an in-vivo measurement of underlying molecular biology. These issues relate to improved quantification of the measurements, improved image reconstruction and processing, and the use of blood plasma data in combination with kinetic models.

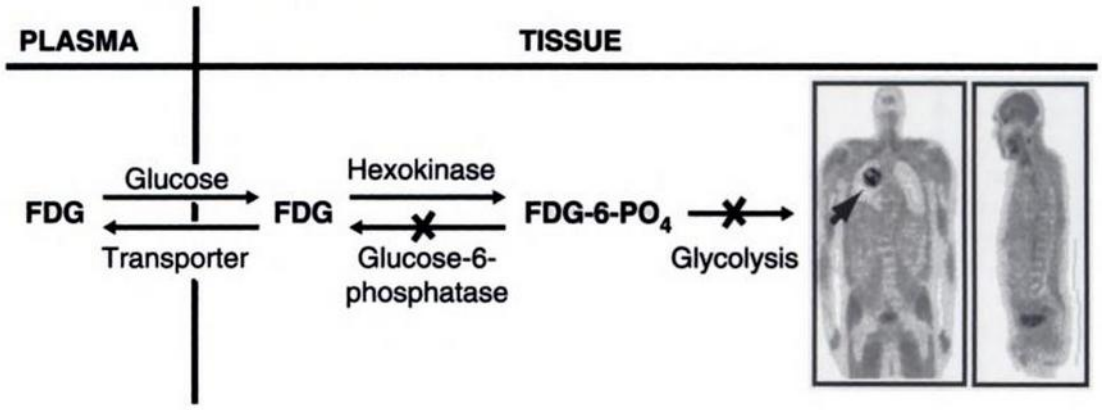

Figure 1. 1 Tracer kinetic model for FDG illustrating forward and reverse transport between plasma and tissue, as well as hexokinase phorsphorylation. PET scans to the right are coronal and saggital images of a patient with nonsmall cell carcinoma of the lung (arrow).

1.1 Quantitation of FDG Uptake in In-vitro Cell Studies

FDG has been found to be a useful tracer in PET oncology studies, but the biologic interpretation of the FDG-PET signal in malignant lesions remains complicated to date. This problem can be addressed by in vitro approaches that allow the measurement of FDG uptake under controlled conditions. Data from these experiments may be used to develop working hypotheses for the interpretation of patient data. Although in vitro studies may suffer from the differences between the in vitro and the in vivo situation, they are valuable tools for the detection of general cellular reactions to media environmental change such as a consequence of the exposure of cells to high glucose levels. A commonly cell culture procedure is presented in figure 1.2. First, flask with millions of cells is taken out from the incubator to the hood and the

cell culture media inside was sucked out; Second, trypsin was added to dissociate cells from surface and another 10mL cell culture media was added to flask; All the media mixed with cells was then suck out and release to a 15mL vial; Third, the cells will be separated from the media by centrifuge, the media will be washed out and fresh media was added to the cells, the cells should be mixed well with the fresh media; Fourth, 20 uL of the mixed media was sucked out and added onto hemocytometer to count cell numbers; Fifth, after the cell concentration (/mL) is calculated, cells will be plated into each well of a cell culture plate. Usually, the plate with loaded cells will be incubated for 24 hours before it was used for tracer uptake experiment. In the FDG uptake experiment, FDG media will be added to each well and the whole plate will be incubated for another 60 minutes. Then the media is washed out with PBS and the cells are lysed. The media with lysed cells will be transferred to the vials that are used for gamma counting (Fig. 1.3).

One concern for the in-vitro cellular FDG uptake studies not commonly recognized is the glucose content in cell culture media used for the uptake experiment. Because glucose and FDG compete for transport and phosphorylation, this may result in alterations in FDG uptake. A few studies have been performed to investigate the effect of glucose concentration on cellular FDG uptake. Torizuka et al. have performed in-vitro experiments on human adenocarcinoma cells (*7*), and primary lung and breast cancer(*8*). It was found that human adenocarcinoma cells do not significantly change FDG uptake with chronic hyperglycemia while acute hyperglycemia markedly reduces uptake of FDG, indicating that the fasting state is necessary for FDG studies on these cells; For lung and breast cancer, in vitro studies showed a much lower phosphorylation rate of FDG in breast cancer cells in hyperglycemia environment than it was in lung cancer cells. Zhuang HM et al. (*5*) tested the effect of high glucose levels on FDG uptake in inflammatory tissue (mononuclear cells) and malignant legions (mesothelioma cells), the results suggested that below a certain level (~250mg/dL), elevated glucose concentration might not make any difference in FDG uptake in inflammatory cells, while observed FDG uptake by malignant cells decreased as glucose concentration increased. All these studies illustrate the complexity of

glucose uptake in tumor cells, and more basic studies are needed to increase our understanding of effect of physiological environment on cellular FDG uptake.

Another problem may be the influence of the washing procedure on the radiotracer concentration for scintillation count. Too many washing steps with PBS may wash away significant number of cells that are adhesive to the bottom; too little may not be enough to clear the extra-cellular radioactivity completely. Haberkorn et al (*9*) had shown that the measured radioactivity was found to be stable for the tracer of FDG after two washing steps with PBS.

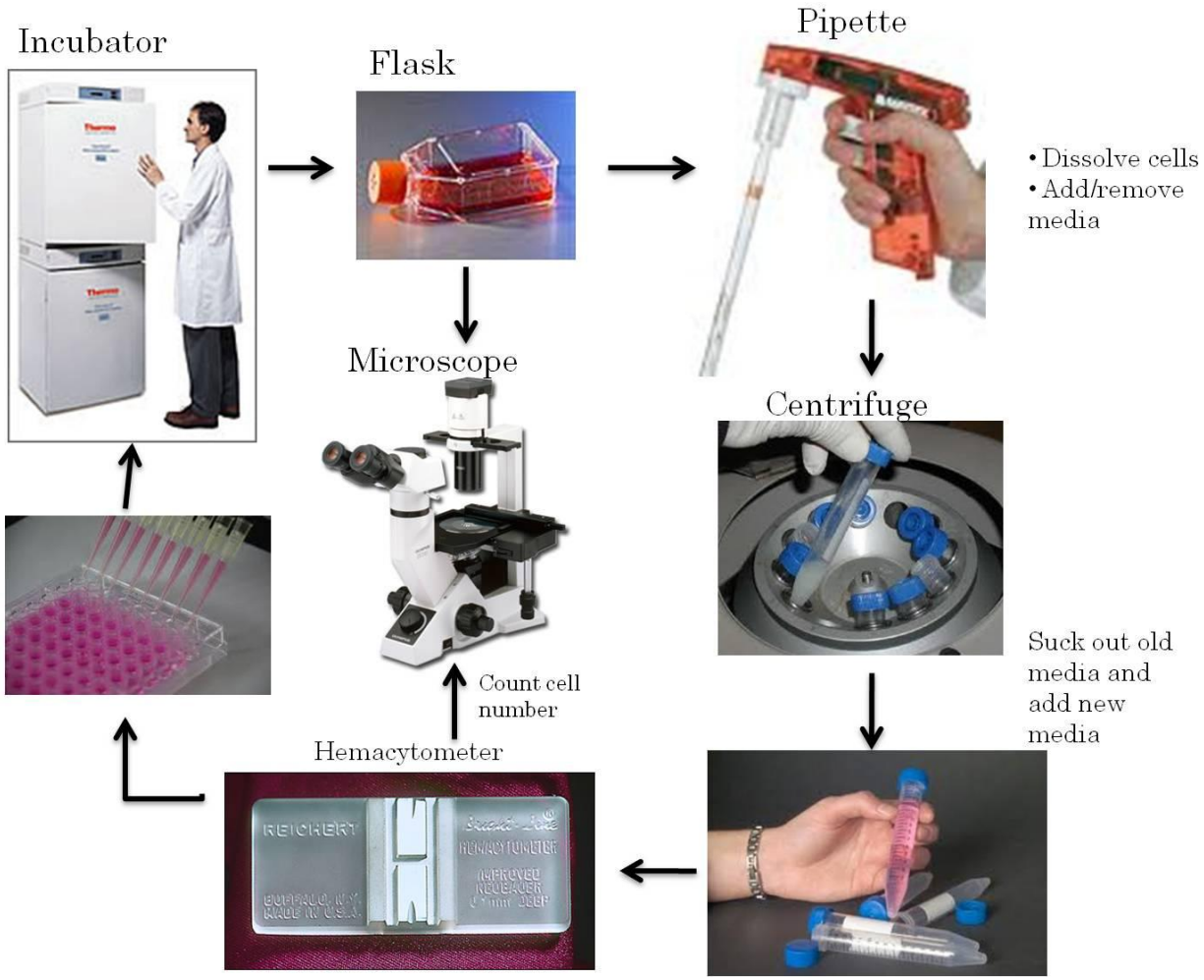

Figure 1. 2 Procedures of cell culture, cell number counting and cell plating in in-vitro study

Figure 1. 3 A gamma counter that is used for measuring gamma radiation emitted by a radionuclide.

1.2 Quantitation of FDG uptake in PET

FDG-PET provides a unique means of non-invasive assessment of tumor metabolism. The uptake of FDG into tissue reflects both transport and phosphorylation of glucose. FDG is transported across the cell membrane by the same carrier molecules as glucose and subsequently is phosphorylated by hexokinase. In contrast to glucose, FDG-6-phosphate cannot be further metabolized since this would require the presence of an oxygen atom at the C-2-position. Such trapping mechanism enables the measurement of FDG concentration in cells and results in high contrast between tumor and normal tissues shown in FDG-PET images. FDG-PET has a well-established role in the diagnosis and staging of a wide variety of cancers. Quantitative analysis of

tumor FDG uptake and qualitative image interpretation by experienced observers give complementary information for differentiation between benign and malignant lesions (*10-15*). Moreover, quantification of tumor glucose metabolism is essential for evaluation of tumor response to chemo- and radiotherapy. Lymphoma is among the first tumor types to be investigated with FDG-PET and the assessment criteria for early response to chemo- or immunotherapy is well established (*16, 17*); Clinical studies in breast cancer and adenocarcinoma of the lung suggested that serial FDG-PET studies allow the prediction of response early in the course of chemotherapy (*18, 19*). These days, the potential advantages of FDG-PET for delineation of the target volume in radiotherapy planning are also investigated by a few clinical studies (*20, 21*). Although the technology to precisely control the delivery of a radiation dose is well developed, the fundamental problem of determining what region of tissue needs to be targeted still exists.

Several approaches have been applied for quantitation of FDG uptake in tumor. The most simple and commonly used techniques are standardized uptake value (SUV) and simplified tracer kinetic modeling using the "Patlak-Gjedde" analysis, which provide highly reproducible parameters of tumor glucose utilization. More complex modeling approaches that determine individual rate constants for FDG transport and phosphorylation have also been applied, but not widely used in clinical studies due to complex acquisition protocols and arterial blood sampling during data acquisition. This section focuses on introduction of these three quantitation methods.

1.2.1. Standardized Uptake Value

Standardized uptake value (SUV) is the most common index used to measure tracer accumulation in PET studies. The SUV is a semiquantitative measure of normalized radioactivity concentration in PET images. To measure SUV, a 2D or 3D region of interest (ROI) is firstly delineated on a target (i.e., tumor or normal tissue) using an interactive image analysis software. Calculation of SUV is very simple and requires the measurement of radioactivity concentrations at a fixed time point. Therefore, static PET image with significant less scanner time than dynamic acquisition protocols could be used for the measurement. The measured radioactivity

within the ROI is normalized to the average radioactivity concentration in the body, which is approximated as the injected dose divided by the body size. Common body size measurements are based on the patient's body weight, lean body mass, or body surface area, with body weight being the most frequently used.

$$SUV = \frac{Radioactivity\ concentration\ in\ tissue}{Injected\ radioactivity/Body\ size} \quad (1)$$

It has been reported that SUV generated by normalization of FDG uptake to patient body weight (SUV_{bw}) overestimates FDG uptake in heavy patients, as their fraction of body fat (with low FDG uptake) is often increased. Normalization to body surface area or lean body mass has been shown to be more preferable than normalization to body weight in heavy patient (*22*). However, the differences between the normalization methods appear to be small for regular size patients with breast cancer (*23*).

When used for quantitation of FDG uptake in tumors, SUV is usually described in two ways: the mean or maximum SUV of all voxels within the ROI (SUV_{mean} and SUV_{max}, respectively). SUV_{mean} incorporates information from multiple voxels, making it less sensitive to image noise. However, measured SUV_{mean} will vary depending on which voxels are included in the ROI and may require additional image segmentation tools for delineation of the target, so it is sensitive to ROI definition and is subject to intra- and inter-observer variability(*24*). SUVmax is the highest voxel value within the ROI, so it is independent of ROI definition (assuming the voxel with the highest radioactivity concentration is included). Studies performed by Matthias R. Benz et al.(*25*) indicated that different approaches to define ROIs result in considerably different interobserver variability. SUV_{mean} demonstrated a significantly higher interobserver variability than did SUV_{max}. However, SUV_{max} is more susceptible to variations due to statistical noise as well as image reconstruction and parameters after processing (*26*). As shown in figure 1.4(*27*), SUV_{max} has changed substantially due to the changing of field of view (FOV) size from 50 to 70cm. Therefore, the use of SUV_{max} might be limited when studies are performed on different PET scanners or with different acquisition and image reconstruction protocols.

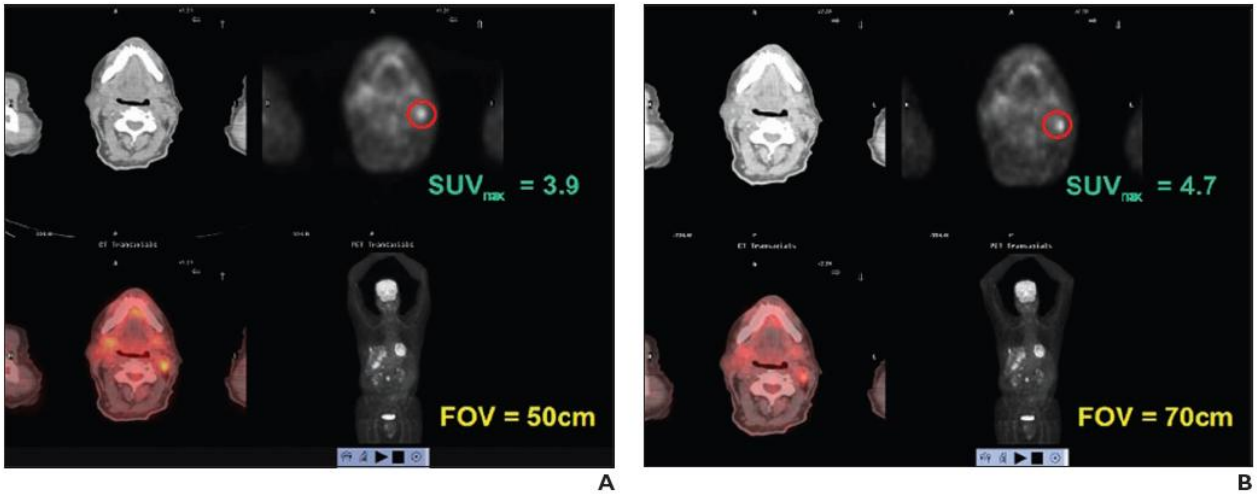

Figure 1. 4 Effect of field of view (FOV) change on standardized uptake value (SUV) measurement of melanoma in 61-year-old man. Initial images were reconstructed with 50-cm FOV (A) and with 70-cm FOV (B) to include area of primary disease. Image reconstruction algorithm was the same for the two images (*27*).

A major disadvantage of the SUV approach in therapy monitoring is the dependency on the time of measurement. Various malignant tumors may possess quite different tracer accumulation and clearance rate, which will be shown later in our tumor studies, result in different shape of time activity curves. The measurement point for SUV quantitation should be tumor-dependent and SUV can only be compared when they are measured at the same time point after tracer injection (*28*) to achieve high reproducibility of glucose metabolic measurements.

1.2.2. Simplified tracer kinetic modeling using "Patlak-Gjedde" analysis

A Patlak-Gjedde plot (*29, 30*) is a graphical analysis technique based on the compartmental model that uses linear regression to identify and analyze pharmacokinetics of tracers. It can be used when there are any number of reversible compartments and at least one irreversible compartment, such as 2 tissue compartmental FDG model (Figure 1.1). Patlak-Gjedde analysis assumes that all the reversible compartments must be in equilibrium with plasma, i.e. the ratio of the concentrations of tracer in plasma and in reversible tissue compartments must remain stable. In these circumstances only the accumulation of tracer in irreversible compartments is affecting the visual distribution volume. Patlak-Gjedde analysis allows

determination of a rate constant K_i for the net influx of FDG in the tissue. K_i can be calculated from the following equation:

$$\frac{ROI(T)}{C_p(T)} = K_i * \frac{\int_0^T C_p(t)dt}{C_p(T)} + (V_e + V_p) \quad (2)$$

Where *ROI(T)* is the tracer concentration in tissue, $C_P(t)$ is the concentration of tracer in arterial plasma. The plot will become linear for the times $T > t^*$ when V_e, the distribution volume of the reversible part (the ratio of the concentration in the reversible compartment to plasma) is constant. The slope of the linear phase represents the transport rate K_i (Figure 1.5). This technique requires dynamic data acquisition and measurement of a blood time-activity curve unless a reference region that contains only reversible compartments exists(*30*), such as cerebellum in FDOPA studies. The reference region can be included in the model, and the plasma curve is 'cancelled out'. The only difference in the calculation is that plasma curve is replaced with reference region curve.

Weber et al (*28*) has studied the reproducibility of several parameters including SUV and K_i that are used to quantify the tumor glucose metabolism by FDG-PET. The results showed that the values of K_i can be measured with the same reproducibility as SUV. The main advantage of K_i is that it takes into account changes in the whole-body distribution of FDG. Therefore, measurement of the input function and calculation of uptake constant K_i may be preferable to the use of SUV when the distribution volumes of FDG changes due to environmental changes, such as change of blood glucose levels. However, it was also found that variability of K_i could be increased due to patient movement during acquisition, especially when the size of the lesions is still small. Quantitative studies for evaluating FDG uptake in lung cancer (*31*) also supported the same conclusion that SUV and graphical Ki can be measured reproducibly. In general, SUV and K_i are both high reproducible parameters for quantitation of glucose metabolism in PET studies.

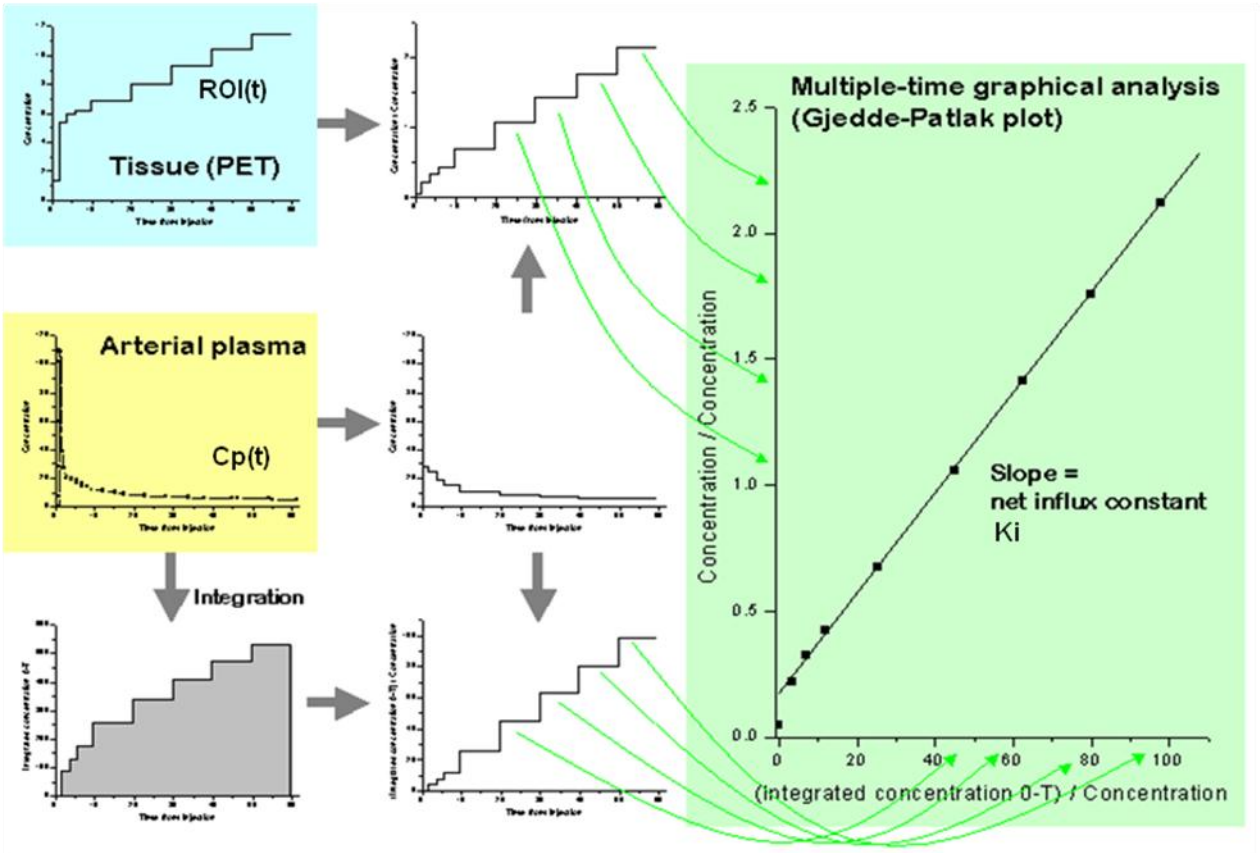

Figure 1. 5 Patlak-Gjedde analysis for irreversible tracer.

1.2.3. Tracer kinetic modeling in FDG-PET

PET imaging provides radioactivity measurements in the tissue of interest. The images of tracer distribution can be usefully applied to answer clinical and scientific questions. Generally speaking, the concentration of radioactivity in a given tissue region at a particular time post-injection primarily depends on two factors. First, and of the most interest, is the local tissue physiology, for example, the blood flow or glucose metabolism in that region. Second is the input function, i.e., the time-course of tracer radioactivity concentration in the blood pool, which defines the amount of the tracer before it enters the target tissue. A mathematical model is used to describe the relationship between the tissue concentration and the physiological parameters

that affect the uptake and metabolism of the tracer in several compartments. Regional physiological parameters could be estimated by the model fitting to the measured tissue and blood concentration. Several steps are involved for developing a model for a specific radioactivity tracer. First, a model is constructed based on the expected distribution of the tracer in body and target area. Usually, such model is complex and has many physiological parameters to be solved; second, with some basic assumptions, one or more simpler models that include less parameters could be derived based on the initial one; finally, validation of the models is performed to select the model that fits the measured data best and produces the most reliable estimates of physiological parameters. In terms of FDG, a two tissue compartmental model is usually enough to describe the process (*32*). FDG and glucose enter cells by the same transport enzyme and are both phosphorylated by the enzyme hexokinase. However, deoxyglucose is not a substrate for the next enzyme in the glycolytic pathway, so deoxyglucose-6-phosphate accumulates in tissue. In this way, the tissue signal directly reflects the rate of metabolism, since there is little clearance of metabolized tracer. The compartmental model for FDG is shown as figure 1.6, C_p is the concentration of FDG in plasma; $\mathbf{C_1}$ is the activity concentrations of FDG in tissue; C_2 is the activity concentration of phosphorylated FDG in tissue. $\mathbf{K_1}$ (min^{-1}) and $\mathbf{k_2}$ (min^{-1}) are the putative rate constants at which FDG crosses the cell membrane; and $\mathbf{k_3}$ (min^{-1}) and $\mathbf{k_4}$ (min^{-1}) are the putative rate constants of phosphorylation and dephosphorylation of FDG, respectively.

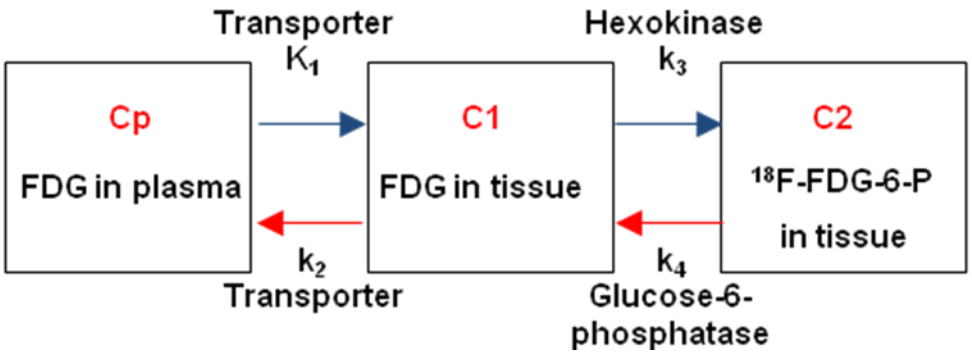

Figure 1. 6 Two tissue compartmental model for describing FDG kinetics in tissue.

The model could be interpreted by two differential equations, one for each tissue compartment:

$$\frac{dC_1}{dt} = K_1 C_p(t) - K_2 C_1(t) - K_3 C_1(t) + K_4 C_2(t) \quad (3)$$

$$\frac{dC_2}{dt} = K_3 C_1(t) - K_4 C_2(t) \quad (4)$$

An outflux term in Eq. 3 ($-K_3 C_1(t)$) has a corresponding influx term in Eq. 4 ($+K_3 C_1(t)$). The solution to these coupled differential equations, for the case of an ideal bolus input, is as follows:

$$C_1(t) = C_p[A_{11}\exp(-\alpha_1 t) + A_{12}\exp(-\alpha_2 t)] \quad (5)$$

$$C_2(t) = C_p A_{22}[\exp(-\alpha_1 t) - \exp(-\alpha_2 t)] \quad (6)$$

$$\alpha_1 = (k_2 + k_3 + k_4 - \sqrt{(k_2 + k_3 + k_4)^2 - 4k_2k_4})/2 \quad (7)$$

$$\alpha_1 = (k_2 + k_3 + k_4 + \sqrt{(k_2 + k_3 + k_4)^2 - 4k_2k_4})/2 \quad (8)$$

Here, the time course of each compartment is the sum of two exponentials. The measured tissue radioactivity will be the sum of radioactivity in both tissue compartments, which is $C_1(t) + C_2(t)$. The equations are non-linear with respect to the model rate constants except K_1.

In reality, the input to the tissue is the continuous blood time activity curve, which equals a series of bolus injections. So the tissue response is a sum of the individual response to each bolus input. The responses are scaled in magnitude and shifted in time to match each bolus input. The mathematical calculation for the response to continuous input function could be completed by convolution using softwares (i.e MATLAB). Figure 1.7 (*33*) demonstrated the concept of bolus and continuous input function and theirs tissue response.

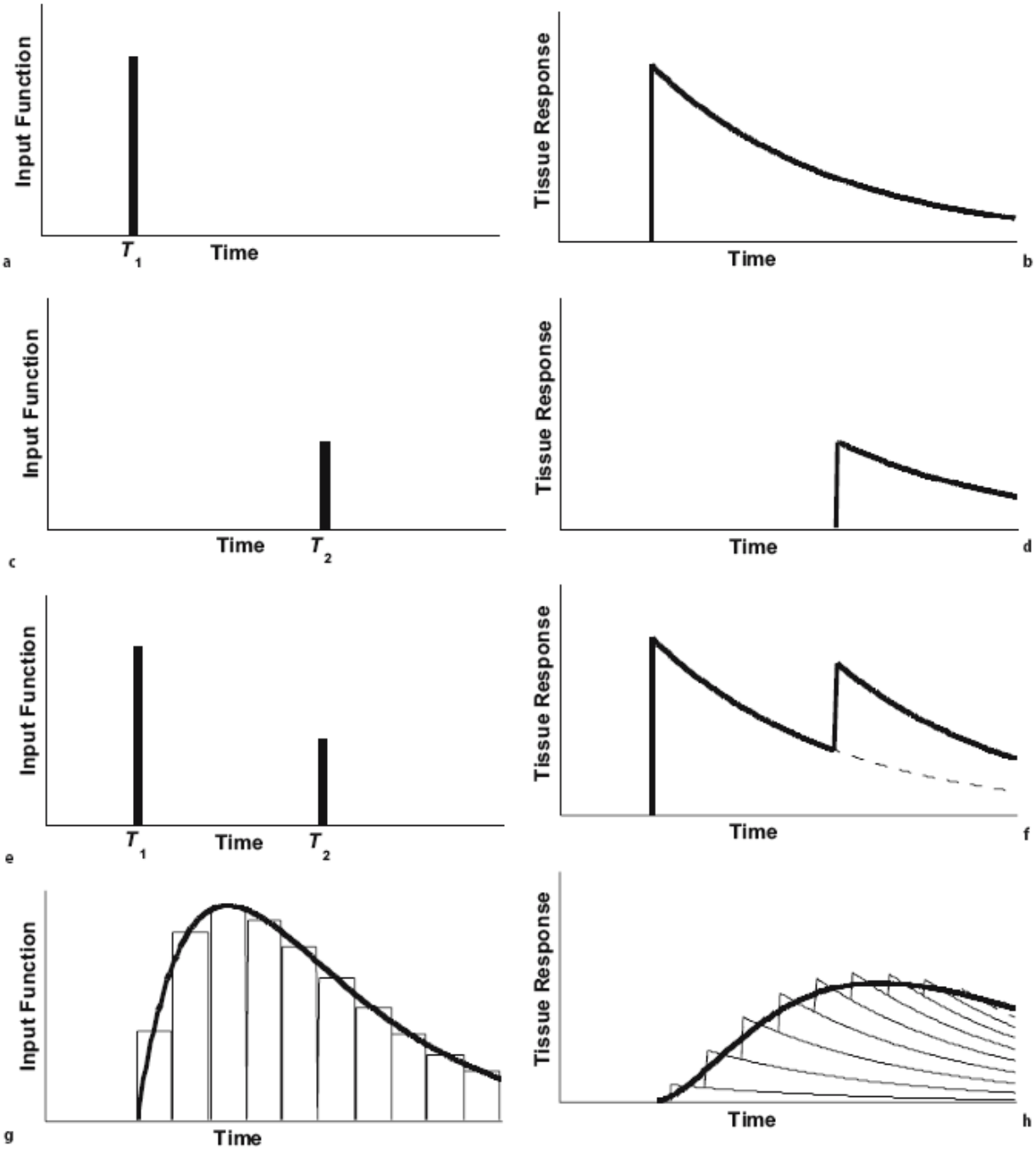

Figure 1. 7 Tissue responses for different input function (*33*).

The input function is essential to determine the kinetic rate constants using the radioactivity data measured with the PET scanner. The input function, usually derived from the

arterial blood samples, requires complex protocol to be acquired. Nowadays, different approaches are tested to infer the shape of the arterial input function with less invasive methods. An alternative to blood sampling is to derive the arterial input function directly from the dynamic images with or without limited blood smaples. Clinical study of ^{11}C-Flumazenil kinetic in human brain (*34*) demonstrated that the shape of the tracer plasma curve could be obtained from the intact flumazenil fraction in plasma in three arterial samples and the internal carotid artery time-activity curve (TAC). Joonyoung et. al (*35*) implemented factor analysis (factor images of right ventricle, left ventricle, and myocardium) to extract the blood input function of FDG and 1-^{11}C-acetate in rats and mice. Using prior information of tracer kinetics in some tissues, Gregory Z. Ferl et. al (*36*) developed a robust method for accurately estimating the plasma time activity curve of FDG by use of mice PET data and 2 blood samples.

Many trade-offs must be considered when a model is used for quantitation of tracer uptake (*37*) . Tracer kinetic modeling offers a number of advantages compared to the empirical measures (ex., SUV measurement). It can produce quantitative estimates of one or more physiological parameters and explain the cause of different levels of tracer uptake between subjects. It may improve the signal to noise characteristics of the data by reducing intersubject variability. However, the application of mathematical modeling also has disadvantages. Usually, modeling procedures are more complex, requiring longer scanning time, blood sampling, and complex data processing.

1.3 Factors affecting Quantitation of FDG uptake in Tumors

FDG-PET has been widely used in clinical and preclinical studies for measurement of distribution of glucose metabolism in the subjects. FDG is a glucose analog that accumulates preferentially in malignant cells due to their higher glucose metabolism and is useful for detecting/staging various cancers, including lung cancer, melanoma, lymphoma, colorectal cancer, breast cancer, cervix cancer, and head and neck malignancies (*4*). Quantitative assessment of therapy-induced changes in tumor FDG uptake may allow prediction of tumor response and patient outcome very early in the course of therapy(*38*). In order to get reliable measurement of glucose metabolism, it is critically important to understand the variables that can affect the quantitation of FDG uptake in tumors. Many biologic factors will affect the FDG distribution in the body. Technologic factors will also affect how close the image based data analysis is to the physical FDG distribution. In this section, we will address the factors that need to be considered in FDG measurements.

1.3.1. Biological Factors

A. Body Composition

Body composition is a source of variability because the FDG distribution is weight dependent. Heavier patients often have a higher percentage of body fat, which comsumes less FDG than muscle tissue. Clinical FDG PET studies performed by K.R Zasadny and R.L Wahl (*39*) showed that in heavy patients, SUVs for normal tissues (lung, liver, marrow, spleen, blood, and normal breast) were up to twice those of lighter patients. Comparison of SUVs among patients with different body compositions will result in unreliable estimates. Even comparison of

SUVs between examinations of the same patient can be flawed if the patient has lost or gained weight during the course of treatment. SUV calculated using lean body mass or body surface area can be used to account for the body composition rather than body weight, but it is still unclear whether these correction can make SUV better correlated with glucose metabolic rate (*18*, *40*).

B. Blood Glucose Levels

Blood glucose level is also a major factor that affects FDG uptake in tissues. FDG is in competition with glucose because they use the same enzyme (hexokinase) during phosphorylation process. K-P Wong et. al (*41*) studied a group of mice with different dietary condition and blood glucose levels. The results showed that FDG uptake constants of the myocardium and skeletal muscle are significantly correlated with dietary condition but not with blood glucose level. Conversely, FDG uptake constant of the mouse brain varies inversely with blood glucose level, but the metabolic rate of glucose has no correlation with blood glucose level and dietary condition. Kazuo Kubota et. al (*42*) found that liver uptake is elevated with higher blood glucose level. In vitro studies in ovarian adenocarcinoma (*7*) indicate that FDG accumulation in cancer cells will decline with increasing glucose level in the medium. Langen et al. (*2*) studied a group of patients with bronchial cancer. FDG was measured first under fasting state and then 2 days later during intravenous infusion of glucose. The results suggested that the SUV of FDG uptake in bronchial carcinomas is influenced significantly by plasma glucose levels. While the FDG uptake constant K_i acquired by the Patlak approach was less dependent on the plasma glucose level and is preferable to SUV when high reproducibility is

needed. Lindholm et al. (*3*) used oral glucose loading to elevate the blood glucose level in patients with head and neck cancer and found similar results. Zhao et. al (*43*) indicated that FDG uptake and the effects of hypoglycemia and hyperglycemia seem to depend on lesion activity, including the histological type and malignancy grade of tumors. All these studies showed that the intrasubject/intersubject variations in blood glucose levels can have highly significant effects on quantitation of FDG uptake, especially when SUV is used. Although the absolute amount of FDG uptake in most cancer cells could be increased with lower blood glucose level, the actual tumor visualization may not be improved due to the changes in background FDG uptake. For example, Ishizu et al. (*6*) found that the FDG uptake ratio of tumor to cortical gray matter in glioblastomas increased 27% with glucose loading, although the SUV in tumor is decreased. Therefore, understand of the glucose effect in quantitation of FDG uptake in different lesions is critically important.

C. Blood Insulin Levels

Insulin can induce a host of effects on vascular cells, including traditional metabolic actions such as glucose transport and utilization(*44*), protein synthesis and cellular proliferation(*45*). In addition, insulin also has vascular-specific actions that are particular to vascular tissues (*46*). It is well known that several tissues, including heart tissues, muscle and fat, have a large number of highly insulin-sensitive Glut-4 glucose transporters. In these tissues, Glut-4 expression levels at the cell surface are markedly increased under hyperinsulinaemia owing to Glut-4 translocation from vesicles to the membrane(*47*). Thus, hyperinsulinaemia markedly increases the level of glucose uptake in these tissues. Usually, insulin-induced

hypoglycaemia shifts FDG uptake from the tumor to insulin-sensitive tissues and reduce the tumor to background ratio (*48-50*). These studies all involved insulin infusion into the animal or patient to alter the circulating insulin level, thus significantly altered the blood glucose level. It is necessary to investigate the effect of insulin on glucose metabolism in tumors without any human intervention.

D. Tumor Configuration and Partial Volume Effect

Partial volume effect (PVE) occurs when radioactive counts from a source or focus ‘‘spill out’’ into a region that is volumetrically larger in the reconstructed image than its physical size. The recovery coefficient (RC) is usually used to correct PVE and can be defined as the ratio of the measured activity in a region of interest divided by the true activity. Severity of PVE could be affected by a number of factors, such as scanner resolution and object geometry. Hoffmanet al. (*51*) addressed the effect of object size on quantitation of PET image and found that the accuracy in quantitating isotope concentrations is strong related to the object size and larger recovery coefficient is required to compensate for partial volume effect on smaller object. Usually, recovery coefficient is measured in a phantom with various sizes of spheres and applied to actual patient data. Such correction will introduce problems if the object geometry is not uniform, especially for tumors with necrotic cores. The latest study performed by Mathieu al. (*52*) investigated the clinical impact of partial-volume effect correction on the quantitation of FDG PET image in esophageal cancer patients. The results showed that PVE correction increased the value of SUV measurement (maximum, peak, and mean), but did not add clinical value as a predictive factor to therapy response; Using the same threshold, metabolic tumor volume

delineated on PVE-corrected images were systematically smaller by on average -10%±5%, resulting in a mean volume difference of -4±3cm^3 on 3 different tumors (Figure 1.8). This finding suggest that the PVE correction could be critical important for measurement of FDG uptake in early treatment.

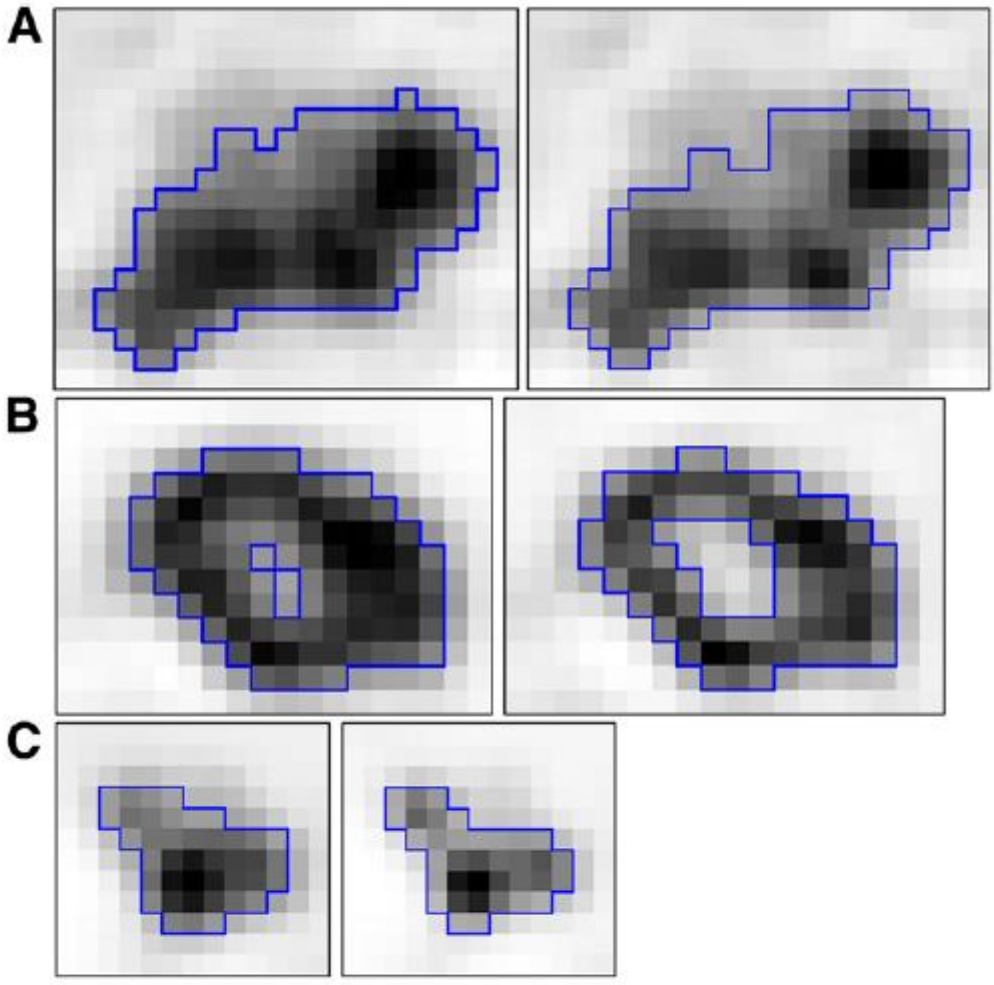

Figure 1. 8 Original (left) and PVE corrected (right) PET images with large, slightly heterogeneous tumor (A); tumor with necrotic core (B); and small, homogeneous tumor (C) (*52*).

1.3.2. Technical Factors

A. Interscanner Variability

PET scanners made from different manufacturers have different physical properties and different acquisition and reconstruction protocols. The calibration factor used to convert the measured counts to actual radioactivity is also different. In 2009, the American College of Radiology Imaging Network published results about the qualification of 169 PET scanners and found that 12% sites are unable to maintain accurate SUV calibrations without additional training or supervision. They also showed differences up to 6% among averages over all scanners of the same model (*53*). Other than the calibration factor, spatial resolution is another important factor that will affect the quantitation of PET images. Small object whose size less than twice the full width half maximum (FWHM) needs correction for partial volume effect.

B. Image Reconstruction Parameters

A number of studies have been done to investigate the impact of image reconstruction and processing parameters on SUV. Adams et. al (*27*) studied effect of several iterative reconstruction parameters include image matrix size, postsmoothing, field of view (FOV) size, TOF versus non-TOF reconstruction, number of iterations, and image matrix placement on measured SUV. The results suggested that the same FOV and reconstruction parameters should be used for baseline and follow-up studies to reduce the variability in measurements. Figure 1.9 shows another example of the effects of image reconstruction settings on the maximum SUV (SUVmax) in a lesion (*54*). Difference in SUV_{max} between images in figure 1.9 was due to combined effects of different numbers of iterations and subsets in ordered-subset expectation

maximization (OSEM), different image matrix sizes, and different smoothing filters. The trade-off between noise and resolution is notable. The measured SUV is higher with more iterations but the image noise is also increased a lot.

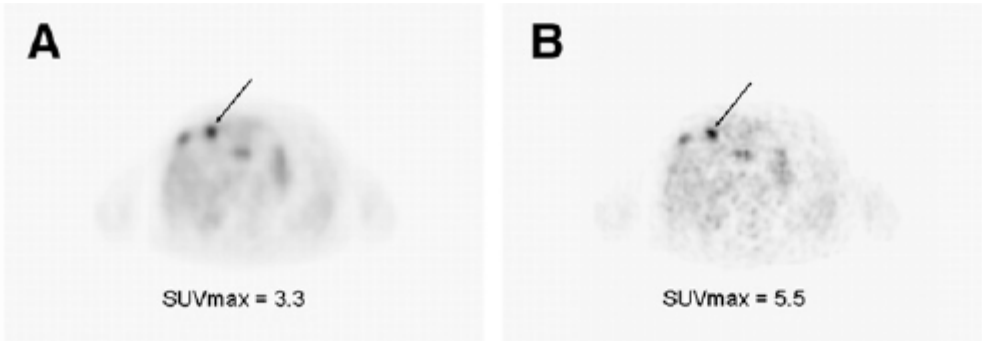

Figure 1. 9 Effects of different image reconstruction settings on SUV_{max} outcome. Arrows indicate the same liver lesion with 2 different reconstruction settings. (A) PET study was reconstructed by use of ordered-subset expectation maximization (OSEM) with 2 iterations and 8 subsets, image matrix size of 128*128, and postsmoothing with 8-mm FWHM gaussian filter. (B) PET study was reconstructed by use of 4 iterations and 16 subsets, image matrix size of 256 *256, and postsmoothing with 5-mm FWHM gaussian filter (54).

C. Other Factors

Other factors that affect the quantitation of PET images include: residual activity in syringe, incorrect synchronization of clocks of PET scan and dose calibrator, subject movement during the scan and interobserver variability. Heather et. al (*55*) found a change of 16.7% ±36.2% in SUVmax due to different ROI placement by different readers, indicating that automated analytic tools to assess tumor response to therapy might be helpful to enhance the reproducibility in quantitative FDG PET measurements.

Chapter 2 SPECIFIC AIMS

The effect of blood glucose levels on the measurement of FDG uptake in various tumors is necessary to be investigated due to the competition between FDG and glucose. This problem can be addressed by in vitro and in vivo approaches. In vitro experiment allows the measurement of FDG uptake under controlled conditions and is a valuable tool for the detection of general cellular reactions to media environmental change. Traditionally, cells are culture in multi-well plates and the cellular uptake of FDG is measured separately using a gamma counter. The procedure is labor intensive and is not able to produce kinetics parameters of FDG in tumor cells. With our newly developed microfluidic-beta camera system, dynamic imaging of tracer uptake in cells could be acquired and makes the extraction of a tracer's uptake/clearance kinetics in cell lines possible. Meanwhile, the design of the flow channels allows simultaneously and continuously measuring tracer uptake in cells under different media composition.

Mouse PET study has served as an important preclinical method to explore tissue biology and body physiology with or without intervention in nowadays. Studies with small animal PET make the quantification of physiological parameters more practical than clinical human studies. Kinetic modeling of mouse PET data is well developed and is used to study diseases, to evaluate therapies or new drugs, and to gain insight into molecular processes in-vivo. However, few longitudinal mouse PET studies have been implemented with systematic and complete quantitative analysis of FDG uptake in tumors. With our successful development of mini-invasive methods for quantitative mouse FDG-PET, the application of quantitative mouse PET could be expanded to longitudinal tumor studies. Furthermore, the dependency of the

physiological parameters on several biological factors can be investigated systematically. Specifically, we propose the following three aims:

Aim1: Examine the transport and uptake kinetics in tumor cells using a microfluidic multi-chamber cell culture chip coupled with PSAPD camera (MF-PSAPD)

- To design and validate a new kinetic strategy for extracting FDG transport and uptake information in MF-PSAPD system.
- To examine the effects of media glucose level on tumor FDG uptake constant and other kinetic parameters

Aim 2: Examine the effects of medium composition on FDG uptake kinetics in two different tumor cell lines in traditional multi-well cell culture plates

- To examine the effects of media glucose level on FDG uptake constant and lumped constant in different types of tumor
- To examine the effects of media free fatty acid level on FDG uptake in different types of tumor

Aim 3: Quantitative analysis of longitudinal FDG-PET studies on tumor-bearing mice.

- To develop reliable procedure for quantitative analysis of longitudinal FDG-PET studies
- To establish the temporal course of FDG kinetics in tumor without human intervention
- To examine the effects of blood glucose level on tumor FDG uptake constant and glucose metabolic rate in two different types of tumor

- To examine the effects of tumor configuration on tumor FDG uptake constant and glucose metabolic rate in two different types of tumor

Chapter 3 IN VITRO TRACER KINETIC ASSAY ON A PSAPD-COUPLED MICROFLUIDIC CHIP

3.1 Introduction

Glucose transport and sequestration rate constants in tissues have been extensively studied using 2-deoxy-2-[18F]fluoro-D-glucose (FDG) and kinetic modeling, in both human and animal positron-emission tomography (PET) imaging. Data acquired from dynamic PET imaging can provide tissue kinetic information, which is useful for quantitative estimation of regional biological processes in living subjects that can help disease diagnosis and treatment monitoring (*33*). Although quantitative analysis can provide more useful information (*56*), long scan times, limited spatial resolution and other practical issues such as the requirement of determining an arterial input function have limited the use of dynamic studies in routine PET imaging. Traditional in vitro tracer uptake assays using microplates (*57*) can measure the cellular uptake of FDG, but are not able to provide reliable kinetic information related to membrane transport and cytosolic sequestration rates separately. Traditional in vitro procedures are also laborious and time consuming, require a large number of cells, on the order of 10^4~10^6, and disturbance or removal of the cell cultures at each measurement data point.

Microfluidic devices (*58*) offer a robust analytical tool that allows rapid analysis of cellular responses to external stimuli in parallel and have opened up new opportunities for in vitro assays. A recently developed imaging system that combines a microfluidic chip and a position sensitive avalanche photodiode (PSAPD) (*59*) offers a new method of conducting in vitro tracer uptake assays with a small number of cells and allows cell incubation to be easily set

to any desired condition (*60*). The whole system is shown in figure 3.1. The advantages of this new technology include: i) the ability for *in vitro* imaging of cells in the microfluidic chip without major disturbance or removal of the cell cultures, in contrast to traditional radiometric methods, ii) high photon detection sensitivity that allows measurements of low radioactivity levels, iii) accurate digital control of the cell incubation conditions, enabling automatic control of tracer flow in and out of microfluidic chips and iv) simultaneous measurement of multiple samples on a microfluidic chip (*61*). With these advantages, time activity curves (TAC) of tracer concentration in each chamber/well in the microfluidic chip can be measured and tracer kinetic information such as transport rate constants in cells can be estimated using a proper tracer kinetic model.

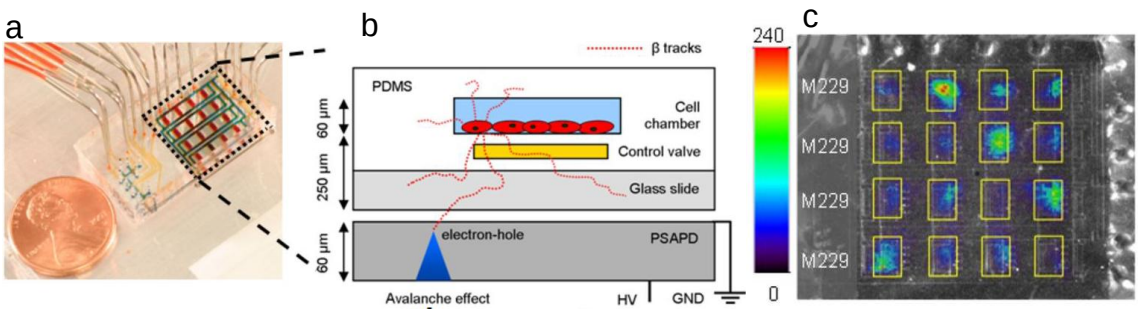

Figure 3. 1 (a) Configuration of a 4 by 4 microfluidic chip (b) Schematic diagram of the cross section of a typical microfluidic chip and the PSAPD detector. In the center of the chip is a cell chamber where radioactive cells and solutions can be loaded. Beneath the channel are a series of substrate layers that can be used to control the flow of solutions. The chip is placed on a glass slide and then on top of the PSAPD detector. (c) Region of interest (ROI) drawn on each chamber. Color bar decribes the magnitude of tracer uptake in cells.

The volumes of each chamber although small, ~ 50 nL, is still relatively large when compared to the space occupied by the cultured cells. This large difference presents a challenge when trying to estimate the kinetic parameters with bolus injection or constant infusion (CI) (*62*).

Bolus delivery with immediate clearance would yield very little radioactivity in the cultured cells to be reliably measured, while CI of radio-tracers through the wells would give a high background activity, that compromises the ability of the integrated platform to measure the transport and uptake rate constants. New tracer kinetic assay strategies are thus needed to overcome these difficulties. In this section, we report a novel switching strategy for extracting cellular uptake information. The switching strategy consists of multiple medium-infusion cycles, each of which has a tracer incubation (TI) period followed by a background-removed (BR) period (tracer-free medium). An approach to obtain an optimal switching schedule (OSS) design that would provide the most reliable parameter estimates of the tracer transport and phosphorylation rate constants in the cultured cells was also investigated.

Optimal designs of PET scanning protocols (SP) have been reported before (*63-65*). Various criteria have been proposed to objectively assess the adequacy of the PET sampling intervals in terms of the precision of the estimated parameters (*64*). Mazoyer et al. (*63*) proposed the use of the determinant of the Fisher information matrix (i.e.,the D-optimal criterion) as a guide to the selection of the SP in PET data analysis and used this technique to select the PET SP from a predetermined fixed number of SP's. Kewei Chen et al. (*65*) also used the same criterion to select PET SP with the four parameter FDG model. Leow et al.(*66*) combined simulated annealing with Component-wise Metropolis Monte Carlo simulation to solve the optimization problem. In this work, we use the simulated annealing to derive an optimal switching schedule (OSS) based on the optimization of the D-optimal design criterion. The four-parameter FDG model is used to demonstrate the use of the OSS design in parameter estimation. The optimal

design also allowed us to study issues related to how the switching schedule affects the reliability of the estimated parameters and what the minimal number of TI and BR periods should be in order to achieving a robust estimate of the model parameters.

The performances of three schedules: constant infusion (CI), the equal-period switching strategy (ESS) with equal cycles of TI and BR and OSS were demonstrated by performing actual tracer experiments on the integrated system using U87, P8 and CaP8 cell lines (*67*) and the tracer ^{18}F-FDG. The conventional ^{18}F-FDG model (*32*) with proper adjustments for the switching conditions was used to fit the measured kinetic data to estimate the values of the transport and phosphorylation rate constants.

The uptake of ^{18}F-FDG in tumor cells is susceptible to various physiological variables in the body that include plasma substrate levels such as glucose(*1, 2*). Our previous study in mice(*41*) showed that the effect of glucose on ^{18}F-FDG uptake constant could be varied in different organs and tissues. Therefore, the robustness of the FDG uptake value can be improved if such effect is better understood and accounted for (*5, 42*). In this work, we monitored the uptake of ^{18}F-FDG in tumor cell lines in response to specific glucose levels.

3.2 Methods

3.2.1 The Switching Media Perfusion Strategy and Its Optimal Design

A. The Switching Strategy

The novel switching strategy consisted of multiple medium-infusion cycles, each of which had a tracer incubation (TI) period followed by a background-removed (BR) period. In the TI period, cells were incubated with tracer containing medium and the PSAPD detector recorded

the beta particle counts from the well that included activities from both outside and inside the cultured cells. In the BR period, extracellular medium was cleared from the well and tracer containing medium was replaced by tracer-free medium (in less than 1 second for each well), therefore the recorded counts were only from cells. The switching strategy is illustrated in figure 3.2.

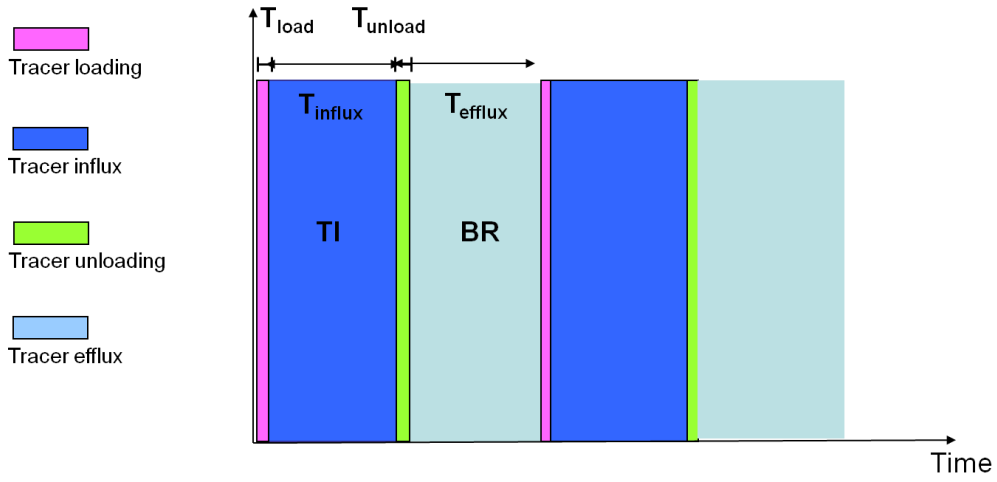

Figure 3. 2 Switching schedule with repeated cycles consists of TI and BR periods for media perfusion on a cell culture chip. In each cycle, cells were first incubated with tracer containing medium (TI period) and the beta camera recorded the total activity in the well that included activities from both outside and inside the cells. After that, extracellular medium was cleared from the well and tracer containing medium was replaced by tracer-free medium (BR period). The cycles will be repeated until the end.

B. Theory of Optimal Design

The objective of the optimal design of the switching strategy was to vary the time lengths of each TI and BR periods to achieve the most reliable estimates of the model parameters with a minimal number of switches. Fewer numbers of switches is desirable since it would minimize any potential effects of switching on cells. In the optimal design, number of switches is fixed and the length of each period is optimized first. Therefore, every optimal switching schedule (OSS) is

correspondent to a number of switches. Then the optimal number of switches is determined by comparing the value of cost function among OSS with different number of switches. Three steps were applied in the procedure for optimizing the period length:

First, for each period, the tracer concentration in cells and extra-cellular space can be calculated by solving the differential equations of the compartmental model that govern the tracer kinetics of in cells. With a set of initial conditions: the tracer concentration in the medium, the number of TI and BR periods, and the length of each period and preselected kinetic parameter values, the time activity curve (TAC) under any tracer perfusion strategy can be generated. In this work, the initial schedule was set as equal-period switching strategy (ESS) with equal cycles of TI and BR and the total imaging time was 120min.

Second, the reliability of the estimated parameters was evaluated in terms of the Fisher information matrix of the estimated parameter vector $\hat{k}$, as described by DiStefano(*68*). Briefly, a first-order approximation for the variance-covariance matrix of the parameter estimates, $\mathrm{COV}(\hat{k})$, was used and can be described by

$$\mathrm{COV}(\hat{k}) \approx M^{-1} \qquad \text{Eq. 1}$$

where $\hat{k}$ is the estimated parameter vector of *k*; $\mathrm{COV}(\hat{k})$ is the variance-covariance matrix of $\hat{k}$; M^{-1} is the inverse of the Fisher information matrix *M*, which is a measure of the amount of parameter information in the data. The element in the jth row and pth column of *M*, denoted by m_{jp}, was calculated by the following equation

$$m_{jp} = \sum_{i=1}^{n} \frac{1}{\sigma^2(t_i)} \left[\frac{\partial y(t_i,k)}{\partial k_j}\right] \left[\frac{\partial y(t_i,k)}{\partial k_p}\right] \quad \text{Eq. 2}$$

where t_i is the mid time point in each period i (TI or BR period); $y(t_i, k)$ is the averaged activity within the period i with a predefined parameter vector $\hat{k}$; $\sigma^2(t_i)$ is the variance of the measurement at time t_i . Equations 1 and 2 relate the switching schedule t_i (i = 1,2, . . . , N) to $\mathrm{COV}(\hat{k})$ which gives a measure of the precision of $\hat{k}$. The determinant of $\mathrm{COV}(\hat{k})$ was used as the criterion for optimizing the switching protocol. Optimizing a switching schedule that has a minimal determinant of $\mathrm{COV}(\hat{k})$ is equivalent to maximizing the determinant of the Fisher information matrix, det(M).

Thrid, in order to find the OSS that gave the maximal "energy"/cost function (det(M)), a simulated annealing algorithm based on heuristics from an annealing process (*69*) was used. The basic idea of the algorithm is to combine local and global search in order to get more accurate global solutions by appending a suitable energy with an artificial "temperature", which help escape the problem of getting stuck in a local maximum occasionally. Probability of accepting a bad solution is decreased as the "temperature" decreases (Eq. 3), and in the final stages it became similar to a gradient based search.

$$p_{ij} = e^{-(E_j - E_i)/T} \quad \text{Eq. 3}$$

Where E_i is the energy of the old switching schedule and E_j is the energy of the proposed new switching schedule, p_{ij} is the probability of accepting the new switching schedule. Considering our optimal design, the energy is the determinant of the Fisher information matrix (Eq. 2)

corresponding to a specific switching protocol. With a properly chosen "temperature" (T) and a cooling rate, the switching schedule could be optimized by approaching the maximal energy. Several typical sets of model parameters (k) were tested in the optimal design.

C. The Microfluidic Beta Camera Considerations

The microfluidic chip contained multiple wells for automated and separate cell deposition and medium perfusion control (Figure 3.1). A fluidic network was designed and integrated with embedded pneumatic valves and peristaltic pumps in order to individually address the microfluidic wells with varying solutions and reagents (*70*). The average time required for each medium switching, as measured in advance in actual experiments by using dyed medium, was approximately 10 second in total per transition period, during which the measurements were not used for estimating the model parameters. Therefore, a constraint on the minimal length of the intervals was incorporated in the optimal design procedure. The microfluidic beta camera system measured continuously the total activity inside each well with a time frame of 10 seconds. The length of each TI and BR period was thus not allowed to be shorter than 2 minutes.

Assume the variance at each period is proportional to the measured count rate in each interval and is inversely proportional to the interval length, the variance structure of the measurement error (*71*) is described as

$$\sigma^2(t_i) = \frac{\alpha * y(t_i, k)}{\Delta I_i} \qquad \text{Eq.4}$$

where interval ΔI_i is the length of period i, and the coefficient α is a proportionality constant related to the radiotracer concentration in the medium and the measurement sensitivity of the PSAPD detector.

3.2.2 FDG Studies

A. ^{18}F-FDG Kinetic Model and Parameter Estimation

We used the regular three compartment FDG model to describe the kinetics of FDG uptake in cells. The system of differential equations for the cellular uptake of FDG is:

$$\frac{dc_1}{dt} = -K_1 \times \frac{1-V_b}{V_b} \times c_1 + k_2 \times \frac{1-V_b}{V_b} \times c_2 \quad \text{Eq.5}$$

$$\frac{dc_2}{dt} = K_1 \times c_1 - k_2 \times c_2 - k_3 \times c_2 + k_4 \times c_3 \quad \text{Eq.6}$$

$$\frac{dc_3}{dt} = k_3 \times c_2 - k_4 \times c_3 \quad \text{Eq.7}$$

$$V_b = 1 - \frac{V_{cell}}{V_{well}} \quad \text{Eq.8}$$

where, c_1 and c_2 are, respectively, the extracellular and intracellular activity concentrations of FDG in nCi/ml; c_3 in nCi/ml is the intracellular activity concentration of phosphorylated FDG. V_{cell} is the volume of total cells in a well, V_{well} is the volume of a well on the chip, V_b is the volume ratio (Eq.8) of extracellular space to well space; K_1 (min^{-1}) and k_2 (min^{-1}) are the putative rate constants at which FDG crosses the cell membrane; and k_3 (min^{-1}) and k_4 (min^{-1}) are the putative rate constants of phosphorylation and dephosphorylation of FDG, respectively. A solution of the system of differential equations (Eqs.5-7) was used to generate the TACs in

computer simulations and fit the TACs derived experimentally from the PSAPD-generated tracer kinetic data. The model parameters were estimated based on a nonlinear weighted square approach with the Levenberg-Marquardt algorithm (*72*). In the model fitting, the weight (*w*) assigned to each measurement period *i* was

$$w_i = \frac{1}{\sigma_i^2} = \frac{\Delta I_i}{y(t_i,k)} \qquad \text{Eq.9}$$

B. Computer Simulations

Parameter estimates derived using different tracer infusion strategies—CI, ESS and OSS were compared by computer simulation under a few different sets of parameter values and with different measurement noise levels. First, for each set of parameters ($k(K_1,k_2,k_3,k_4)$, V_b) and a infusion strategy, a noise TAC was generated using Eqs. 5-7. The input function, which represents the FDG concentration in the medium that flows into the well at the beginning of each period, was defined as a binary function with repeated one-and-zeros (repeated pairs of [1, 0]s) corresponding to the switching schedule. The input function for CI was considered as an ESS with the functional value always equal to one. Second, pseudo noise, corresponding to the variance structure of the measurement shown in Eq. 4, was added to the simulated total activity function. A total of 4 different sets of *k* values, 2 different V_b and 2 different noise levels were chosen to simulate the measured kinetics for each of the two infusion strategy schedules. For each condition, 120 noise realizations were simulated. For each realization, the model estimation was performed to give the estimated values of the *k* parameters. Mean and variance of each of the estimated parameters among the 120 realizations were calculated.

C. Experiments on Microfluidic Beta Camera

1) The Microfluidic Beta Camera

The microfluidic beta camera is an integrated radiometric imaging system (Figure 3.1), capable of measuring tracer uptake of a small population (1-200) of cells in a real-time fashion. This platform consists of two major components: i) A microfluidic chip and ii) a PSAPD beta camera. The microfluidic chip contained multiple wells for automated and separate cell deposition and medium perfusion control. For parallel cell culturing, cell suspensions were sequentially loaded into wells by gravity. A fluidic network was designed and integrated with embedded pneumatic valves and peristaltic pumps in order to individually address the microfluidic wells with varying solutions and reagents. The solid state PSAPD detector was placed in close contact with the microfluidic chip. It is a beta particle counting device and is capable of providing dynamic imaging of radioactivity emitted from inside the cultured cells and the surrounding medium.

2) Image reconstruction

The microfluidic beta camera system measured continuously the total activity inside each well with a time frame of 10 seconds for all studies. 2 dimensional images were generated using a modified Anger-type logic(*73*). Regions of interest (ROIs) were automatically drawn on each well of the chip. The time-activity curve (TAC) associated with each well was calculated by projecting the corresponding ROIs onto the dynamic beta images. The measured count rates within each TI or BR period were averaged to give data points used for model fitting.

3) FDG Uptake Study of Tumor Cells on Chip

To examine the reliability of the optimal design of the medium infusion schedule on the integrated system, human glioma U87, prostate cancer cell lines P8 and CaP8 was used for FDG kinetic study. Preparation and deposition of the cells in the wells in the PDMS chip followed the procedure previously described (*74*). Cells were incubated in wells in an array of 3×4 wells array for 24 hours before performance of FDG uptake assay studies. The dimensions of each well were $1.6 \times 0.6 \times 0.055 mm^3$ (corresponding to a volume of 53 *nL*). Approximately 200 cells were plated onto each well in advance. Cells were automatically fed with fresh culture medium composed of Dulbecco's Modified Eagle Medium (DMEM, Fischer Scientific, U.S.A.) every 12 hours according to a computer controlled schedule. The integrated platform was maintained at 37 ℃ and was enclosed in an incubator containing an air mixture of 74% oxygen, 20% nitrogen, 5.1% CO_2 and 0.9% argon.

ESS of 12 cycles (5min interval for each TI and BR period) was tested on U87 cell line before the application of the optimized schedule. FDG solution diluted with 3 different concentrations of glucose medium (50, 100, 150 (m*g/dL*)) to an activity concentration of 37 MBq*/mL* was used for U87 to check the effect of physiology environment on the kinetic estimates of cells. For each chip, a total of 4 replications for each glucose condition were measured in each experimental run. During the TI period, the cells in each well were incubated in the FDG solution. During the BR period, the extra-cellular FDG was washed away using DMEM cell culture medium that contained the same glucose level as at the beginning of the study for that well. Total dynamic imaging time was 120 min for each experimental run.

In the experiments that utilized optimized switching schedule, FDG solution diluted with 3 different concentrations of glucose medium (100, 150, 200 (m*g/dL*)) to an activity concentration of 37 MBq*/mL* was used, respectively for 3 sets of 4 wells (Figure 3.3). For each chip, a total of 4 replications for each glucose condition were measured in each experimental run. The experimental procedure was repeated on the same chip with the same cells over 3 days using three different tracer infusion strategies. On the first day, ESS of 12 cycles (5min interval for each TI and BR period) was used. On the second day, OSS of 5 cycles was performed. CI with only TI period was performed on the last day. This three-day experimental procedure was performed twice, resulted in 8 studies for each condition (one tracer infusion strategy with one medium glucose concentration). Model parameters were estimated from each kinetic TAC and were averaged among the 8 studies under the same conditions.

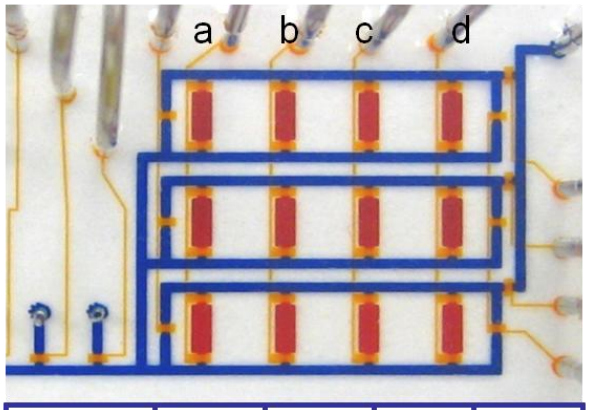

Glucose (mg/dL)	a	b	c	d
100	CaP8	CaP8	CaP8	CaP8
150	CaP8	CaP8	CaP8	CaP8
200	CaP8	CaP8	CaP8	CaP8

Figure 3. 3 Experimental setup for FDG uptake assays on chip. ^{18}F-FDG solution diluted with 3 different concentrations of glucose medium (100, 150, 200 (m*g/dL*)) to an activity concentration of 37 MBq*/mL* was used, respectively for 3 sets of 4 wells. Cell line CaP8 was loaded in each well.

D. Statistical Analysis

For the computer simulation studies and the experimental result characterization, the mean, standard deviation (STD), the coefficient of variation (CV), and the bias of each estimated model parameters were calculated to characterize the simulation results. For the experimental result characterization, the mean, STD and CV of the estimated model parameters were used. Existence of dependency of the estimated parameter values on the glucose level in the incubation medium was also examined by F-test, using the Statistical Package for the Social Sciences (SPSS, IBM Corp.).

3.3 Results

Computer simulations were implemented using MATLAB on a Microsoft Windows XP system. The average computation time for determining an OSS schedule was usually less than 10 min and the number of iteration steps needed for convergence was less than 1000 iterations. For model fitting of one TAC (either simulated or experimental data), convergence was obtained within 60 seconds for CI and within 30 seconds for OSS (usually less than 40 iterations) when the residual sum of squares reached a minimum.

3.3.1 The Optimized Switching Schedule for Tracer Infusion on Chip

A. Effects of the Number of Switching Cycles in the OSS

Since the optimization function is dependent on the model parameters (i.e., values of k's), OSS schedule as a function of the number of switching cycles for each set of k values was

examined. The number of cycles was gradually decreased from 12 to 3 while maintaining a fixed 120min total imaging time. Three sets of model parameters were used, as shown in Table 3.1, the values of determinant (of the Fisher Information matrix) for OSS with different number of switches were calculated for each condition. It was found that the optimized switching schedule always had the largest determinant for the 5-cycle OSS. Table 3.2 shows the optimal schedules with 7 different numbers of cycles under the condition of one set of parameters (K_1=0.14 /min, k_2=0.15 /min, k_3=0.05 /min and k_4=0.005 /min) with a fixed V_b value (V_b =0.95). The switching times of the 5-cycle OSS (alternating between TI and BR periods) are at 0, 9,11,28,43,46,76,79,108 and 111 min. Based on these results, the 5-cycle OSS is the most efficient optimized medium infusion schedule for extracting the kinetic estimates and was selected to be used for real experiments.

Number of switching cycles	det(*M*)		
	K_1=0.14,k_2=0.025 k_3=0.01,k_4=0.005	K_1=0.14,k_2=0.15 k_3=0.05,k_4=0.005	K_1=0.52,k_2=0.02 k_3=0.008,k_4=0.005
12	1.34E+07	5.38E+05	3.08E+07
10	1.67E+07	5.67E+05	4.24E+07
7	2.22E+07	6.18E+05	5.59E+07
6	2.23E+07	6.89E+05	6.42E+07
5	2.32E+07	6.92E+05	6.72E+07
4	2.13E+07	6.37E+05	6.61E+07
3	9.23E+06	2.58E+04	2.93E+07

Table 3.1 Determinant values (of Fisher information matrix) of optimized switching schedules with 12, 10, 7, 6, 5, 4 and 3 cycles under different set of k parameters. V_b is fixed at 0.95.

Number of switching cycles	Optimal switching time points
12	5,7,13,15,26,28,33,35,37,48,70,72,81,83,98,100,103,105,109,111,115,117
10	5,7,13,15,27,29,34,45,47,73,87,89,101,103,108,110,114,116
7	9,11,18,20,34,47,49,76,78,109,114,116
6	6,8,15,17,31,45,47,78,80,111
5	9,11,28,43,46,76,79,108,110
4	11,15,38,57,59,102,104
3	8,13,58,102,104

Table 3.2 Optimized switching schedules with 12, 10, 7, 6, 5, 4 and 3 cycles when *k* is set at K_1=0.14 /min, k_2=0.15 /min, k_3=0.05 /min and k_4=0.005 /min. V_b is fixed at 0.95.

B. Comparison of Values of the Determinant (of Fisher Information Matrix) among 5-cycle OSS,12-cycle ESS and CI under Different Conditions

The procedure of optimal design was performed for 3 different sets of *k* and V_b values, and the values of determinant (of the Fisher Information matrix) for CI, 12-cycle ESS and 5-cycle OSS under these conditions are shown in Table 3.3. The results indicate that the 5-cycle OSS always yielded larger determinant values than those of 12-cycle ESS and CI. When V_b was increased from 0.91 to 0.99, the determinant value of OSS decreased much less than that of CI, which indicated that the use of OSS would be more important when the number of cells in the well was small. When K_1 was increased from 0.14 to 0.52 (or K_1/k_2 is increased from 0.14/0.15 to 0.52/0.02), the determinant value of CI was increased significantly (order of 10^4~10^7) while the determinants of the OSS were increased less (order of 10~10^3). Although the values of the determinant for the OSS were not the same for different combinations of *k* and V_b, the actual

OSS schedules were similar for different conditions (Table 3.4). In other words, the OSS schedule was shown to be relatively insensitive to k and V_b values.

$k(K_1,k_2,k_3,k_4)$	Tracer uptake assays	det(M)		
		$V_b = 0.91$	$V_b = 0.95$	$V_b = 0.99$
K_1=0.14,k_2=0.025, k_3=0.01,k_4=0.005	CI	2.25E+06	2.13E+05	1.34E-01
	12-cycle ESS	4.28E+06	3.74E+05	5.08E+02
	5-cycle OSS	1.29E+08	2.32E+07	6.70E+04
K_1=0.14,k_2=0.15, k_3=0.05,k_4=0.005	CI	3.72E+03	3.88E+01	1.16E-04
	12-cycle ESS	9.88E+04	7.29E+03	7.75E+00
	5-cycle OSS	5.10E+06	6.92E+05	1.95E+02
K_1=0.52,k_2=0.02, k_3=0.008,k_4=0.005	CI	4.02E+07	1.18E+07	1.79E+02
	12-cycle ESS	2.92E+07	3.68E+06	5.19E+03
	5-cycle OSS	4.60E+07	3.08E+07	4.26E+05

Table 3.3 Determinant values (of Fisher information matrix) among CI, 12-cycle ESS and 5-cycle OSS under different combination of k and V_b values

k and V_b	Optimal switching time points for a 5 cycle OSS
K_1=0.14,k_2=0.025, k_3=0.01,k_4=0.005 V_b=0.91	9,11,28,42,44,75,77,109,111
K_1=0.14,k_2=0.15, k_3=0.05,k_4=0.005 V_b=0.95	9,11,28,43,46,76,79,108,110
K_1=0.52,k_2=0.02, k_3=0.008,k_4=0.005	9,11,27,43,45,78,80,110,112

V_b=0.99

Table 3.4 Pattern of a 5-cycle OSS under different combination of k and V_b values

3.3.2 Performance Comparison among Different Schedules from Computer Simulation

Over the 120 realizations, the average value, Bias% and CV% of the kinetic parameter estimates for the two schedules (12-cycle ESS, 5-cycle OSS and CI) under four different sets of sets of K, Vb values and noise levels are shown in table 3.5. ESS and OSS had a much smaller Bias% and CV% compared to those of CI, with the largest CV% improvement in K_i ($K_i = \frac{K_1 \times k_3}{k_2 + k_3}$) from 53% to 9% in OSS. When V_b was increased from 0.95 to 0.99, CI gave the worse result (e.g., bias% of K_i was increased from 2% to 18%), which is consistent with the decrease in the determinant value of the Fisher information matrix shown before (Table 3.4) and confirms the validity of the optimization procedure used for generating the OSS schedules. When the measurement noise level was doubled (factor α increased from 0.1 to 0.2 which was selected to be consistent with preliminary measurements), the estimates by CI also deteriorated most and gave larger variance of the estimates compared to those of ESS and OSS.

Parameter values	Tracer uptake assays	Bias%					CV%				
		k1	k2	k3	k4	Ki	k1	k2	k3	k4	Ki
α=0.1, V_b=0.95	CI	9%	110%	390%	310%	10%	31%	174%	248%	402%	150%
k1=0.14, k2=0.025	12-cycle ESS	2%	60%	275%	131%	18%	11%	119%	198%	133%	59%
k3=0.01, k4=0.005	5-cycle OSS	1%	13%	48%	66%	4%	11%	60%	117%	102%	44%
α=0.1, V_b=0.95	CI	52%	126%	18%	20%	2%	100%	147%	69%	214%	26%

k1=0.1, k2=0.2	12-cycle ESS	37%	125%	27%	3%	1%	68%	133%	63%	72%	17%
k3=0.05, k4=0.005	5-cycle OSS	0%	0%	1%	5%	1%	5%	12%	14%	35%	6%
α=0.1, V_b=0.99	CI	171%	277%	30%	36%	18%	203%	223%	64%	190%	48%
k1=0.1, k2=0.2	12-cycle ESS	19%	45%	8%	6%	3%	39%	76%	35%	40%	13%
k3=0.05, k4=0.005	5-cycle OSS	0%	1%	0%	1%	0%	8%	15%	12%	27%	9%
α=0.2, V_b=0.99	CI	248%	343%	-11%	-56%	-17%	239%	232%	82%	543%	53%
k1=0.1, k2=0.2	12-cycle ESS	32%	78%	18%	-7%	1%	42%	74%	38%	54%	12%
k3=0.05, k4=0.005	5-cycle OSS	-1%	-1%	-4%	-14%	-3%	13%	29%	23%	52%	9%

Table 3.5 Bias% and CV% of 120 realizations of CI, 12-cycle ESS and 5-cycle OSS under four different combinations of k, V_b and noise level α

3.3.3 Application of the Different Media Infusion Schedules to microfluidic beta camera experiments

For the experimental result characterization, the mean, STD and CV of the estimated model parameters were calculated. Convergence of model fitting of one TAC was obtained within 60 seconds when the residual sum of squares reached a minimum.

A. Application of the 12-cycle ESS to Microfluidic Beta Camera Experiments

For physical experiments on the microfluidic system, a control experiment was performed first. FDG was infused into the chamber without cells and the results showed that the washing was effective in removing the FDG from the chambers. Number of cells in each well was counted before and after experiment and no significant difference was observed. The 12-cycle ESS was implemented to measure FDG kinetics in U87, P8 and CaP8 cells. Figure 3.4 showed the FDG kinetics in U87. It is observed that the FDG uptake constant K_i is decreased when the medium glucose level is increased from 0.5g/L to 1.5g/L (Left panel of figure 3.4).

When checking the FDG concentrations in medium and cell compartments separately (Left panel of figure 3.4), we found that when medium glucose level is 1g/L, FDG-6-PO_4 concentration in cells is almost twice that under the condition of 1.5g/L glucose level.

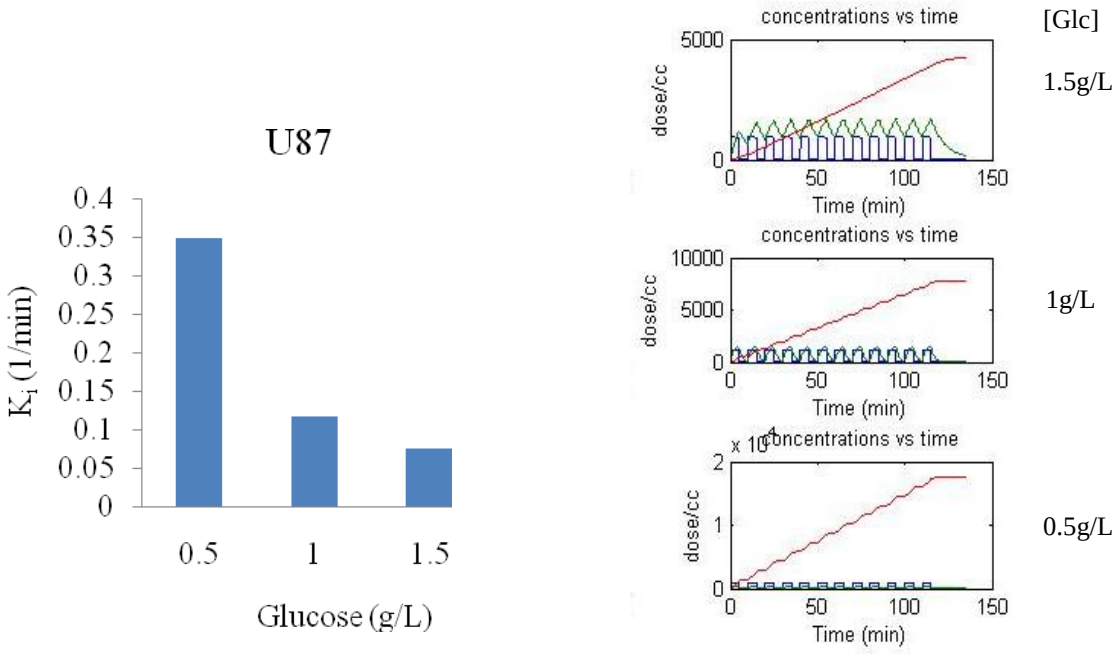

Figure 3. 4 Left: FDG uptake constant K_i under 3 different glucose concentrations ([Glc]); Right: Estimated FDG concentrations in medium (blue) and cells (green), FDG-6-PO_4 concentration in cells (red).

B. Application of the 5-cycle OSS to Microfluidic Beta Camera Experiments

The 5-cycle OSS, 12-cycle ESS and CI (the same schedules used in the simulations) were implemented to measure ^{18}F-FDG kinetics in CaP8 cells. The performances among three schedules were compared based on the variability of the estimated model parameters.

The measured kinetics data were fitted well by the model of Eqs. 5-7 and a set of typical fitting results of the three infusion strategies are shown in figure 3.5. The correlation coefficient (R) between the measured data and the corresponding model-predicted values was evaluated in

each fitting. For all OSS studies, the R value was 0.999 ±0.0003 and the slope was 0.987 ±0.009; for CI studies, the R value was 0.992 ±0.002 and the slope was 0.985 ±0.005; for ESS studies, the R value was 0.998 ±0.0002 and the slope was 0.986 ±0.002. In all the model fitting procedures, the parameter value of V_b was fixed at 0.95, which was estimated based on the cell number and chamber volume in the microfluidic chip. The value of k_4 for tumor cells was assumed to be close to 0 (*75-79*) and was also fixed at 0.005/min here to make the model fitting more stable and to give more reliable parameter estimates. If the values of k_4 or V_b were allowed to be variable during the model fitting, the variability of the estimates in some runs increased drastically (e.g., the CV% of Ki for CI was increased more than twice, from 36% to 74%). Averaged estimates of the k parameters under the 3 different conditions of OSS, CI and ESS (4 replicates for each condition) are shown in (4 replicates for each condition) are shown in Table 3.6. For the condition of 200mg/dL glucose medium, the CV% of the estimated K_i was, 29%, 28% and 20% for CI, ESS and OSS, respectively. A decrease of the variability on the estimates of K_1, k_2 and k_3 were also shown for OSS as compared to those of CI.

Since the experiment with 4 runs of each glucose condition was implemented on the same chip twice to get the total 8 runs, the inter-experiemental variability was also checked for different glucose conditions. For OSS, no significant differences in K_1, k_2, k_3 and K_i were found in all glucose conditions ($P>0.05$) between two experiments; For K_i, the smallest P-value was 0.32 with the condition of 200mg/dL medium glucose concentration. The similar conclusions were also found in ESS. However, for CI, differences in k_2 and k_3 were significant in all glucose conditions ($P<0.05$) between two experiments, only K_1 and K_i resulted in the P-value larger than

0.05. These results indicate that the switching schedule is more stable than CI when they are applied on the chip.

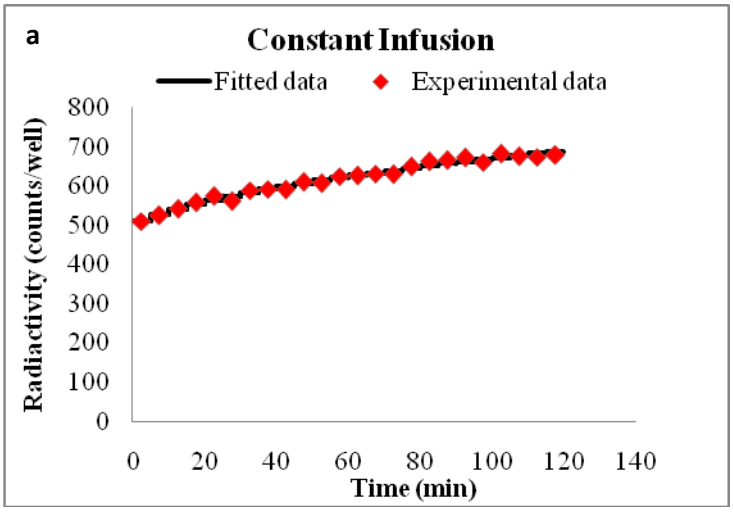

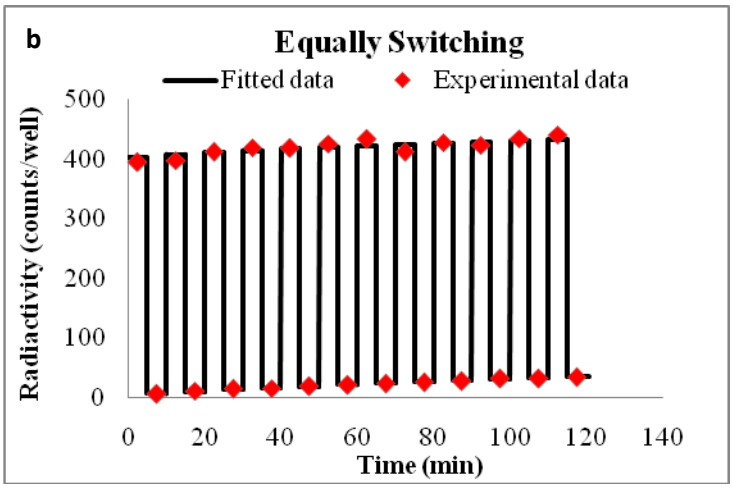

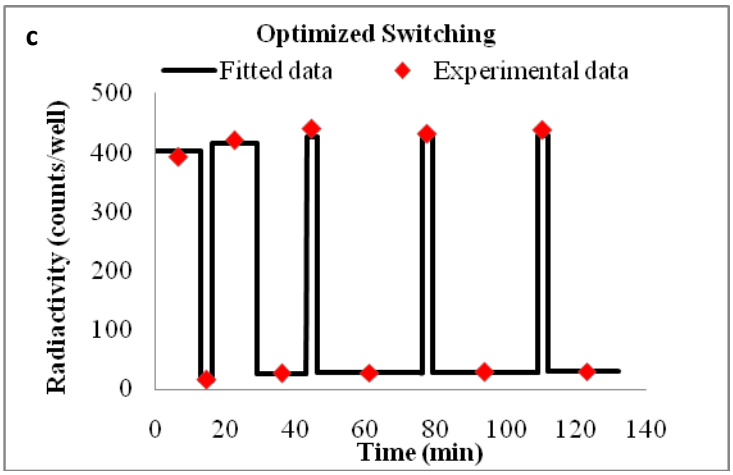

Figure 3. 5 Experimental data from microfluidic Beta Camera with CI, 12-cycle ESS and 5-cycle OSS were all well fitted with the compartmental model.

K_1

	OSS			CI			ESS		
Glucose	mean	std	CV%	mean	std	CV%	mean	std	CV%
1	0.4516	0.1203	27%	0.2438	0.0608	25%	0.1535	0.0678	44%
1.5	0.3649	0.0550	15%	0.2177	0.0611	28%	0.1205	0.0357	30%
2	0.2782	0.0895	32%	0.1710	0.0942	55%	0.0661	0.0114	17%

k_2

	OSS			CI			ESS		
Glucose	mean	std	CV%	mean	std	CV%	mean	std	CV%
1	0.3801	0.1058	28%	0.1623	0.0778	48%	0.1920	0.0778	96%
1.5	0.3427	0.0450	13%	0.1430	0.0516	36%	0.2895	0.0516	86%
2	0.4878	0.1814	41%	0.1674	0.1414	84%	0.1946	0.1414	161%

k_3

	OSS			CI			ESS		
Glucose	mean	std	CV%	mean	std	CV%	mean	std	CV%
1	0.0914	0.0446	49%	0.0873	0.0547	63%	0.1773	0.0543	31%
1.5	0.0839	0.0098	12%	0.0671	0.0064	10%	0.3567	0.3536	99%

2	0.0803	0.0113	14%	0.0642	0.0317	49%	0.2740	0.2862	104%

K_i

	OSS			CI			ESS		
Glucose	mean	std	CV%	mean	std	CV%	mean	std	CV%
1	0.0807	0.0061	8%	0.0789	0.0063	8%	0.0721	0.0043	6%
1.5	0.0711	0.0035	5%	0.0688	0.0043	6%	0.0680	0.0390	57%
2	0.0437	0.0085	20%	0.0492	0.0141	29%	0.0453	0.0129	28%

Table 3.6 Mean, STD and CV% of estimated k among 5-cycle OSS, CI and 12-cycle ESS performed on microfluidic beta camera

C. Relationship of Model Parameters to the Glucose Level in the Cultivating Medium

Functional relationships between the derived kinetic parameters of OSS and the medium glucose concentration ([glc]) indicate that the glucose transport and utilization in these cells was well regulated. Based on the results of OSS, estimates of k_2 and k_3 were not correlated with the medium glucose level (p=0.358 and 0.554, F-test), while K_1 and K_i were correlated with the medium glucose level (p=0.012 and 0.000, F-test); the values of K_1 and K_i were inversely proportional to the glucose concentration in the medium (R=0.651, p=0.022 for K_1 and R=0.790, p=0.002 for K_i). The cellular glycolytic rate ($GR= K_1*k_3/(k_2+k_3)*$[glc]) was not affected by medium glucose level (p=0.778, F-test). For CI, K_1 was not correlated with the medium glucose level (p=0.250, F-test) and the inverse relationship of K_1 versus glucose level was not significant due to the large variability of the estimates (R=0.012, p=0.614). Like the results from OSS, K_i from CI was also correlated with the medium glucose level (p=0.009, F-test) and the inverse relationship with medium glucose level was significant (R=0.335, p=0.003). Estimates of k_2, k_3 and GR from CI experiment were not correlated with the medium glucose level (p>0.05, F-test), (p=0.642 for GR, p=0.883 for k_2 and p=0.563 for k_3).

3.4 Disussion

In this work, the optimal design of the novel switching schedule and its application in tracer kinetic assays with a microfluidic beta camera has been investigated. This approach was examined with computer simulation and was tested with real experimental data.

The OSS design on parameter estimation was derived based on different number of cycles (Table 3.1 and 3.2). It was noted that the 1) The OSS with 5 cycles always yield the largest determinant of the Fisher information matrix among 3 different sets of model parameters 2) effects of decreasing the number of cycles on the determinant of the Fisher information matrix was small 3) the patterns of the OSS all had longer TI period in the beginning and longer BR period later, regardless of the number of cycles selected 4) the determinant of the Fisher information matrix increased first in value with decreased number of cycles from 12, but started to decrease when the number was below 5. Therefore, the most effective OSS to extract kinetic information with minimum number of switching cycles was a 5-cycle OSS.

The effect of using 5-cycle OSS and CI on parameter estimation was compared by computer simulation based on 4 sets of typical parameters first. The simulation results showed that reasonably good parameter estimates could be obtained with the optimized switching schedules (Table 3.3 and 3.5), in which OSS produced the estimated K_1-k_4 values with better accuracy and precision than CI. The simulation results also indicated that OSS was insensitive to the values of k and V_b over the range of conditions studied (Table 3.4). The parameter estimation accuracy with CI was relatively poor and large biases in the estimates of K_1-k_4 were observed (Table 3.5). This is likely caused by the high background noise from extracellular space

simulated. For OSS, however, as background removed period was applied, the noise generated for those periods were much smaller than those of CI. Therefore, a better approximation of the noise variance can be made and more reliable and good parameter estimates obtained.

Kinetic experiments have demonstrated that the 5-cycle OSS is useable for estimating FDG uptake constant in the microfluidic beta camera system. All experimental data were well fitted by the regular FDG model with residuals consistent with random noise (Figure 3.5). In terms of the effects of medium glucose level on the individual values of K_1, k_2, k_3, K_i, GR, a clear inverse relationship was found for K_1 and K_i estimates obtained with the 5-cycle OSS. However, for the studies with constant infusion strategy, K_1 was not related to medium glucose level. In vitro study on ovarian adenocarcinoma (*7*) showed a enhanced FDG uptake in cells with lower media glucose concentration. Clinical studies on pancreatic malignancies (*1*) and bronchial carcinomas (*2*) also demonstrated that FDG uptake into most human cancer cells is inhibited by increasing media glucose levels because of direct competition between FDG and D-glucose for uptake and incorporation into cultured tumor cells and cancers. Our results are consistent with those findings. The inverse relationship showed that the Cap8 cells were able to adapt to changes in the glucose level in the medium by regulating the membrane transport of glucose into cells, and thus maintaining stability in the cellular glycolytic environment. Results on K_i obtained from OSS showed a clearer inverse relationship between FDG transport rates and glucose levels than CI. Due to our lack of knowledge of the true value of cellular kinetic parameters of CaP8 cells in the particular medium environment, only precision of the estimated parameters was evaluated (Mean, STD and CV were shown in Table 3.6). Based on the value of experimental kinetic

parameters K_1-k_3 in CaP8 cells, computer simulation was performed again to compare the 5-cycle OSS and CI. It was found that a 5-cycle OSS still improves the accuracy and precision of the estimated K_1-k_3 more than 2 folds than CI (Table 3.7). Averaged on the 6 parameter sets, the Bias% and CV% of K_1 for OSS was 3% and 23%, for CI was 27% and 86%. Nonetheless, Bias% and CV% of K_i from both OSS and CI are lower than 10% for all conditions. This explained that in the experimental results (Table 3.6), only the average value of K_i from OSS and CI are similar under each glucose level.

Parameter values	Tracer uptake assays	Bias%				CV%			
		K_1	k_2	k_3	K_i	K_1	k_2	k_3	K_i
α=0.1, V_b=0.95	CI	16%	32%	-4%	-1%	75%	115%	28%	5%
K_1=0.4516, k_2=0.3801 k_3=0.0914, k_4=0.005	5-cycle OSS	1%	0%	-1%	0%	20%	23%	10%	3%
α=0.1, V_b=0.95	CI	25%	50%	-5%	-2%	112%	186%	29%	5%
K_1=0.3649, k_2=0.3427 k_3=0.0839, k_4=0.005	5-cycle OSS	1%	-1%	-2%	0%	22%	27%	10%	4%
α=0.1, V_b=0.95	CI	50%	67%	-11%	-3%	115%	140%	35%	8%
K_1=0.2782, k_2=0.4878 k_3=0.0803, k_4=0.005	5-cycle OSS	3%	2%	1%	0%	30%	31%	15%	6%
α=0.1, V_b=0.95	CI	13%	44%	-2%	-1%	59%	133%	42%	6%
K_1=0.2438, k_2=0.1623 k_3=0.0873, k_4=0.005	5-cycle OSS	3%	5%	-4%	-1%	23%	44%	15%	2%
α=0.1, V_b=0.95	CI	15%	47%	2%	-1%	56%	122%	37%	6%
K_1=0.2177, k_2=0.1430	5-cycle OSS	5%	8%	-3%	-1%	18%	32%	11%	2%

k_3=0.0671, k_4=0.005									
α=0.1, V_b=0.95	CI	41%	106%	1%	-2%	101%	168%	47%	10%
K_1=0.1710, k_2=0.1674 k_3=0.0642, k_4=0.005	5-cycle OSS	5%	7%	-2%	-1%	22%	35%	9%	3%

Table 3.7 Bias% and CV% of 120 realizations of CI and 5-cycle OSS under six different parameter sets (each set has different K_1-k_3, *same* k_4, V_b and α) based on the results from experiments in CaP8 cell line.

However, from the experiment, the improvement in variations (CV%) of the estimated parameters by using the 5-cycle OSS was not as large as predicted from the computer simulations compared to CI. The lower than expected reduction in variability of the estimates in the experimental results may be due to the variability of the switching operation. Generally speaking, the variability sources can be categorized into two types. One comes from systemic technical factors (e.g., flow rate, image resolution, linearity of detection sensitivity, chip configuration, materials that are used for the bottom of the chip and dose calibrator for FDG). Another type is associated with tumor responses to systemic biochemical changes (from TI to BR period) and the change of cell numbers. These factors will be discussed below.

The microfluidics is a pneumatic pressure-driven chip-based system(*80*), which means local forces to direct droplet movements was generated by active control of gas pressure applied off-chip. This pressure was adjusted manually and was not the same day to day. So, the flow rate might not have been stable, and might be dependent on how big the pressure difference was. The effect of flow rate, such as shear stress(*81*), though was assumed very small and could be neglected on cellular biological state, may still affect the clearance of extracellular tracer during

BR period in OSS. Therefore, the model fitting described in Eq. 4-6 would not be accurate without considering the tracer residuals that was left outside the cellular space during BR period. Improvement of pressure control can be achieved by using a more precise pressure regulator in the future.

The spatial resolution of the PSAPD detector was approximately 680 μm full width half maximum (FWHM) with the current microfluidic chip design, which includes a 150 μm thick glass slide and 100 μm of plastic between the source and detector (Figure 3.6). The FWHM was calculated from the Gaussian function that described the line profile acquired with the use of the FDG line source. As the source-to-detector distance was increased, The FWHM was increased (Figure 3.6). If the source-to-detector distance can be decreased, such as by eliminating the substrate layers, the system spatial resolution could be improved down to 400 μm FWHM. The dimension of each well on chip was $1600 \times 600 \times 55\ \mu m^3$ and the width of the well is narrower than the 680 μm FWHM. Therefore, the partial volume effect (PVE) needs to be accounted for the measurement of FDG activity in each well. Recovery coefficients for different size of the well could be measured for correction the PVE effect.

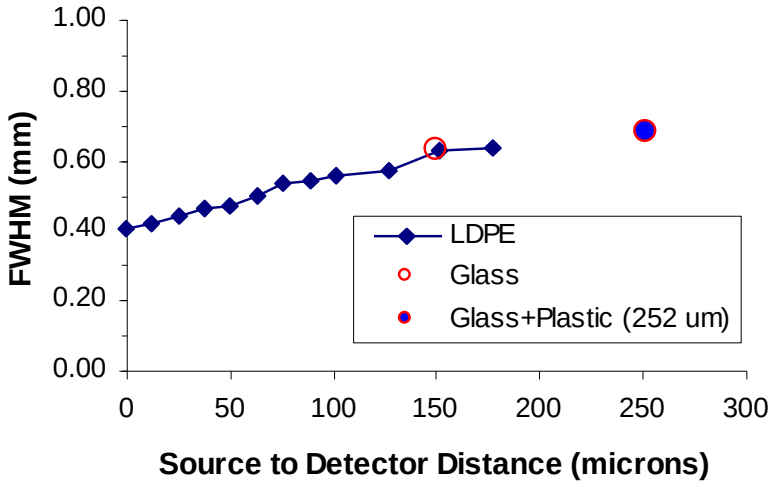

Figure 3. 6 The FWHM is plotted as a function of source to detector distance using various layers of plastic films and a single 150 μm glass slide.

The range of ^{18}F positrons through plastic is less than 1000 μm and approaching very low energies the range decreases exponentially (*82*). Therefore small changes in the source-to-detector distance can have a large impact on the range of the positrons and the detection efficiency. The absolute sensitivity as a function of plastic film thickness was measured for PSAPD detector in the control experiment (Figure 3.7). In the current microfluidic chip design, with a 150 μm thick glass substrate plus an additional 100 μm of plastic between the source and detector, the absolute sensitivity is approximately 3%. As the height of the microchamber is only 55 μm, detection sensitivity of beta camera is assumed to be linearly related to the depth of each well in such small dimension and is not accounted in the model fitting. The actual signals detected by the PSAPD are different, depending if the radioactive molecules distribute (i) evenly throughout a chamber as in the case with no cells or (ii) mainly to the bottom location as in the

case with cells. If the detector sensitivity could be calibrated without and with cells and applied in image reconstruction, more precise FDG uptake could be measured.

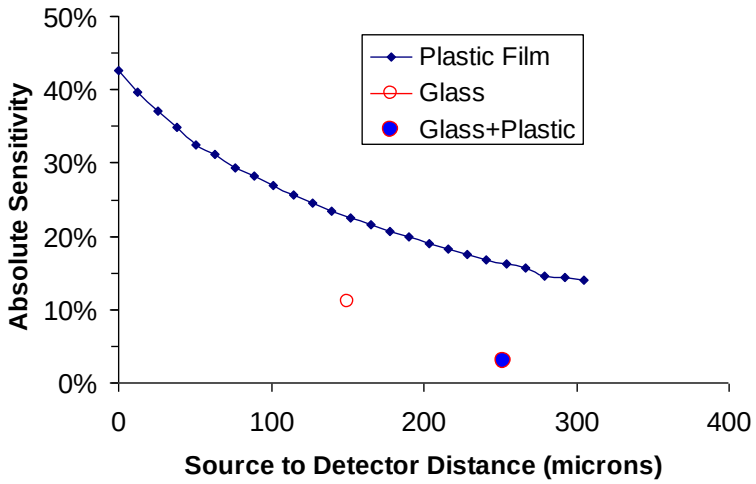

Figure 3. 7 Absolute sensitivity for Tl-204 source as a function of plastic film and a single 150 μm thick glass slide.

The chip configuration and materials are another two issues to be considered. Each well could have dimensional variation, which was hard to measure accurately after the microchip was made. So the chamber volume was not homogeneous. The volume ratio V_b of 0.95 in the model fitting for all experimental data used in the present study was only a gross estimate. The bottom of the chip was made with polydimethylsiloxane (PDMS), which may have absorption of the tracer, FDG, during the experiment and may have enhanced the background on the measurement.

For the three day consecutive experiments, cell numbers were counted before each experiment. It was found that the percent change in cell numbers was about ±5% from the first day to the third day, in terms of cell volume percentage in a well would be ±0.25%, which is too small to affect the cellular kinetic parameters.

3.5 Conclusions

The microfluidic beta camera platform with a kinetic switching strategy for tracer incubation was shown to provide reliable estimates of cellular FDG transport and uptake constants. Results on the real experiments showed that U87 and CaP8 cell lines can regulate well the glucose transport into cells to maintain their glycolytic metabolic rate (i.e., it can adapt well to environmental glucose level changes). Both computer simulations and real tracer kinetic experiments indicated that the reliability of the model parameters can be improved with an optimal design of fewer switching cycles. The optimized schedule also has the practical advantages of simplifying the tracer incubation protocol and reducing any potential disturbance to the cultured cells caused by the perfusions during the switches between the TI and BR periods.

Chapter 4 IN VITRO FDG STUDIES ON TUMOR CELLS USING REGULAR CELL CULTURE PLATE

4.1 Introduction

Cancer cells show increased metabolism of both glucose and amino acids, which can be monitored with 2-[18F]fluoro-2-deoxy-D-glucose (FDG) and positron emission tomography (PET) imaging. FDG uptake is higher in fast-growing than in slow-growing tumors is considered to be a good marker of the grade of malignancy (*10-12*). Although in vitro studies may suffer from the differences between the in vitro and the in vivo situation, they are valuable tools for the detection of general cellular reactions to media environmental change such as a consequence of the exposure of cells to high glucose levels. In our previous chapter, we have showed our effort to study FDG uptake in tumors in vitro. The transport and uptake kinetics in tumor cells in a microfluidic-PSAPD platform could be extracted with the use of a new switching medium infusion procedure (Figure 3.2). It was found that the FDG uptake constant K_i had a significant inverse correlation with the medium glucose levels in glioblastoma (U87) and prostate cancer (CaP8), while no significant relationship were found between k_2, k_3 and medium glucose levels. For the in vitro FDG uptake studies performed on regular cell culture plate, human ovarian adenocarcinoma cells has been studied (*7*). The human ovarian adenocarcinoma cells were cultured in medium containing 100 or 300 mg/dl of glucose and measured the FDG uptake at multiple time points (days) after the initial culture. It was observed that the FDG uptake in tumor cells with chronic hyperglycemia (cells grown at 300 mg/dl of glucose for 51 and 72 days and assayed at 100 mg/dl of glucose) was only decreased by 10%, while acute hyperglycemia (cells

grown at 300 mg/dl of glucose for 51 and 72 days and assayed at 300 mg/dl of glucose) markedly reduces uptake of FDG by 70%, as compared to cells grown and assayed at 100 mg/dl of glucose. Both results shown above indicate the necessary to investigate the effect of medium glucose level on FDG uptake studies.

Other physiological factors in the cell culture medium, such as fatty acid (*83, 84*), may also affect the FDG uptake in tumor cells. It has been well known that fatty acids are important sources of fuel for metabolism (*85*). Many cell types can use either glucose or fatty acids for this purpose. In particular, heart and skeletal muscle prefer fatty acids. It has been found that elevated plasma free fatty acid level increased insulin-suppressed hepatic glucose output and reduced the insulin-stimulated glucose uptake in tissues (*86*). However, no in vitro studies have revealed the effect of medium free fatty acid level on glucose metabolism in tumor cells. We performed in vitro FDG uptake experiments on regular cell culture plate to investigate the relationship of medium glucose/free fatty acid level and FDG uptake in several tumor types. Moreover, we studied the effect of glucose levels on [18F]-3'-fluoro-3'-deoxy-L-thymidine (FLT) uptake in tumors. FLT is transported by the same nucleoside carrier as thymidine and is also phosphorylated by the same enzyme, S-phase–specific thymidine kinase 1 (TK1), which leads to intracellular trapping of radioactivity within the cytosol (*87, 88*). TK1 is a principal enzyme in the salvage pathway of DNA synthesis. Thus, FLT as a PET tracer is used to marker cell proliferation. Some preclinical and clinical studies have suggested that FLT uptake is considerable in malignant tissue but much less in inflammatory cells than is FDG uptake (*89-91*). Decreased uptake of FDG is seen in hyperglycemic patients and can cause false negative results

(*3*). To the best of our knowledge, no studies have been reported the effect of glucose levels on FLT uptake in tumor due to the different pathway FLT incorporated with from the glucose metabolism. However, it would still be necessary to confirm that the use of FLT could avoid the issue of decreased tumor uptake in hyperglycemia patients.

Since FDG and glucose differ with regard to transport across the membrane and phosphorylation through the initial step in the glycolysis, FDG net uptake must be converted into glucose net uptake by the lumped constant (LC) (*92*). LC is a term based on the principles of competitive substrate kinetics that corrects for the differences in transport and phosphorylation between FDG and glucose. A direct and simple approach to measure the value of LC in rats has been studied by Sokoloff et al. (*93*). The procedure requires accurate determination of the arterial-venous differences of the FDG and glucose concentration so that the blood samples need to be taken from the subjects. To measure LC in cell lines in vitro, cellular glucose utilization can be precisely determined by measuring the difference of medium FDG and glucose concentration before and after tracer incubation. Thus the glucose effect on LC could also be investigated.

4.2 Materials and Methods

4.2.1 Cell Culture

Human glioblastoma cancer cell line U87, prostate cancer cell line PC3, mammary cell line MDA-MB-231 were used. D-(+)-glucose (10% w/v), obtained from Sigma (St. Louis, MO), was added to glucose-free RPMI to obtain the desired final glucose concentration (~50, 100, 150, 200 or 450 mg/dl). The 100mg/dL glucose media was used to make the cell culture media with 0,

25, or 50 μM/L free fatty acid (linoleic (18:2) acid). Cells were seeded at an initial density of ~0.8 x 10^4 to 1.5 x 10^4 cells per 0.36 cm^2 area in a 96-well tissue culture plate (BD Falcon) or at an initial density of ~1.5 x 10^5 to 3 x 10^5 cells per 3.8 cm^2 area in a 12-well tissue culture plate (BD Falcon), fed with the media containing different glucose levels or FFA levels. The number of cells seeded in the plate depends on the area each cell occupied when they are flat attached to the bottom area. The size of glioblastoma cancer cell line usually is twice the size of the other cell lines. So less number of U87 cells was plated for the tracer uptake experiment compared to the other tumor types.

At confluency, cells were dissociated with 0.05% trypsin-0.02% EDTA and used in the experiments or otherwise subcultured. Viable cell number was assessed by the Trypan blue dye exclusion technique using an Olympus (Lake Success, NY) IMT-2 inverted microscope. All experiments were conducted in a humidified incubator containing 5% CO_2 at 37 ℃. The media glucose level was measured at initial cell plating and the end of the tracer uptake experiment with a glucose and lactate analyzer (SensorStar, DiaSys Diagnostic Systems, Germany) (Figure 4.1).

4.2.2 FDG and FLT Uptake Studies

The tracers FDG and FLT were diluted in glucose-free RPMI media to obtain a final concentration of 0.5 μCi/100 μL in the solutions that were used in the tracer uptake experiments. Tracer uptake assay was performed 24-hour after initial cell culture on the plate. Tracer uptake into cells was determined at the same media glucose level as the growth media; that is, cells grown at 100 mg/dl of glucose were assayed at 100 mg/dl of glucose and those grown at 200

mg/dl of glucose were assayed at 200 mg/dl of glucose. The tracer solution was added to each well and the incubation continued for another 60 min at 37 ℃. Hank's Balanced Salt Solution (HBSS), ice-cold, was used to stop tracer incorporation, and cells were washed three times with the same buffer. Cells were lysed in 100 µl of 0.3*M* NaOH and 1% sodium dodecyl sulfate. After that, the media in each well was transferred into a sterile glass tube (Borosilicate heavy wall, Fisherbrand) to measure the radioactivity with a well counter. The experiment procedure is shown as Figure 4.1.

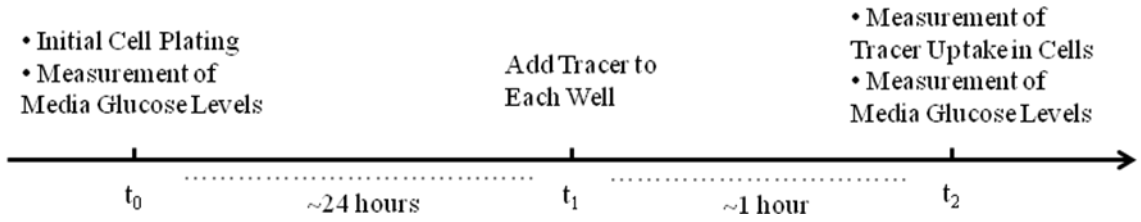

Figure 4. 1 Experiemental procedure for measuring media glucose levels and cellular tracer uptake.

4.2.3 Lumped Constant and Glucose Utilization Rate

The lumped constant (LC) was calculated as the ratio of normalized FDG uptake to normalized glucose uptake in cells (Eq. 4.1). The glucose utilization rate (GR) was determined in two ways as shown in Eq. 4.4 and Eq. 4.5. The GR_{LC} that is derived from the FDG uptake and lumped constant was compared to GR that was directly calculated from absolute change of media glucose levels.

$$LC = \frac{\text{FDG uptake\% per hour}}{\text{Glucose uptake\% per hour}} \qquad \text{Eq. 4.1}$$

$$\text{FDG uptake\% per hour} = \frac{\text{Celluar\_FDG}_{t2}}{\text{Total\_FDG}_{t2}} / (t_2 - t_1) \quad \text{Eq. 4.2}$$

$$\text{Glucose uptake\% per hour} = \frac{[glc]_{t0} - [glc]_{t2}}{[glc]_{t2}} / (t_2 - t_0) \quad \text{Eq. 4.3}$$

$$GR = \frac{[glc]_{t0} - [glc]_{t2}}{(t_2 - t_0) \times 60} \ (\text{g/min/l}) \quad \text{Eq. 4.4}$$

$$GR_{LC} = \frac{\text{FDG uptake\% per min} \times [glc]_{t2}}{\text{LC}} \ (\text{g/min/l}) \quad \text{Eq. 4.5}$$

Where t_0 is the time when cells are initially seeded in the plate, t_1 is the time when tracer is added to the plate and t_2 is the time when the tracer uptake in cells is measured, which is corresponding to the time schedule shown in Figure 4.1. Cellular_FDG is the measured FDG count rate in cells and Total_FDG is the measured FDG count rate in the well that includes both FDG inside the cells and FDG outside the cells.

4.2.4 Data Analysis

Glucose and tracer uptake was normalized to the total activity added to each well and expressed as percentage uptake per 10^3 viable cells. Mean and standard deviation (STD) of the tracer uptake and lumped constant in each tumor type were calculated for each condition (one of five glucose levels or one of three free fatty acid levels). Correlation of FDG or FLT uptake normalized by the number of viable cells as a function of the glucose or FFA level was also examined. To account for the effect of glucose on FDG uptake in tumor cells, the FDG uptake data was regressed with the following equation:

$$Y = \frac{a}{b + [glc]} \quad \text{Eq. 4.6}$$

where Y denotes the FDG uptake, [glc] represents the media glucose level with the unit mg/dl or g/l and the parameter b was to account for the competition between ^{18}F-FDG and glucose. Statistical comparisons were based on F-tests and $P < 0.05$ was considered to be statistically significant.

4.3 Results

4.3.1 Media Glucose Levels

The media glucose levels were monitored only for the cells grown in 12-well plate since the minimum measurable volume required by the glucose analyzer is 800 μl. During the 24-hour incubation, media glucose levels ([glc]) of tumor cells grown at 50 mg/dl, 100mg/dl and 150mg/dl all decreased, but with different amount when normalized to original media glucose levels. The change of media glucose levels in three different tumor types: MDA-MB-231, U87 and PC3 were shown in Figure 4.2. The results were averaged on three replications for each condition (one tumor type with one media glucose level). It was observed that the hourly glucose uptake were highest when the cells were cultured and assayed at 100 mg/dl [glc] for all the cell lines, but all declined when the glucose level increased to 150 mg/dl. PC3 used the most glucose per hour compared to the other two cell lines at all three different glucose conditions (e.g., at 100 mg/dl [glc], PC3: 2.71%±0.12%; U87: 0.82%±0.11%; MDA-MB-231: 0.46%±0.02%).

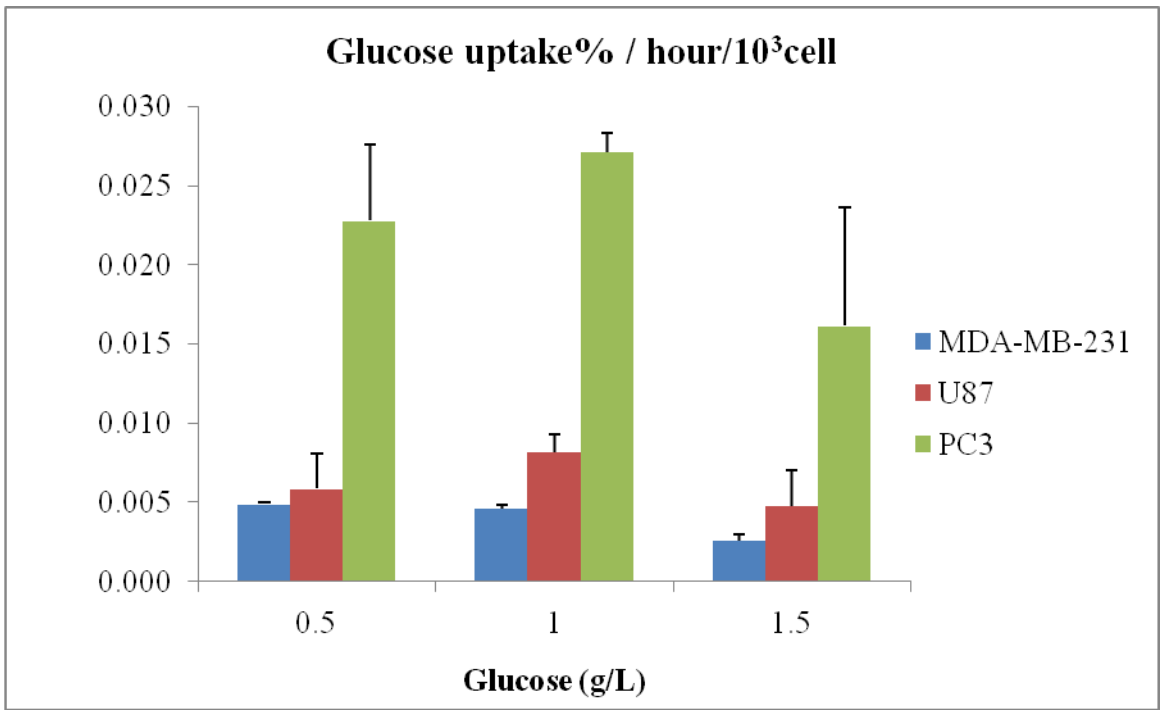
Glucose uptake% / hour/10³cell
0.030
0.025
0.020
0.015
0.010
0.005
0.000
0.5
1
1.5
Glucose (g/L)
MDA-MB-231
U87
PC3

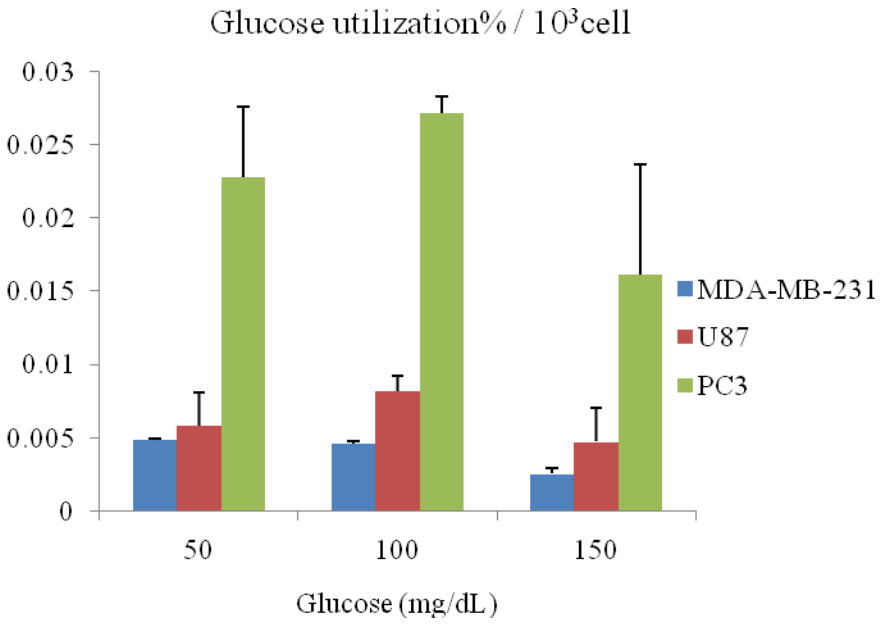
Glucose utilization% / 10³cell
0.03
0.025
0.02
0.015
0.01
0.005
0
50
100
150
Glucose (mg/dL)
MDA-MB-231
U87
PC3

Figure 4.2 Glucose uptake in different tumor cell lines cultured in the media with different glucose levels. The results were averaged on three replications for each condition (one tumor type with one media glucose level).

4.3.2 Effect of Media Glucose levels on FDG Uptake

FDG uptake into the cells decreased with the elevated media glucose levels in all three tumors, but with a different significance of inverse relationship. As shown in figure 4.3, based on eight replications for each condition (one tumor type with one media glucose level), the relationship between the cellular FDG uptake (y-axis) verses the glucose concentration (x-axis) in the medium is Y=0.088/(4.883+[Glc]) for MDA-MB-231 (R=0.2417), Y=0.0282/(0.5046+[Glc]) for PC3 (R=0.8686) and Y=0.017/(0.16+[Glc]) for U87 (R=0.8304). At the same glucose level (e.g., 1.0 g/L), the FDG uptake is quite different among the three cell lines: PC3 showed the highest FDG uptake among the three cell lines, which was correspondent to the rank of cellular glucose uptake (Figure 4.2).

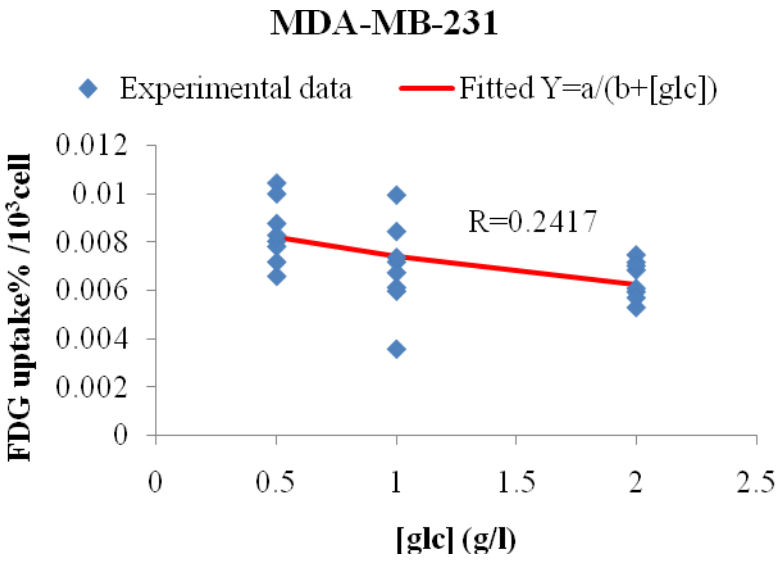
MDA-MB-231
Experimental data
Fitted Y=a/(b+[glc])
FDG uptake% /10³cell
0.012
0.01
0.008
0.006
0.004
0.002
0
R=0.2417
0
0.5
1
1.5
2
2.5
[glc] (g/l)

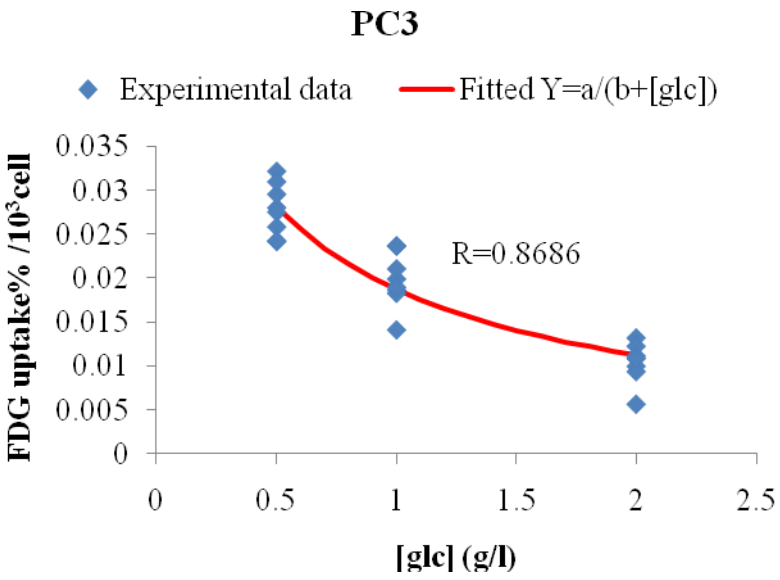
PC3
Experimental data
Fitted Y=a/(b+[glc])
FDG uptake% /10³cell
0.035
0.03
0.025
0.02
0.015
0.01
0.005
0
R=0.8686
0
0.5
1
1.5
2
2.5
[glc] (g/l)

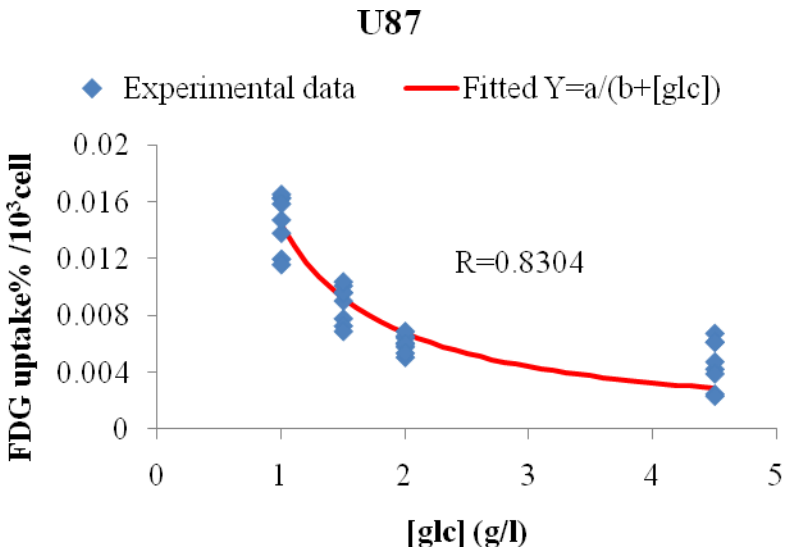

Figure 4.3 FDG uptake in three different tumor cell lines: MDA-MB-231, PC3 and U87 cultured in the media with different glucose levels (g/l). The experimental data (blue diamond) was regressed with the Eq. 4.6 that was used to accounts for the glucose effect on the FDG uptake.

4.3.3 Effect of Media Glucose levels on Lumped Constant and Glucose Utilization Rate

The lumped constant (LC) and glucose utilization rate (GR) were calculated based on the Eq. 4.1 to Eq. 4.5. Effect of media glucose levels on LC and GR was examined on two tumor types: PC3 and U87, and the results were shown in Figure 4.4, based on three replications for each condition (one tumor type with one media glucose level). It was found that the media glucose levels had no correlation with the value of LC in both cell lines (F-test, PC3: R=0.0202, P=0.715; U87: R=0.0071, P=0.8294). GR calculated based on FDG net uptake and LC (Eq. 4.5) was not dependent on the media glucose levels for both tumor types (P>0.05). While GR

calculated directly from the ratio of FDG net uptake to glucose net uptake (Eq. 4.4) had significant positive correlation with media glucose levels ($P<0.05$) for U87.

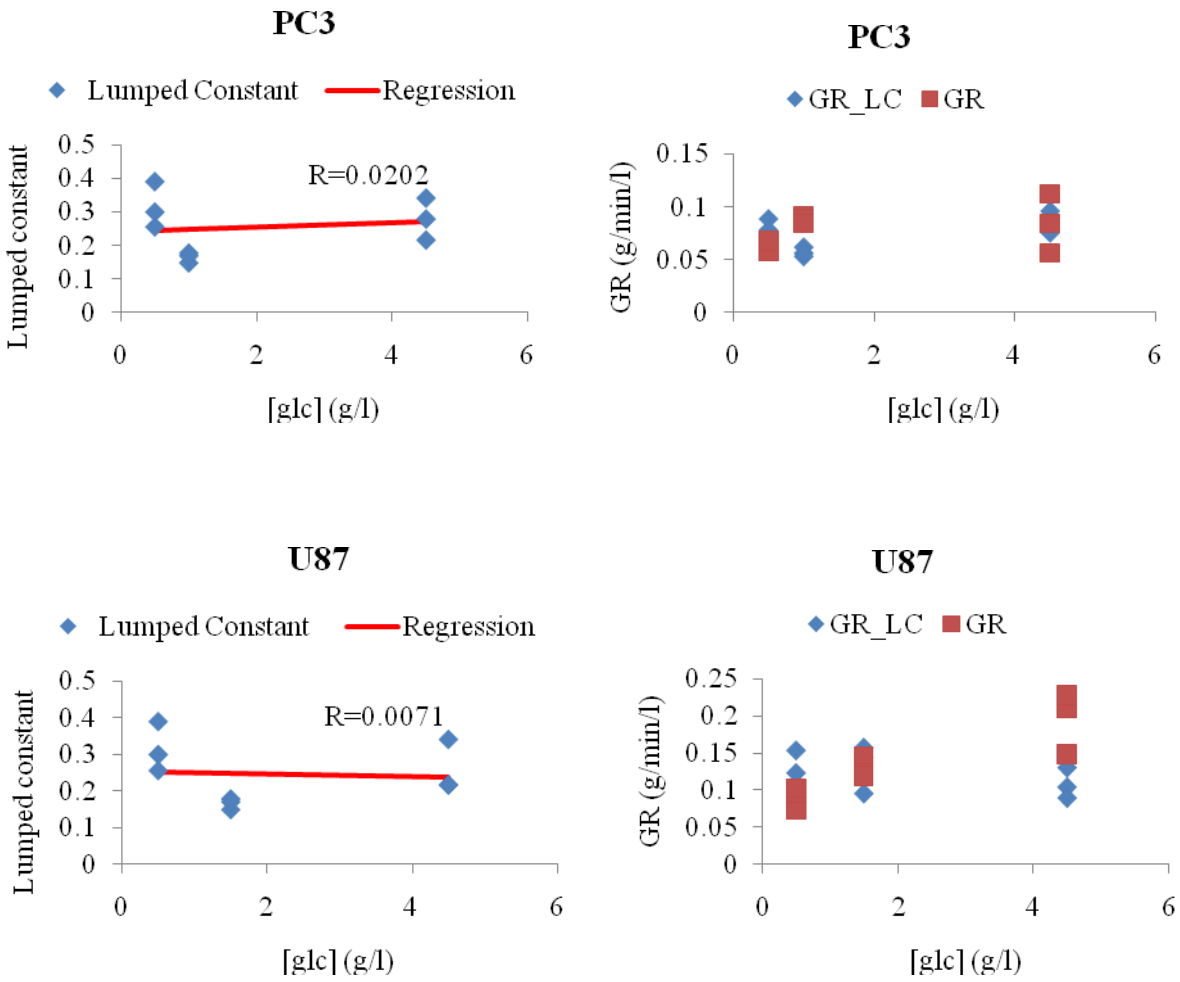

Figure 4.4 Effect of media glucose levels on lumped constant (LC) and glucose utilization rate (GR). In the graph, GR and GR_LC represent the GR calculated from Eq. 4.4 and Eq. 4.5, respectively.

4.3.4 Effect of Media Glucose levels on FLT Uptake

Effect of media glucose levels on FLT uptake into the tumor cells was examined on two tumor types: MDA-MB-231 and PC3. Based on four replications for each condition (one tumor type with one media glucose level), as shown in Figure 4.5, no correlation was found in both cell lines with the value of slope not significant differ from 0 (F-test, MDA-MB-231: R=0.0148, P=0.6541; PC3: R=0.1259, P=0.1775).

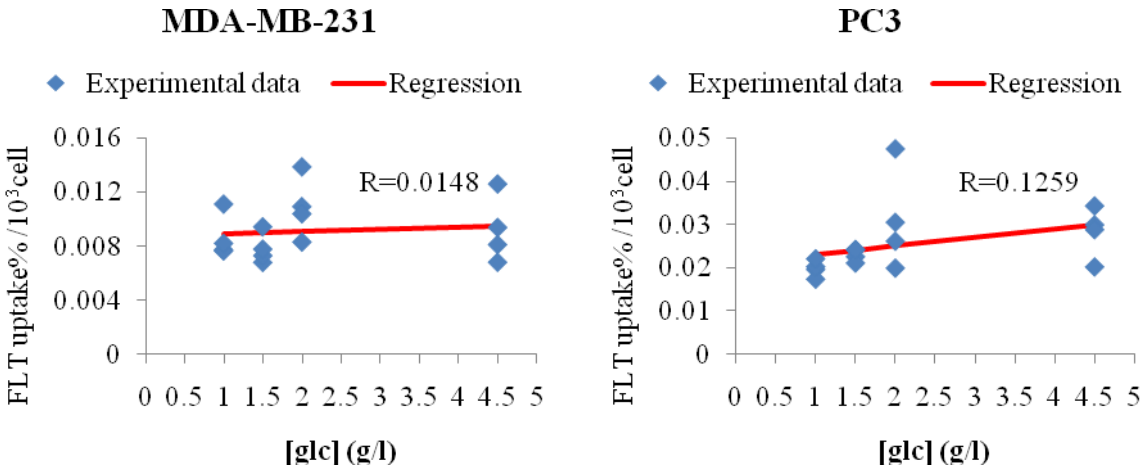

Figure 4. 5 FLT uptake in two different tumor cell lines: MDA-MB-231 and PC3 cultured in the media with four different glucose levels (g/l): 1, 1.5, 2, 4.5.

4.3.5 Effect of Media Free Fatty Acid levels on FDG Uptake

The media free fatty acid (FFA) levels were changed from 0 to 50 μM/l and the FDG uptake was measured in two cell lines: MDA-MB-231 and PC3. From the results shown in Figure 4.6, based on eight replications for each condition (one tumor type with one media

glucose level), cellular FDG uptake was not affected by the FFA level (F-test, MDA-MB-231: R=0.0015, P=0.8586; PC3: R=0.0014, P=0.8627).

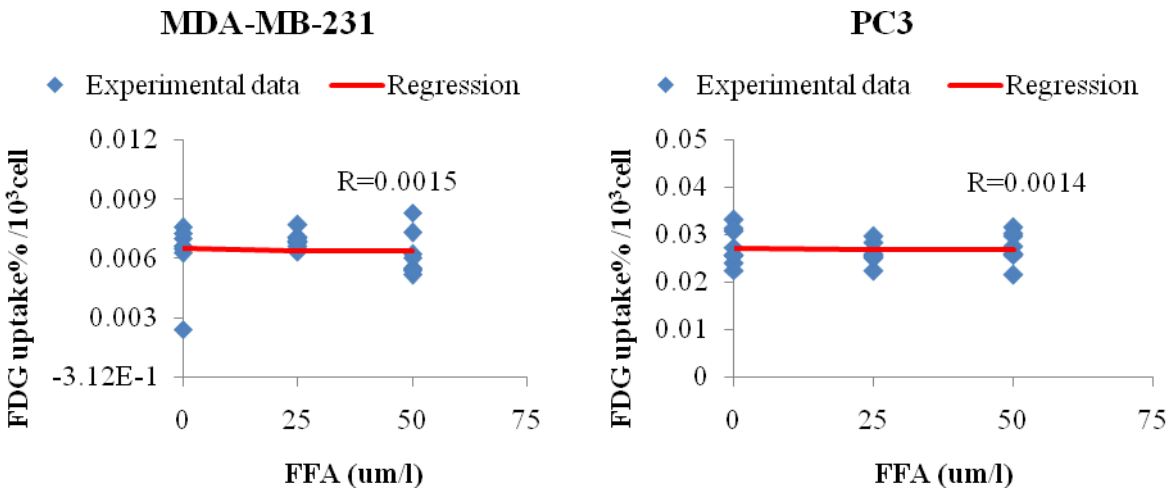

Figure 4. 6 FDG uptake in two different tumor cell lines: MDA-MB-231 and PC3 cultured in the media with three different free fatty acid (FFA) levels (μM/l): 0, 25 and 50.

4.4 Discussion

We have performed in vitro studies on several tumor types: MDA-MB-231, PC3 and U87 with the use of multi-well cell culture plate and have investigated the effect of two physiological factors: media glucose levels and media free fatty acid levels on the cellular uptake of two commonly used tracers: FDG and FLT.

4.4.1 FDG Studies in Tumor Cells

The FDG uptake was measured in all three tumor cell lines. In vitro studies demonstrated that exposure of these human tumor cell lines to hyperglycemia (2 g/l of glucose) reduced tumor

uptake of FDG tracer, as compared to tracer uptake of cells grown at the 0.5 g/l glucose level (Figure 4.3). However, only slightly reduction of FDG uptake was found in the mammary tumor MDA-MB-231 when compared to the prostate tumor PC3 and glioma U87. The FDG uptake in MDA-MB-231 is not affected as much by medium glucose level over the normal physiological glucose range as those of the other two cell lines are, which resulted a much larger coefficient b ($b=4.883$ for MDA-MB-231, $b<1$ for PC3 and U87) in the regression model (Eq. 4.6), where b was to account for the competition between FDG and glucose. It was also noted that the inverse relationship in U87 was agreed with what we found from the in vitro experiments performed on microfluidic system (Section 3.3.3 A).

Reported results in the literature on effect of blood glucose levels on a few other types of tumors were somewhat controversial. Most studies have demonstrated that ^{18}F-FDG uptake into human cancer cells are inhibited by increasing blood/media glucose levels because of direct competition between FDG and D-glucose for uptake and incorporation into tumor cells and cancers (*1, 2, 7, 94, 95*). In vitro studies with human ovarian adenocarcinoma (*7*) showed that acute hyperglycemia markedly reduces uptake of FDG in tumor cells. In vivo studies on rodents by Wahl et al. (*95*) have demonstrated that FDG uptake into human mammary carcinoma is inhibited by increasing media glucose levels. Our results from PC3 and U87 data were consistent with these findings. However, animal studies performed by Torizuka (*96*) indicated that the uptake of FDG in mammary carcinoma was reduced for insulin-induced hypoglycemia. Likewise, the mammary cancer MDA-MB-231 presented a inverse relationship with a smaller coefficient

of determination (R=0.2417) from the regression model (Figure 4.3). These may indicate that glucose uptake mechanism could be different in different tumor types.

LC is a term based on the principles of competitive substrate kinetics that converts FDG uptake rate to glucose utilization rate. Measurement of LC is complicated in vivo since both the arterial-venous concentration differences of the FDG and that of the glucose need to be determined accurately (*93*). In rat brain, the LC was found to be relatively stable within normoglycemic range (*97*) and decreased very slowly in hyperglycemic conditions (*98*). We showed that the value of LC from in vitro experiments for both tumors are smaller than 1 (PC3: 0.253 ± 0.057; U87: 0.654 ± 0.220), indicating that U87 has higher glucose utilization rate than PC3. It was also found that the calculated lumped constants were not correlated to the glucose levels for either PC3 or U87 cell line (Figure 4.4). LC in gliomas had been estimated by clinical PET studies before (*99*) with the value of 1.4 ± 0.46, where as in non-tumor-bearing contralateral brain tissue the value of LC was 0.86 ± 0.14. The difference between the in vitro and in vivo glioma studies is expected since the biological environment for tumor growth is quite different. However, in vitro experiments are much simpler and still could provide useful biological information between different tumor types.

Not only tested with different media glucose levels, FDG uptake was also examined with different media free fatty acid (FFA) levels (Figure 4.6) in MDA-MB-231 and PC3. No significant correlation was found between the FDG uptake and media FFA levels in both cell lines.

4.4.2 FLT Studies in Tumor Cells

In contrast to FDG studies, our FLT studies (Figure 4.5) have demonstrated that FLT uptake in tumor cell lines MDA-MB-231 and PC3 is not affected by the change of media glucose levels. This may indicate that FLT is a potentially more cancer-specific PET tracer and do not need the correction of glucose concentration in quantitative analysis as some of the FDG-PET studies (*27*). However, in comparison with FDG, FLT uptake is lower in nearly all cases, resulting in a lower sensitivity in targeting tumor tissues (*87, 89, 91*). Futhermore, the relation between proliferation and TK1 activity is not always fully understood (*100*). Advantages of using FLT-PET are still controversial and the high manufacturing cost of FLT tracer in UCLA has slowed down the pace of FLT-PET researches.

4.4.3 In Vitro Experiments: Comparison Between Microfluidic System and Regular Plate

In Chapter 3, we have presented a novel in vitro approach to explore the FDG uptake kinetics in cells, with the use of a microfluidic beta camera system (Figure 3.1) and a switching tracer infusion protocol (Figure 3.2). It has shown the FDG uptake in tumor cells under different physiological conditions (i.e. different media glucose levels) could be measured automatically without any human intervention during the tracer uptake period. Furthermore, time activity curve (TAC) that reflects the dynamic change of FDG uptake in cells according to the change of time was able to be derived. With the acquired TAC and a kinetic model for switching protocol on chip (Eqs. 3.5-3.8), kinetic parameters were derived and the reliability of these estimates have been approved. All of the above quantitative analysis of FDG uptake in cells is hard to be realized on the in vitro experiment performed on regular cell culture plate. From the experiments

on the regular multi-well plate that were shown in this chapter, I found that it was time and labor consuming even to measure FDG uptake in cells at a single time point, and the cells must be lysed before any radioactivity measurement. Plus, inter-operation variation was introduced due to different cellular washing protocol or different experimental executer. Although owning so many advantages compared to the regular cell culture plate, the microfluidic chip still have its own limits. First, the volume of each well (μl scale) is very small and it is hard to measure the concentration change of the physiological factors in media, such as media glucose levels; Second, the optimal design of the chip has not been achieved yet and the manufacturing of the microfluidic chip is not as mature as the regular plate. It can be foreseen that the microfludic chip will be explored a lot more in future in cell experiment and its possibility in various biological applications would be valuable by scientists, but whether it can replace the regular cell culture plate or not is unknown, or at least not in near future.

4.4.4 Implications in Further In Vitro and In Vivo Tumor Studies

Both glucose transport and the subsequent phosphorylation of glucose by hexokinase are thought to be the key steps in glucose utilization, especially with respect to FDG uptake. Because glucose-6-phosphatase activity is reported to be low in tumor cells (*101*), the in vitro studies have focused mainly on two types of well-known proteins, glucose transporter (GLUT) and hexokinase. The expression level of GLUT in tumor cells is known to be higher than that in normal cells(*102-104*). However, the effect of medium glucose level on GLUT expression and hexokinase activity to glucose metabolism, and also FDG uptake, is still unknown. To determine the relationship between glucose level and GLUT expression or hexokinase activity in FDG

uptake, we plan to study different tumor cell lines in vitro with respect to 2-deoxyglucose (DG) uptake, hexokinase activity, and the the amount of GLUT1-5 expressed on the plasma membrane.

We have found that different tumor cell lines may response differently to the elevated media glucose levels in in vitro studies. It will be interesting to learn whether it is the same or not in small animal PET studies, which we had extensive experiences with. MDA-MB-231 and U87 would be good candidates for tumor implantation since both tumor cell lines are very aggressive with similar glucose utilization rate (Figure 4.2), but with different relationship in FDG uptake and media glucose levels (Figure 4.3).

4.4 Conclusions

FDG uptake in the tumor cell lines all decreased with the increased medium glucose level, but not with the change of media free fatty acid levels. Furthermore, the relationships between FDG uptake and media glucose levels are different among different tumor types, indicating different transporter/hexokinase adaptation to glucose level in the extra-cellular environment. Lumped constant and FLT uptake is not affected by media glucose levels.

Chapter 5 IN VIVO FDG-PET STUDIES ON MICE WITH TUMORS

5.1 Introduction

Small animal positron emission tomography (PET) imaging is being used increasingly in preclinical biomedical research for investigation of tumor biology. The use of glucose analogue 2-[18F]fluoro-2-deoxy-D-glucose (^{18}F-FDG) for the in vivo measurement of local glucose utilization with oncological animal models have been a valuable tool for evaluation of early response to treatment. Longitudinal imaging overcomes the limitation of single time-point imaging and enables tracking of the natural history of disease and provides qualitative and quantitative assessments of the effects of an intervention. The antineoplastic drugs evaluated in these studies were either conventional chemotherapy agents (*105*) or inhibitors of the tumor transduction signal (*106*) or radiation therapy (*107*). Reduction in ^{18}F-FDG uptake from its baseline value is usually used as an indicator of the tumor response to treatment. However, large inter-animal variability in imaging measurements of different animals could mask out the true effects in terms of the time course of changes. Standard uptake value (SUV) (*108*) is the most popular semiquantitative measure of normalized radioactivity concentration in PET images and can be influenced by a variety of biologic and technical factors (*27*). The effect of plasma glucose concentration on ^{18}F-FDG uptake has been investigated before. Studies evaluating the usefulness of correcting for blood glucose level gave conflicting results: some have found a benefit in normalizing SUV by blood glucose (*18, 94*), some have found no benefit (*109, 110*). Our previous work also suggested that ^{18}F-FDG uptakes in different non-tumor tissues are controlled differently (*41*). It is likely that the value of SUV may not necessarily reflect directly

the glucose utilization rate in the tissue of concern and adjustments for glucose level should be done cautiously. The results also suggested that different mechanisms of regulating glucose utilization existed among different tumor cells. In vitro study on ovarian adenocarcinoma (*7*) demonstrated that ^{18}F-FDG uptake into human cancer cells was suppressed by high media glucose levels. However, Dr. Torizuka (*96*) indicated that the uptake of ^{18}F-FDG in mammary carcinoma is reduced for insulin-induced hypoglycemia. Our in vitro studies presented in chapter 3 and 4 also demonstrated the effect of media glucose levels on FDG uptake was varied in different tumor cell lines. A strong inverse relationship was found in most tumor types (U87, PC3 and CaP8), whereas not in mammary cell line MDA-MB-231.

In this work, we addressed the effect of blood glucose level and tumor size on both SUV and ^{18}F-FDG uptake constant K_i by using an input function for quantitation of biological function in two different tumors: U87 and MDA-MB-231, which have shown different adaptation to the change of glucose levels in in vitro studies. The input function was derived from dynamic PET images using only one tail veil blood sample taken at the end of the scan (*36*), so the animal did not need to be sacrificed after each scan and longitudinal studies could be performed. The use of an input function for quantitation of biological function reduces many effects due to systemic biochemical or physiological variations.

5.2 Materials and Methods

5.2.1 Animal Models and PET Imaging

Animals and Tumor Models

Twenty 6- to 8-week-old SCID white mice were maintained in a strict defined-flora, pathogen-free environment in the AALAC accredited Animal Facilities of the Department of Radiation Oncology, UCLA. Human glioblastoma cell line U87 and breast cancer cell line MDA-MB-231 were used for mouse tumor model. Both cell lines were cultured in Dulbecco's modification of Eagle's medium (DMEM) supplemented with 10% fetal bovine serum and 1% antibiotics–antimycotic solution before injection. Cells were injected (11 mice was injected with MDA-MB-231 cells and 9 mice was injected with U87 cells) subcutaneously as single-cell suspensions in phosphate buffer saline (PBS; $\sim 2 \times 10^6$ MDA-MB-231 or $\sim 6 \times 10^5$ U87 cells in 100 μl PBS). When the diameter of the tumor grew to approximately 2.5 mm diameter, PET scan was performed once a week on the same animal until the diameter of the tumor exceeded 10 mm. Tumor size was measured weekly with a caliper and the volume was calculated as $0.5 \times L \times W^2$.

Small-animal Imaging

Small-animal PET scans were performed on a microPET Focus 220 scanner (Concorde Microsystems, LLC) and on an Inveon dedicated PET (DPET; Siemens Preclinical Solutions, Inc). For PET and CT scanning, the animal was placed in a prone position inside an imaging chamber specifically designed for small-animal PET and CT imaging to allow for regulated temperature control and anesthesia delivery (*111*). List-mode PET data were acquired for 60 minutes immediately after ^{18}F-FDG injection via a tail-vein catheter (18.28 ± 1.19 MBq, ~60 μL). After the PET scan was completed, a 10-min CT scan was acquired with a small-animal CT scanner (MicroCAT II; ImTek Inc.) for attenuation correction of the PET meaurements.

Blood Sampling

Tail vein blood glucose levels were measured using a blood glucose meter (Abbott AlphaTRAK Glucose Meter) at the beginning and the end of each scan. A single blood sample (~10–15 μL) was collected with a 1cc syringe from the heart at the end of the study (~70-80 min). The whole-blood in the syringe was released to a pre-weighed test tube, weighed, and the radioactivity was counted in a gamma counter (WIZARD 3"; PerkinElmer Life Sciences, Finland).

Image Reconstruction

Frame durations of all the PET studies were 4×1 s, 15×0.5 s, 1×2 s, 1×4 s, 1×6 s, 1×15 s, 3×30 s, 1×60 s, 1×120 s, 3×180 s, 3×900 s and 1×51 s. The attenuation maps derived from the small-animal CT data were used for attenuation correction of the PET data (*112*). The PET data were corrected for random coincidences and dead-time losses, and were reconstructed using the filtered backprojection algorithm with a ramp filter cut off at the Nyquist frequency, resulting in a volumetric spatial resolution of 1.32 mm FWHM (full width at half maximum) at the center of the field of view and a voxel size of 0.4×0.4×0.8 mm^3.

Image Analysis

Image analysis was performed using AMIDE (http://amide.sourceforge.net/) on PET studies without apparent necrotic center shown in the images. The 3D isocontour regions of interest (ROIs) were manually defined for skeletal muscle of the forelegs, liver, and tumor in each mouse on 60 min images. The time-activity curve (TAC) representing the tissue kinetics of ^{18}F-FDG in each tissue of interest was calculated by projecting the corresponding ROIs onto the dynamic

PET images. An elliptical ROI (2.0×1.5×1.5 mm) was drawn on the left ventricle (LV) region. After correction for delay, dispersion, partial-volume and plasma-to-blood ratio (Eq. 2) (*36*), the first minute of this LV TAC was used as the early part of input function (for quantitative analysis of tissue kinetics. The small-animal PET and CT image files, blood sample data, and other experimental information for all studies discussed here are available online at the UCLA Mouse Quantitation Project website (http://dragon.nuc.ucla.edu/mqp/index.html).

5.2.2 Quantitation of FDG PET Images

Semiquantitative Analysis

For semiquantitative analysis, ROIs were generated for each study as described above. Standard uptake values (SUV) were calculated using the formula shown in Eq. 1. Both the highest voxel value within the ROI (SUV_max) and the average ROI value (SUV_avg) were recorded.

$$\text{SUV} = \frac{\text{Radioactivity concentration in ROI (MBq/ml)}}{\text{Injected dose (MBq)/Weight of the animal (g)}} \qquad \text{Eq. 1}$$

Equilibration of 18F-FDG between Plasma and Whole-Blood

A time-dependent plasma-to-whole-blood ^{18}F-FDG equilibrium ratio, $R_{PB}(t)$ (Eq. 2), was determined between ^{18}F-FDG concentrations in plasma and whole-blood for each study:

$$R_{PB}(t) = 0.386e^{-0.191t} + 1.165 \qquad \text{Eq.2}$$

where t is given in minutes. R_{PB} was previously calculated by taking a series of whole-blood samples throughout the course of several studies, centrifuging each sample into plasma and

cellular components, and measuring the ^{18}F-FDG concentration in each fraction as described by Wu et al. (14) and Wong et al. (*41*).

Plasma Input Function

The full plasma time-activity curve (TAC_p) (the full input function) was derived based on the method reported by Ferl et al. (13). The method included the use of the early-time left ventricle (LV) TAC (t < 1 min) (with corrections of delay, dispersion, partial-volume effects, and red blood cell (RBC) uptake, and one cardiac whole-blood sample taken at the end of the study (~70 min). Briefly, the input function was assumed to have 4 exponential components (Eq. 3):

$$TAC_p = A_1 e^{-\mu_1 t} + A_2 e^{-\mu_2 t} + A_3 e^{-\mu_3 t} - (A_1 + A_2 + A_3) e^{-\mu_4 t} \quad \text{Eq. 3}$$

where A_1, A_2, A_3 are unit parameters. The sum of the first three exponential terms were used to describe the very early portion of the serial blood sample data; the fourth exponential term was added to the input function so that TAC_p was forced to be equal to 0 at time 0. All the parameters were estimated by simultaneously fitting the plasma FDG blood curve with Eq. 3, and the muscle and liver TACs with two separate 4K-compartmental FDG models. Bayesian constraints were also added in the model fitting procedure (13).

Kinetic Analysis

Both the PET image and blood data were converted to absolute radioactivity concentration (Bq/mL) using a cross-calibration factor derived from cylinder phantom experiments. The ^{18}F-FDG uptake rate constant K_i ($K_i = K_1 k_2/(k_2 + k_3)$) was estimated via the

Patlak graphical analysis (*113*) using the derived plasma input function and tumor TAC data, by taking the slope of the linear portion from 15–60 min of the plot based on Eq. 4, where $\frac{C_T(t)}{C_P(t)}$ is plotted on y-axis and $\frac{\int_0^t C_P(t)}{C_P(t)}$ is plotted on x-axis:

$$\frac{C_T(t)}{C_P(t)} = \left(\frac{K_1 k_3}{k_2+k_3}\right)\frac{\int_0^t C_P(t)}{C_P(t)} + Int \qquad \text{Eq. 4}$$

$$\text{Int} = \left(\frac{k_2}{k_2+k_3}\right)\frac{C_1(t)}{C_P(t)} + \frac{V_B C_B(t)}{C_P(t)} \qquad \text{Eq.5}$$

where $C_T(t)$ is the total ^{18}F-FDG concentration in the tissue of interest, $C_1(t)$ is the non-metabolized ^{18}F-FDG concentration in the tissue, $C_P(t)$ is the ^{18}F-FDG concentration in plasma, $C_B(t)$ is the total ^{18}F-FDG concentration in tissue vasculature and V_B is the volume fraction of blood in tissue. The early-time tissue data will not be used because an equilibration time (t^*) is needed in establishing a steady-state condition when the intercept (Eq. 5) is constant and the Patlak plot becomes linear. The metabolic rate of glucose (MRGlu) was calculated as $\text{MRGlu} = \text{K}_\text{i}\text{C}_\text{glu}/\text{LC}$ (*97, 114*), where C_{glu} is the mean plasma glucose concentration during the 60-min PET imaging; and LC is the lumped constant that is the ratio of the utilization of deoxyglucose to that of glucose. LC were assumed to be 1.4 for brain cancer U87 (*99*) and 1.0 for mammary cancer MDA-MB-231.

Data Analysis and Functional Relationship Determination

All Data analyses were performed using MATLAB (MathWork, USA). Regression analysis was performed on the tumor uptake (SUV_avg and SUV_max), K_i and MRGlu in the tumor to investigate their relationships with blood glucose level and with tumor size. A P-value < 0.05 was considered statistically significant. K_i and SUVs were first PV corrected by dividing the values by RC of the tumor that was estimated based on a sphere of the same volume of the tumor and a background level of 10% of the activity in the sphere. That is, RC for different tumor sizes was calculated based on a sphere of $\text{diameter} = \sqrt[3]{\frac{3*\text{TumorVolume}}{\pi}}$, the spatial resolution of the microPET scanner, and an assumed background activity level of 10% of the actitivity level of the sphere.

Change of the PV corrected SUV or K_i as a function of the tumor size and blood glucose level were assessed by regressing the PV corrected SUV or K_i with the following equations, which are based on the Michaelis-Menten model (*20*):

$$\text{SUV/RC} = \frac{(a+c*\textit{Tumor Diameter})}{b+[Glc]} \qquad \text{Eq. 6}$$

$$K_i/\text{RC} = \frac{(a+c*\textit{Tumor Diameter})}{b+[Glc]} \qquad \text{Eq. 7}$$

where [Glc] was the averaged blood glucose level of the two measurements at the beginning and the end of the scan. The parameters a and c were to account for the effect of tumor growth in size, b was equivalent to the half satuation glucose concentration of ^{18}F-FDG uptake. Significance of each of the two factors (Tumor Diameter and [Glc]) was assessed by removing one factor at a time from the regression equation in the model fitting. The model or the functional relationship

that best fit the data was selected based on the value of the mean squared error (MSE) resulted from leave-one-out cross-validation (LOOCV) (*115*). For each leave-one-out trial, all the data points from the left-out animal was removed, and the MSE of LOOCV was calculated using the following formula:

$$\mathrm{MSE} = \sum_{i=1}^{n} \frac{\sum_{j=1}^{N-N_i} (K_j - \widehat{K_j})^2}{N - N_i} \qquad \text{Eq. 8}$$

Where n is the number of animal and N is the number of studies used for test, N_i is the number of studies for the ith animal that is left out from the cross validation, and $\widehat{K_j}$ is the estimated j from the model fitting.

5.3 Results

Coronal tomographic images of weekly microPET scans of a mouse implanted with MDA or U87 tumor cells are shown in Figure 5.1. The tumors were barely seen on microPET images by days 28 and 37 for U87 and MDA-MB-231, respectively, after implantation. For MDA-MB-231 tumors, necrotic cores were observed as early as the tumor diameter was about 5mm, while for U87 studies, necrotic cores were observed only in 3 cases after the tumor diameter reached 8mm.

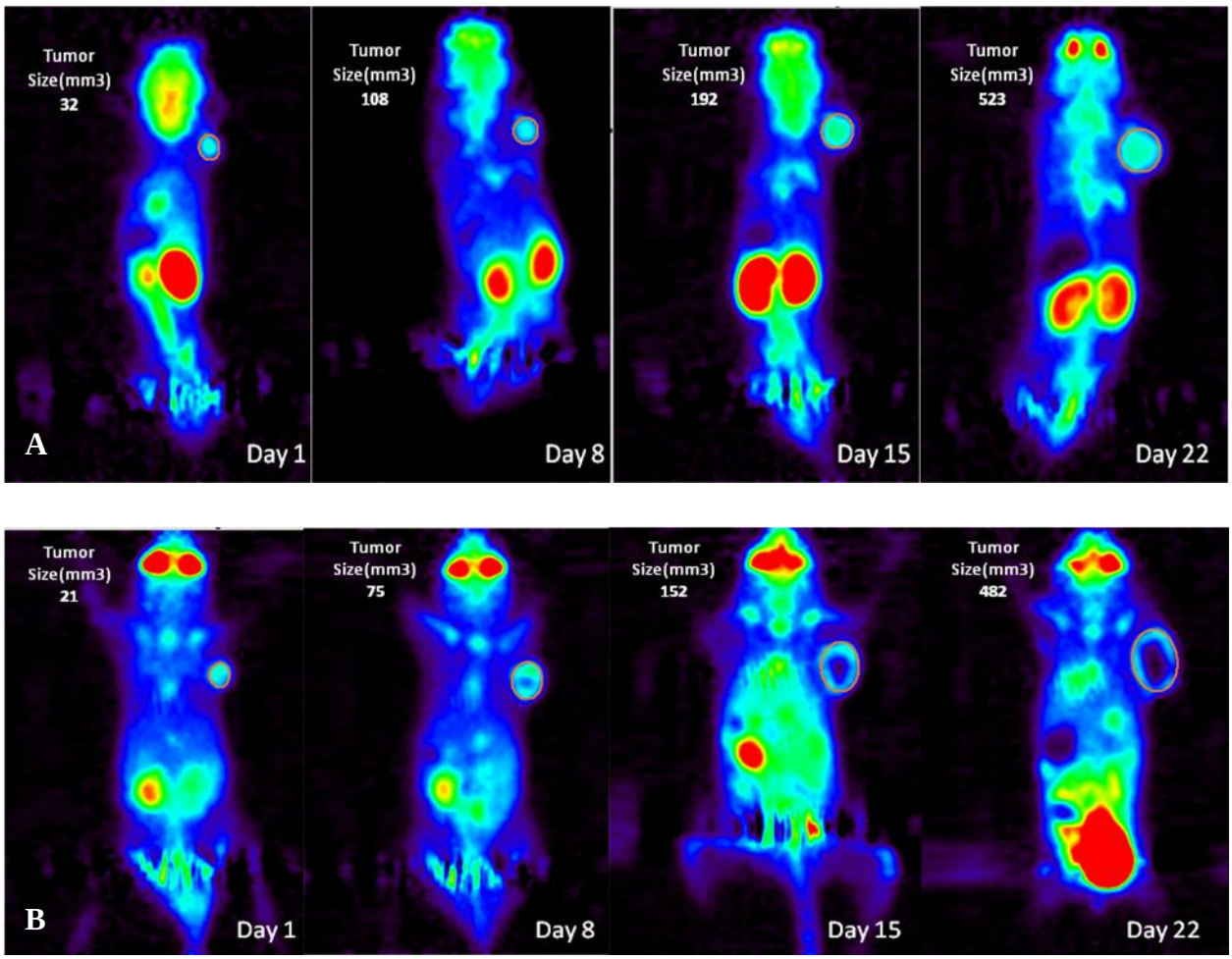

Figure 5. 1 A. Longitudinal FDG PET images of a mouse with human glioblastoma tumor U87 implanted in the shoulder region. B. Longitudinal FDG PET images of a mouse with human mammary tumor MDA-MB-231 implanted in the shoulder region. Compared to the U87 tumor shown in Fig. 1A, necrotic core started appearing early in this case before tumor size became large.

At the beginning time of the PET imaging, the averaged blood glucose levels were 6.882 ±2.517 and 7.792 ±2.520 mmol/L, respectively, for MDA-MB-231- and U87-bearing mice. A modest increase of the blood glucose level was observed at the end of the scan (MDA-MB-231:

8.189±2.245 mmol/L; U87: 8.452±2.373 mmol/L) (probably due to the effect of isoflurane anesthesia (*116*)).

5.3.1 Tumor Size and Tumor Time Activity Curves

The tumor volume and calculated diameter at the time of the first PET scan was 6.063±2.452mm^3 and 2.262±0.332mm for the MDA group and was 5.875±2.644mm^3 and 2.230±0.343mm for the U87 group. Tumor volumes continued to increase over time as shown in Figure 5.2. There was no significant difference (P>0.05) in tumor growth between the two tumor types (Figure 5.2 and 5.3). The largest difference between the tumor sizes of the two tumors was at ~30 days after first PET imaging but the difference were still not significant (P>0.05).

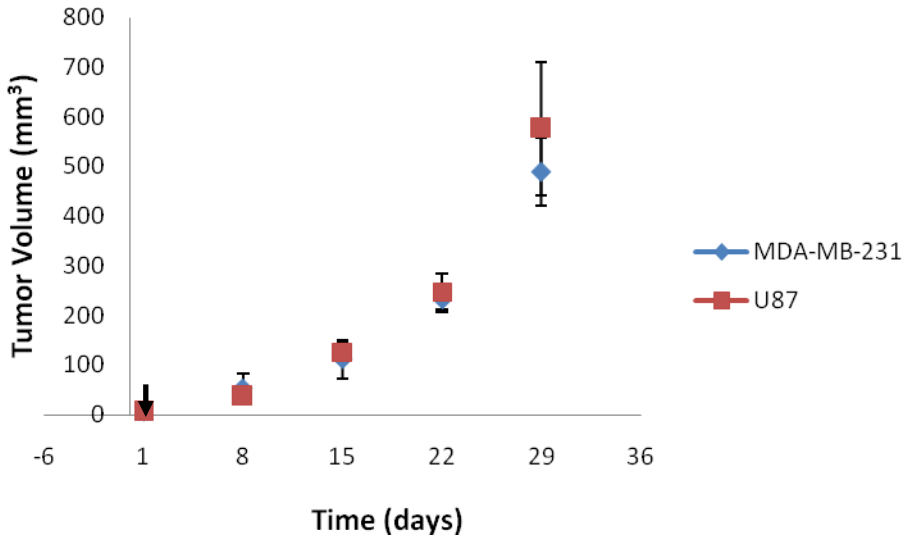

Figure 5. 2 Tumor volume measurements for MDA-MB-231 and U87 mice throughout the experiment. Arrow represents the start time of microPET imaging.

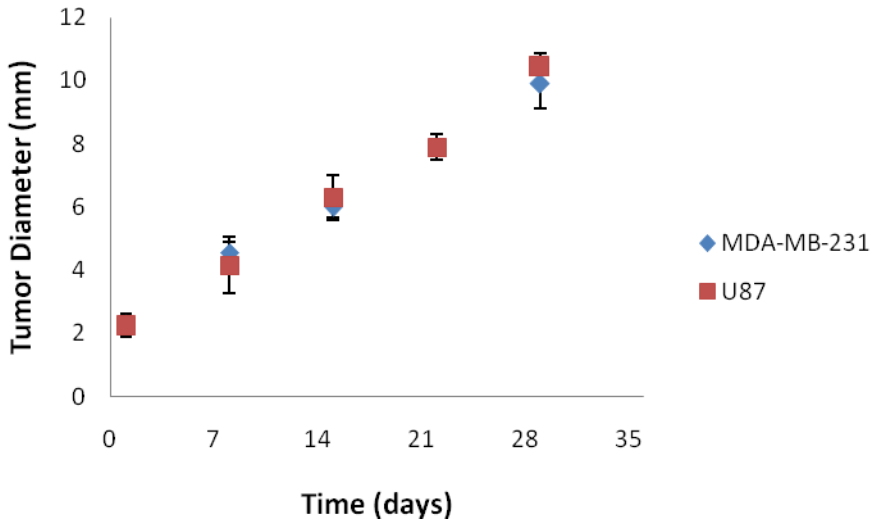

Figure 5. 3 The calculated tumor diameter for MDA-MB-231 and U87 mice throughout the experiment. Day 1 is the first day of FDG PET imaging.

5.3.2 Tumor ^{18}F-FDG Uptake and Metabolic Parameters

SUV_avg or SUV_max could not accurately reflect the ^{18}F-FDG uptake in necrotic tumor and the partial volume effect (PVE) was more difficult to be accounted for since the tumor was heterogeneous after the necrotic core was developed. For evaluation of the effects of blood glucose level, tumor size, and tumor growth, only studies without tumor necrotic cores were investigated in this work. Correlation between SUV_avg and SUV_max was strong for both tumors (MDA-MB-231: R^2=0.9635, P<0.0001; U87: R^2=0.9399, P<0.0001). SUV_avg was thus used for semiquantitative analysis and for model fitting to estimate the model parameter values. SUV_avg was also found to significantly correlate with the Patlak analysis derived K_i (MDA-MB-231: $R^2=0.7913$, $P<0.0001$; U87: $R^2=0.5529$, $P<0.0001$) and with MRGlu (MDA-MB-231: $R^2=0.516$, $P<0.0001$; U87: $R^2=0.419$, $P<0.0001$).

The relationships between tumor size and SUV_avg, K_i and MRGlu in the tumor are shown in Figure 5.4 for MDA-MB-231 and U87 tumors. Linear regression analysis was made based on the data pooled from non-necrotic studies. There was a significant positive correlation between SUV_avg, K_i and MRGlu and tumor size for U87 (SUV_avg: $R^2=0.5686, P<0.0001;$ K_i: $R^2=0.2431, P=0.0272;$ MRGlu: $R^2=0.2167, P=0.0386$) respectively; while no significant correlations of those were found in MDA-MB-231 (SUV_avg: $R^2=0.1514, P=0.1364;$ K_i: $R^2=0.0347, P=0.49;$ MRGlu: $R^2=0.0173, P=0.6273$). Similarly, when we checked the blood glucose effect on SUV_avg, K_i and MRGlu, as shown in **Error! Reference source not found.**5.5, neither tumor SUV_avg nor K_i was found to be correlated with the blood glucose level for MDA-MB-231 (with both slope of regression lines and R^2 not significantly different from zero, $P>0.05$). However, for U87, there was a modest dependence ($P<0.05$ for both SUV_avg and K_i) on blood glucose levels. MDA-MB-231 MRGlu was positively correlated with blood glucose levels ($R^2=0.3993, P=0.0086$), while no significant correlation was found between MRGlu and blood glucose levels for U87 ($P>0.05$).

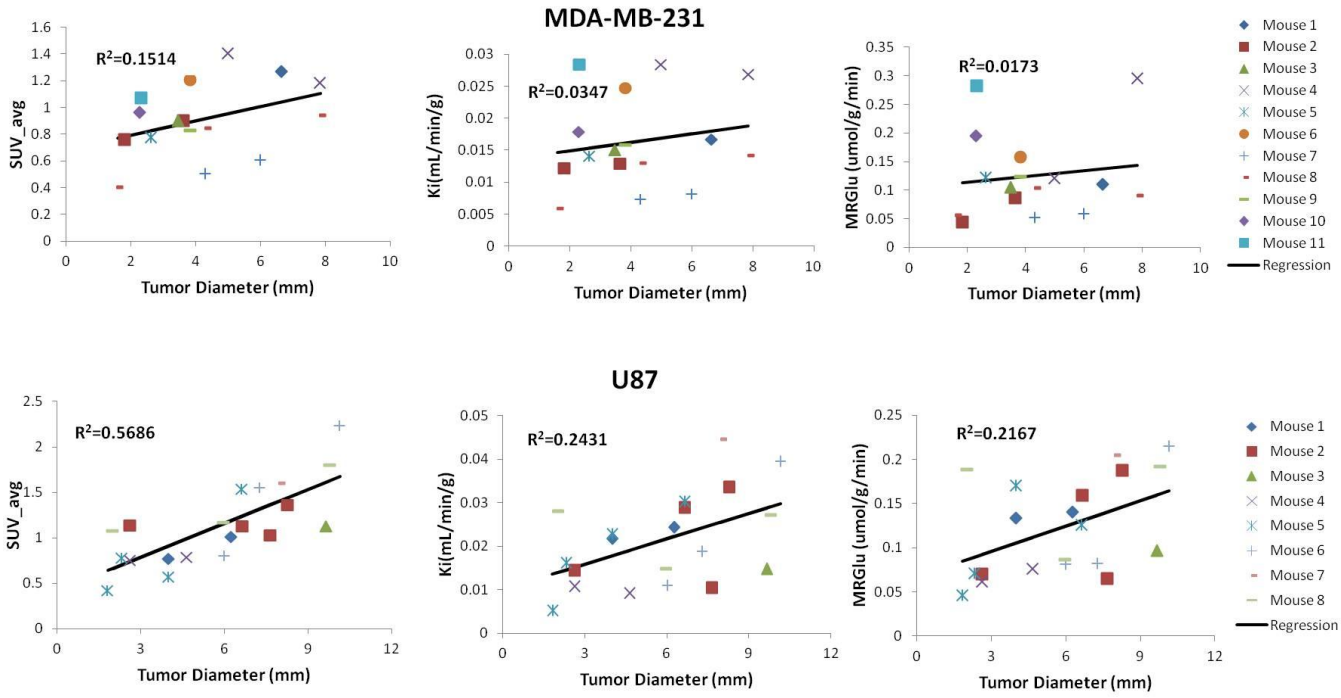

Figure 5. 4 Relationships between tumor diameter and SUV_avg, Ki and MRGlu in mammary cancer MDA-MB-231 and brain cancer U87. The data was pooled from non-necrotic studies only.

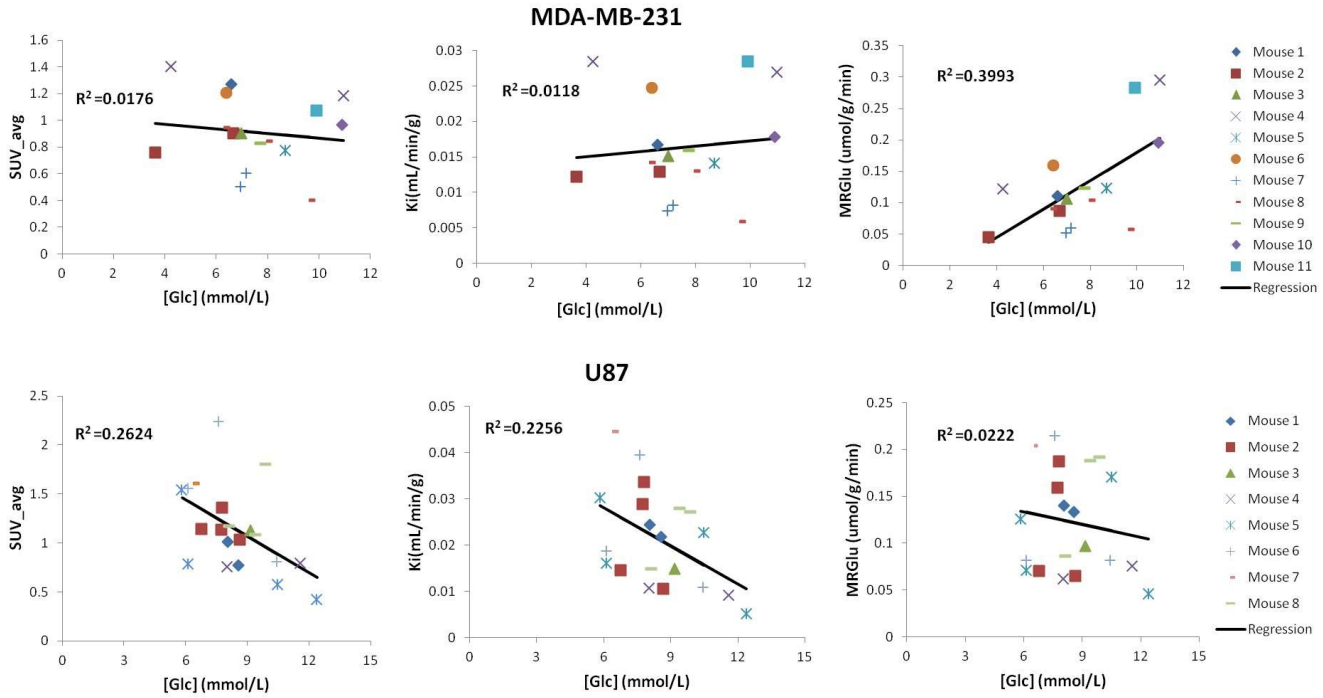

Figure 5. 5 Relationships between blood glucose levels and SUV_avg, Ki and MRGlu in mammary cancer MDA-MB-231 and brain cancer U87. The data was pooled from non-necrotic studies only.

5.3.3 PV Corrected ^{18}F-FDG Kinetics with Blood Glucose Level, Tumor Size and Partial Volume Effect for Non-necrotic Studies

Recovery coefficient (RC) calculated from simulation was used to correct the PVE. The RCs versus sphere radius are shown in Figure 5.6. RCs ranged from 0.34 to 0.93 when the sphere radius was increased from 0.5mm to 10mm.

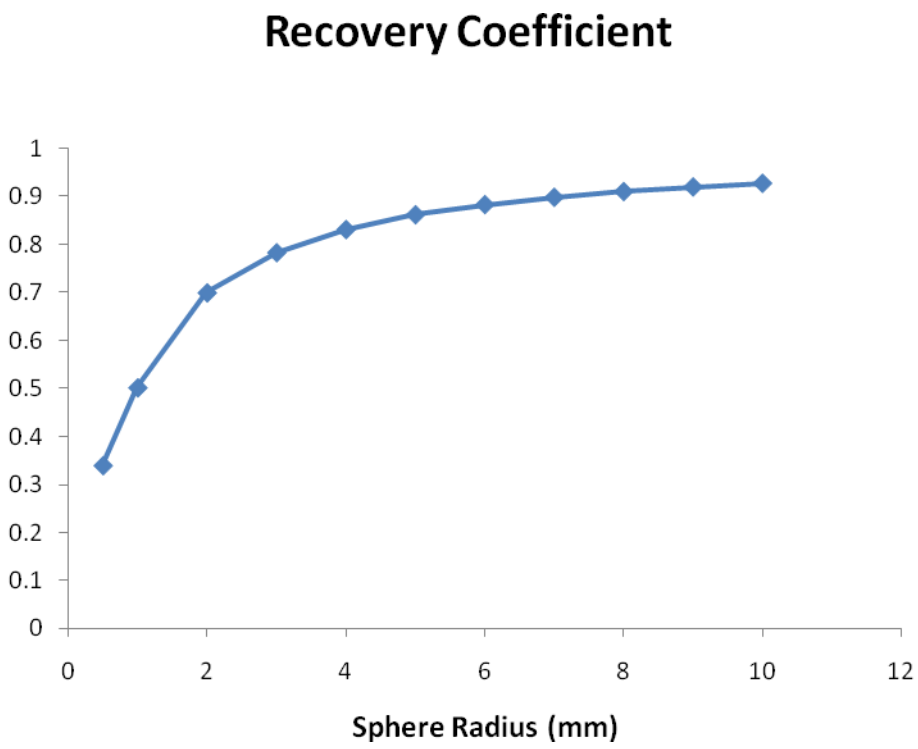

Figure 5. 6 Revocery coefficient (RC) for partial volume correction of 18F-FDG uptake in tumor. Calculated RC was based on the shape of a sphere and the spatial resolution of the microPET scanner.

SUV_avg and ^{18}F-FDG uptake constant K_i in tumor were fitted by the functions of Eq. 6 and Eq. 7, and their various reduced forms (i.e., removing the diameter- or glucose-dependent terms, or both). Leave-one-out cross validation (LOOCV) results that show the most appropriate functional relationships are shown in Table 5.1 and Table 5.2 for both MDA and U87 tumors. The regression model with the lowest MSE value for MDA data was SUV/RC=1.7171 (MSE=2.91E-01) and K_i/RC = 0.034 (MSE=2.40E-04); for U87 data, it was SUV/RC = 4.5445/ (1.129+[Glc]) (MSE=2.04E-01) and K_i/RC = 0.052/(0.2122+[Glc]) (MSE= 9.15E-05). The

results indicated that SUV and ^{18}F-FDG uptake constant K_i in MDA were not affected by blood glucose concentration, in contrast with the case for U87.

		MDA-MB-231		U87	
Model	N	Optimal Parameters	MSE	Optimal Parameters	MSE
SUV/RC = a	1	a=1.7171	2.91E-01	a=1.7931	2.19E-01
SUV/RC = a+c*tumor diameter	2	a=2.1591 c=-0.1115	3.19E-01	a=1.7503 c=0.0008	2.54E-01
SUV/RC = a/(b+glc)	2	a=6.2466 b=2.4541	3.40E-01	a=4.5445 b=1.1290	2.04E-01
SUV/RC = (a+c*tumor diameter)/(b+glc)	3	a=54.4273 b=23.8240 c=-2.8120	3.65E-01	a=4.5427 b=1.1785 c=0.0005	2.49E-01

Table 5. 1 Regression analysis of the PV corrected averaged SUV. Each model's value of mean squared error (MSE) is calculated from leave one out cross validation (LOOCV), which was used to select the most appropriate model that represents the 18F-FDG uptake constants in each tumor type. N is the number of the independent parameters (a,b and c).

		MDA-MB-231		U87	
Model	N	Optimal Parameters	MSE	Optimal Parameters	MSE
Ki/RC = a	1	a=0.034	2.40E-04	a=0.0327	1.40E-04
Ki/RC = a+c*tumor diameter	2	a=0.0404 c=0.0030	2.73E-04	a=0.02926 c=2.06E-05	1.60E-04
Ki/RC = a/(b+glc)	2	a=3.6736 b=117.5432	2.49E-04	a=0.0520 b=0.2122	9.15E-05
Ki/RC = (a+c*tumor diameter)/(b+glc)	3	a=13.3778 b=324.9948 c=-0.7505	2.88E-04	a=0.0517 b=0.2301 c=5.09E-06	9.81E-05

Table 5. 2 Regression analysis of the PV corrected uptake constant Ki. Each model's value of mean squared error (MSE) is calculated from LOOCV. N is the number of the independent parameters (a,b and c).

After the effects of partial volume and blood glucose concentration were accounted for (MDA: corrected_SUV = SUV/RC and corrected_K_i = K_i /RC; U87: corrected_SUV = SUV *(b+[Glc])/RC) and corrected_K_i = K_i *(b+[Glc])/RC), the data did not support any change of SUV or K_i when tumor (of either cell line) grew bigger in size (but before necrotic core development) as shown in Figure 5.7 and Figure 5.8. No significant relationship was found between the corrected_SUV or corrected_K_i and tumor size (Corrected_SUV: R^2=0.1381 and

0.0009 for MDA and U87, respectively; corrected_K_i: R^2=0.093 and 0.0246 for MDA and U87, respectively, P>0.05 for all situations). The corrected_SUV or corrected_K_i was also found to be uncorrelated to blood glucose concentrations with slope of regression lines not significantly different from zero (Corrected_SUV: R^2=0.0006 and 0.0407 for MDA and U87, respectively; corrected_K_i: R^2=0.033 and 0.003 for MDA and U87, respectively, P>0.05 for all situations).

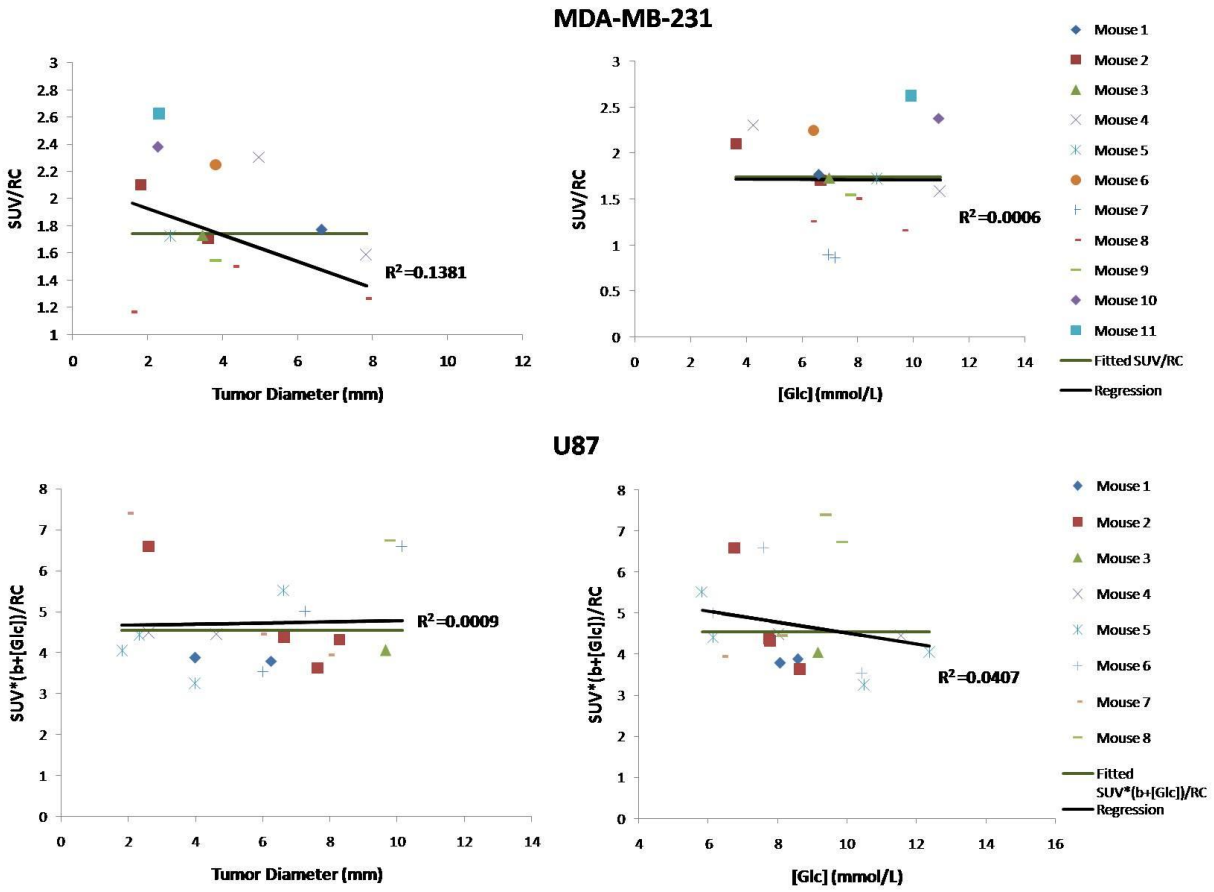

Figure 5. 7 Relationships between corrected SUV and tumor size and blood glucose levels in MDA-MB-231 and U87. The data was pooled from non-necrotic studies only.

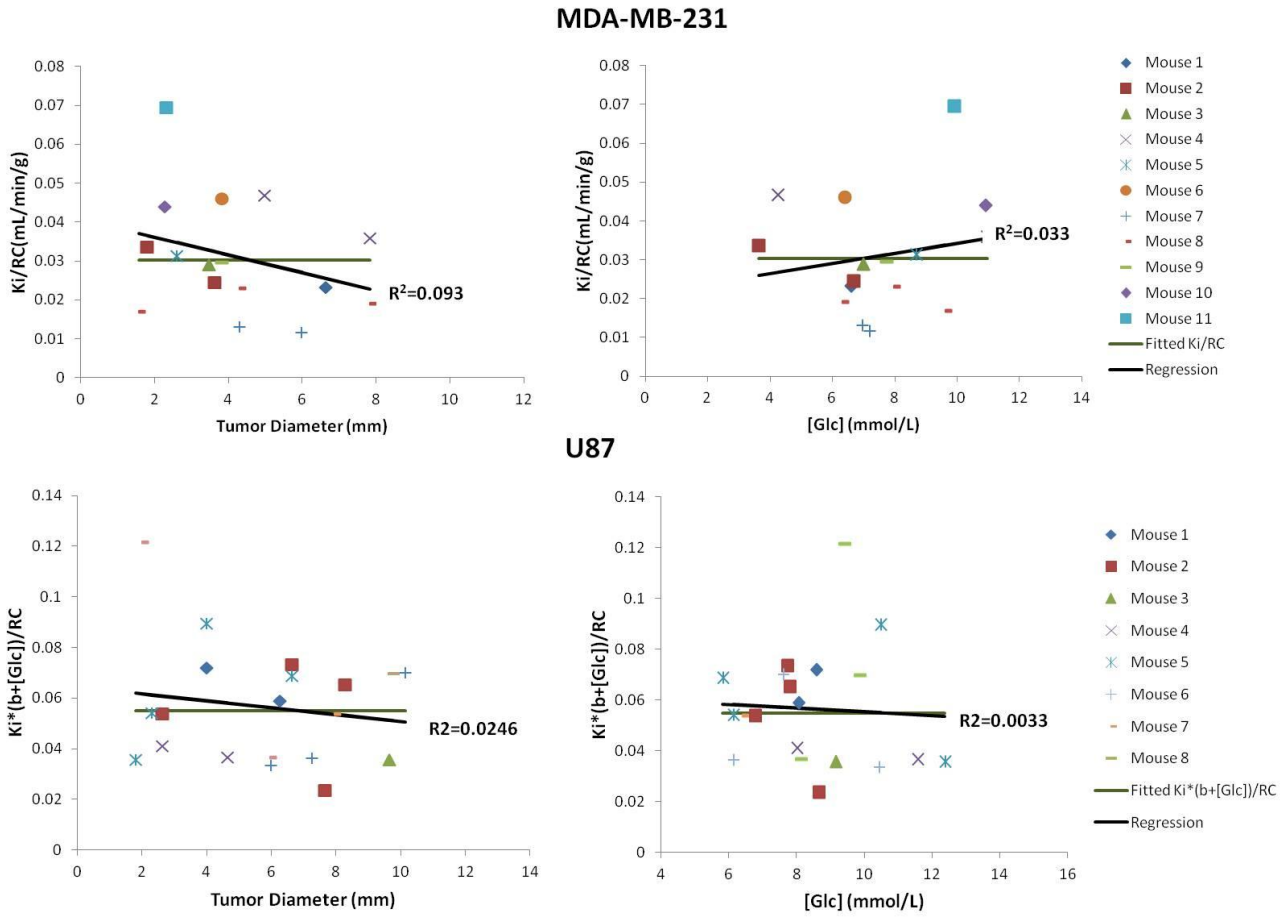

Figure 5. 8 Relationships between corrected_Ki and tumor size and blood glucose levels in mammary cancer MDA-MB-231 and brain cancer U87. The data was pooled from non-necrotic studies only.

5.4 Discussion

In this work, a set of longitudinal quantitative ^{18}F-FDG PET studies were performed on tumor-bearing mice, and the method to account simultaneously for the tumor size, the blood glucose level, and tumor growth has been tested. There were a few prior studies that used ^{18}F-FDG to quantify tumor glucose metabolism in rodents based primarily on semi-quantitative index such as SUV or tumor/background ratio (*117, 118*). While the impact of medium/blood

glucose levels on ^{18}F-FDG uptake in tumor has been well investigated in in-vitro and in-vivo studies (*1-3, 7, 57, 119*), no longitudinal studies have been published to elucidate the associations of both blood glucose level and tumor size with ^{18}F-FDG uptake constant in various tumors. Our quantitative analysis based on ^{18}F-FDG uptake, kinetics analysis and cross validation addresses the effect of blood glucose level and tumor size (for tumors without necrotic cores) in different type of tumors. The results suggested that, accounting for these effects in the fitting of measured data, would lead to improvement in the measurement sensitivity of the true biological signals in the tumors (Figure 5.7 and Figure 5.8).

5.4.1 Observed Differences between MDA-MB-231 and U87

Human breast cancer MDA-MB-231 cells have a high proliferation rate in SCID mice (*120*), so are human glioma U87 cells (*121*). In this work, tumor growth was monitored in longitudinal studies for about 30 days and it was found that MDA-MB-231 and U87 had a similar growth rate after the baseline imaging time point (Figure 5.2). However, MDA-MB-231 developed necrotic cores much earlier than U87 (Figure 5.1), probably due to different angiogenesis rates between the two tumor types. Likewise, the measured time activity curves were also found to be different. After examined the intercepts from the Patlak analysis of both tumors, we found that U87 has a larger intercept (0.505 ± 0.127) than MDA-MB-231 (0.328 ± 0.045). As shown in Eq. 5, the intercept is $\left(\frac{k_2}{k_2+k_3}\right)\frac{C_1(t)}{C_P(t)} + \frac{V_B C_B(t)}{C_P(t)}$, which reflects the fractional blood volume V_B and the distribution volume V_0 of the reversible compartment C_1, i.e. the ratio of concentrations of non-metabolized ^{18}F-FDG in tumor and in plasma. Therefore, the higher intercept of U87 may indicate higher absorption rates of ^{18}F-FDG in U87.

5.4.2 Quantitation of ^{18}F-FDG Uptake using SUV

In PET tumor imaging, SUV is one of the most frequently used indices for characterizing tumor uptake and is becoming increasingly important. However, the value of the use of SUV for interpreting ^{18}F-FDG PET scans was found to be limited because of the considerable overlap between SUV measurements in malignant and benign lesions, and subtle changes of early response to therapy (*19, 122, 123*). The clinical studies indicated that most tumors responding to therapy showed a 20–40% decrease in SUV early in the treatment course (less than 4 weeks after the treatment). Therefore, large variability in SUV measurements could affect the clinical interpretation. It is critically important to understand the variables that can affect the FDG uptakes in the body tissues. Generally speaking, these variability sources can be categorized into two types. One comes from biological factors of the animal (e.g., body size, tumor's size/configuration changes, plasma substrate level, insulin level, and input function variations). Another type is associated with technologic factors (e.g. reconstruction parameter changes and inter-observer variability).

Our MDA-MB-231 data showed that both SUV and MRGlu were relatively constant when tumor grew bigger (Figure 5.4); no correlation was found between SUV and blood glucose levels but MRGlu increased with increasing blood glucose levels (Figure 5.5). Unlike that in MDA-MB-231, SUV in U87 tumor correlates significantly with tumor size and blood glucose levels, indicating that correction for blood glucose level and tumor size is needed in the calculation of SUV to reflect MRGlu. These results also suggested that the glucose uptake mechanism could be different in different tumor types and correcting for blood glucose level or not in the SUV formula should be done cautiously. Reported results in the literature on effect of

blood glucose levels on a few other types of tumors were somewhat controversial. Most studies have demonstrated that ^{18}F-FDG uptake into human cancer cells are inhibited by increasing blood/media glucose levels because of direct competition between ^{18}F-FDG and D-glucose for uptake and incorporation into tumor cells and cancers (*1, 2, 7, 94*). Our results from U87 data were consistent with these findings. However, animal studies performed by Torizuka (*96*) indicated that the uptake of ^{18}F-FDG in mammary carcinoma was reduced for insulin-induced hypoglycemia. Likewise, the mammary cancer MDA-MB-231 presented an uncorrelated relationship with a slight negative slope between ^{18}F-FDG uptake and blood glucose levels (Figure 5.5).

5.4.3 Corrected ^{18}F-FDG Uptake Constant with Blood Glucose Level, Tumor Size and Partial Volume Effect

When tracer uptake in small tumors without necrotic cores was measured, large biases could be introduced by the partial-volume effect (PVE) (*124*). We used calculated recovery coefficient (RC) to reduce the errors attributable to PVE (Figure 5.6). The semi-quantitative analysis showed that the effect of blood glucose level and tumor size on the ^{18}F-FDG uptake should be corrected for U87 data. A model with three independent parameters was used in the present study to account for these factors for the ^{18}F-FDG uptake constant (Eq. 6). Both MDA-MB-231 and U87 data were tested using model fitting. The best model that fitted the ^{18}F-FDG uptake constants was selected based on the smallest mean squared error (MSE) that was calculated from cross-validation (Table 5.1 and 5.2). The results showed that MDA data was best described by the model SUV/RC=1.7171 and K_i/RC = 0.034; for U87 data, it was SUV/RC = 4.5445/ (1.129+[Glc]) and K_i/RC = 0.052/(0.2122+[Glc]).

The U87 K_i was inversely correlated to the blood glucose levels. That is similar to our previous findings on FDG uptake constant in the brain that showed a significant inverse relationship between cerebral ^{18}F-FDG uptake constant and the blood glucose level. It was also consistent with the results of our in vitro studies, which showed that the FDG uptake in MDA is not affected as much by medium glucose level over the normal physiological glucose range as those of U87(*36*). Since U87 is a human cancer cell line originated from the brain, the finding that U87 behaves like brain tissue in glucose metabolism is interesting, but not unexpected. The ^{18}F-FDG SUV and K_i, after corrected for the partial volume effect and blood glucose levels (Figure 5.7 and 5.8), did not show any change when tumor (of either cell line) grew bigger in size (but before necrotic core development) for both MDA and U87. With the use of the corrected_SUV or corrected_K_i, sensitivity of quantitative analysis in different types of tumors is expected to be improved (Figure 5.7 and 5.8). No significant correlation was found between tumor size and blood glucose concentration (R^2=0.0067 and 0.041 for MDA and U87, respectively, P>0.05 for both). This satisfied the independence assumption of the independent variables in the multivariate regression analysis we have used.

The results showed that the values of K_i can be measured with the same reproducibility as SUV. The main advantage of K_i is that it takes into account changes in the whole-body distribution of FDG. Therefore, measurement of the input function and calculation of uptake constant K_i may be preferable to the use of SUV when the distribution volumes of FDG changes due to environmental changes, such as change of blood glucose levels. However, it was also found that variability of K_i could be increased due to patient movement during acquisition, especially when the size of the lesions is still small (*37*). Quantitative studies for evaluating FDG

uptake in lung cancer also supported the same conclusion that SUV and graphical K_i can be measured reproducibly(*38*). In general, SUV and K_i are both high reproducible parameters for quantitation of glucose metabolism in PET studies.

5.4.4 Implications in Further In Vivo Tumor Studies

The present results indicate that ^{18}F-FDG uptake constants in MDA-MB-231 and U87 differ considerably in response to altered blood glucose level, suggesting that ^{18}F-FDG uptake and glucose metabolism are tumor-type dependent. However, more work needs to be done to account for possible effects due to insulin and tumor heterogeneity (when a necrotic core appears) to further improve the reliability of the quantitative measurements and to examine the metabolic stability/change after a necrotic core develops. Insulin can induce a host of effects on vascular cells (*44-46*), including traditional metabolic actions such as glucose transport and utilization(*44*), protein synthesis and cellular proliferation(*45*). In addition, insulin also has vascular-specific actions that are particular to vascular tissues (*46*). Although the effects of insulin on tumor ^{18}F-FDG uptake has been studied by others before (*48-50*), the prior studies all involved insulin injections into the animal or patient to alter the circulating insulin level, which also caused blood glucose level changes. As a result, changes in ^{18}F-FDG uptake could be due to either or both of these factors. Only after the known confounding factors are properly accounted for can one begin to critically assess the temporal changes in ^{18}F-FDG uptake kinetics during normal growth or due to intervention or treatment (*37, 125*).

5.5 Conclusions

Results from the present study showed that ^{18}F-FDG uptake constant in U87 tumor varies inversely with the blood glucose levels; in contrast, MDA ^{18}F-FDG uptake constant is

independent of the blood glucose level, indicating that different transporter/hexokinase adaptation to blood glucose levels exist for the two tumor types. PV and [Glc] corrected ^{18}F-FDG uptake constant was stable as tumor of either cell line grew in size. To make quantitation of ^{18}F-FDG PET images more robust, PV correction is needed. Furthermore, adjustment for blood glucose level should be applied for tumor types that are sensitive to blood glucose levels in their ^{18}F-FDG uptake constants.

Chapter 6 SUMMARY AND CONCLUSIONS

The uptake of FDG into tissue reflects both transport and phosphorylation of glucose by viable cells. However, previous experimental and clinical studies have indicated that the FDG uptake within a tumor mass may be influenced by numerous factors. Biological factors such as tumor grade, hypoxia, cellular proliferation rate and blood glucose concentration have been shown to affect FDG uptake. Generally speaking, the purpose of the work presented in this dissertation was to investigate the effects of several biological factors on a few highly reproducible quantitative parameters of FDG kinetics that are related to tumor glucose metabolism . In vitro studies were firstly performed on a novel cell culture and imaging system (microfluidic beta-camera) to examine the relationship between FDG kinetic parameters in tumor cells and the media glucose levels. Then with the use of multi-well cell culture plate, effects of media glucose levels and media free fatty acid levels on FDG uptake in tumor cells were extensively evaluated. Third, two tumor cell lines were selected based on the results of in vitro experiments for a set of FDG-PET studies on tumor-bearing mice.

Chapter 3 introduced a new tracer infusion strategy to extract the FDG quantitative parameters in tumor cells by using a PSAPD-coupled microfluidic chip. Due to various technical difficulties, extraction of kinetic parameters from in vitro cell culture experiments has not been done by others before. The new switching strategy, which consists of tracer incubation and background-removed periods, overcomes the difficulties caused by bolus injection or constant infusion for quantitation of dynamic cellular tracer uptake data. Furthermore, an optimal switching schedule design was obtained to provide the most reliable parameter estimates of the tracer transport and phosphorylation rate constants in tumor cells. The optimized schedule also

has the practical advantages of simplifying the tracer incubation protocol and reducing any potential disturbance to the cultured cells caused by the perfusions during the switches between periods. Robustness of the novel cell culture protocol and the reliability of the estimates were examined by both computer simulations and real experiments on chip. In addition, response of FDG uptake in tumor cell lines to specific media glucose levels was monitored. It was concluded that the kinetic switching strategy for tracer incubation could provide reliable estimates of cellular FDG transport and uptake constants and the reliability of the model parameters can be improved with an optimal design of fewer switching cycles. The results also indicated that glioma cell line U87 and prostate cancer cell line CaP8 can adapt well to elevated glucose levels in the environment.

The study presented in Chapter 4 was conducted on regular cell culture micro-plate in order to investigate the effect of media glucose levels and free fatty acid levels on FDG uptake in tumor cells. Several different tumor types were tested and conclusions were not all the same at different tumor cell lines. It was found that FDG uptake in the tumor cell lines all decreased with the increased medium glucose level, but not with the change of the free fatty acid level. However, the relationship between FDG uptake and medium glucose level is different for different tumor types, e.g. the FDG uptake in mammary cell line MDA-MB-231 is not affected as much by medium glucose level over the normal physiological glucose range as those of U87 and PC3. The value of the lumped constant appeared not affected by the medium glucose level.

As shown above, in vitro studies of FDG uptake kinetics in cells have been approached by two methods: (1) using a novel microfluidic beta camera system and a switching tracer infusion protocol; (2) using a multi-well cell culture plate. The microfluidic system owns many

advantages over the multi-well plate, such as automatic measurement of time activity curve (TAC) that reflects the dynamic change of FDG uptake in cells as a function of time, extraction of kinetic parameters of cells, less human intervention and time consuming. However, the experimental results from microfluidic system are not as good as predicted from the computer simulations when the switching strategy is applied, indicating that there are still spaces to improve the methodology and the design of the system. The future work may focus on improve the reliability of quantitation on chip for various cellular and tracer experiments.

In chapter 5, in-vivo FDG-PET studies were performed on a set of tumor bearing mice. We hypothesized that the tumor cell lines that responded with strong effects to changes of the medium glucose level in vitro will similarly have a larger effect in vivo. Longitudinal FDG-PET imagings were performed on mice implanted with either U87 or MDA-MB-231. We addressed the effects of blood glucose level and tumor size on both SUV and FDG uptake constant K_i . The input function was derived from dynamic PET images and was used to quantitate the Ki values for both tumor types. Results indicated that there is probably different transporter/hexokinase adaptation to blood glucose level for the two tumor cell lines. The FDG uptake constant, after correction for tumor size and blood glucose level effects, was found stable as tumor grew in size. In other words, to ensure robust quantitation of FDG-PET images, corrections of blood glucose level and partial volume effect are needed for tumors that are sensitive to blood glucose levels in their FDG uptake constants.

The animial FDG-PET studies suggest that FDG uptake and glucose metabolism are tumor-type dependent. Two biological effects: blood glucose level and tumor size are considered. However, more work needs to be done to account for other possible effects such as insulin and

tumor heterogeneity (when a necrotic core appears) to further improve the reliability of the quantitative measurements and to examine the metabolic stability/change after a necrotic core develops. Only after the known confounding factors are properly accounted for can one begin to critically assess the temporal changes in ^{18}F-FDG uptake kinetics during normal growth or due to intervention or treatment.

In conclusion, the effects of blood glucose level on the FDG uptake in various tumor cell lines were investigated in this dissertation in in-vitro and in-vivo situations. Results from microfluidic beta camera system, regular multi-well cell culture plate and FDG-PET studies were consistent and indicated that different tumors have different sensitivity to blood glucose level.

REFERENCES

1. Diederichs CG, Staib L, Glatting G, Beger HG, Reske SN. FDG PET: Elevated Plasma Glucose Reduces Both Uptake and Detection Rate of Pancreatic Malignancies. *J Nucl Med.* June 1, 1998 1998;39(6):1030-1033.

2. Langen KJ, Braun U, Kops ER, et al. The Influence of Plasma Glucose Levels on Fluorine-18-Fluorodeoxyglucose Uptake in Bronchial Carcinomas. *J Nucl Med.* March 1, 1993 1993;34(3):355-359.

3. Lindholm P, Minn H, Leskinen-Kallio S, Bergman J, Ruotsalainen U, Joensuu H. Influence of the Blood Glucose Concentration on FDG Uptake in Cancer--A PET Study. *J Nucl Med.* January 1, 1993 1993;34(1):1-6.

4. Jadvar H, Alavi A, Gambhir SS. 18F-FDG Uptake in Lung, Breast, and Colon Cancers: Molecular Biology Correlates and Disease Characterization. *Journal of Nuclear Medicine.* November 2009 2009;50(11):1820-1827.

5. Zhuang HM, Cort-S-Blanco A, Pourdehnad M, et al. Do high glucose levels have differential effect on FDG uptake in inflammatory and malignant disorders? *Nuclear Medicine Communications.* 2001;22(10):1123-1128.

6. Ishizu K, Sadato N, Yonekura Y, et al. Enhanced Detection of Brain Tumors by [18F]Fluorodeoxyglucose PET with Glucose Loading. *Journal of Computer Assisted Tomography.* 1994;18(1):12-15.

7. Torizuka T, Clavo AC, Wahl RL. Effect of Hyperglycemia on In Vitro Tumor Uptake of Tritiated FDG, Thymidine, L-Methionine and L-Leucine. *J Nucl Med.* March 1, 1997 1997;38(3):382-386.

8. Torizuka T, Zasadny KR, Recker B, Wahl RL. Untreated primary lung and breast cancers: correlation between F-18 FDG kinetic rate constants and findings of in vitro studies. *Radiology.* June 1998 1998;207(3):767-774.

9. Haberkorn U, Morr I, Oberdorfer F, et al. Fluorodeoxyglucose Uptake In Vitro: Aspects of Method and Effects of Treatment with Gemcitabine. *Journal of Nuclear Medicine.* November 1, 1994 1994;35(11):1842-1850.

10. HUBner KF, Buonocore E, Gould HR, et al. Differentiating Benign from Malignant Lung Lesions Using "Quantitative" Parameters of FDG PET Images. *Clinical Nuclear Medicine.* 1996;21(12):941-949.

11. Maurea S, Mainolfi C, Bazzicalupo L, et al. Imaging of adrenal tumors using FDG PET: comparison of benign and malignant lesions. *American Journal of Roentgenology.* July 1, 1999 1999;173(1):25-29.

12. Dehdashti F, Siegel BA, Griffeth LK, et al. Benign versus malignant intraosseous lesions: discrimination by means of PET with 2-[F-18]fluoro-2-deoxy-D-glucose. *Radiology.* July 1, 1996 1996;200(1):243-247.

13. Demura Y, Tsuchida T, Ishizaki T, et al. 18F-FDG Accumulation with PET for Differentiation Between Benign and Malignant Lesions in the Thorax. *Journal of Nuclear Medicine.* April 1, 2003 2003;44(4):540-548.

14. Blumer SL, Scalcione LR, Ring BN, et al. Cutaneous and Subcutaneous Imaging on FDG-PET: Benign and Malignant Findings. *Clinical Nuclear Medicine.* 2009;34(10):675-683 610.1097/RLU.1090b1013e3181b53845.

15. Okada M, Shimono T, Komeya Y, et al. Adrenal masses: the value of additional fluorodeoxyglucose-positron emission tomography/computed tomography (FDG-PET/CT) in differentiating between benign and malignant lesions. *Annals of Nuclear Medicine.* 2009;23(4):349-354.

16. Juweid ME, Stroobants S, Hoekstra OS, et al. Use of Positron Emission Tomography for Response Assessment of Lymphoma: Consensus of the Imaging Subcommittee of International Harmonization Project in Lymphoma. *Journal of Clinical Oncology.* February 10, 2007 2007;25(5):571-578.

17. Cheson BD, Pfistner B, Juweid ME, et al. Revised Response Criteria for Malignant Lymphoma. *Journal of Clinical Oncology.* February 10, 2007 2007;25(5):579-586.

18. Krak NC, van der Hoeven JJM, Hoekstra OS, Twisk JWR, van der Wall E, Lammertsma AA. Measuring FDG uptake in breast cancer during chemotherapy: comparison of analytical methods. *European Journal of Nuclear Medicine and Molecular Imaging.* 2003;30(5):674-681.

19. Takahashi R, Hirata H, Tachibana I, et al. Early [18F]Fluorodeoxyglucose Positron Emission Tomography at Two Days of Gefitinib Treatment Predicts Clinical Outcome in Patients with Adenocarcinoma of the Lung. *Clinical Cancer Research.* January 1, 2012;18(1):220-228.

20. Moule RN, Kayani I, Moinuddin SA, et al. The potential advantages of 18FDG PET/CT-based target volume delineation in radiotherapy planning of head and neck cancer. *Radiotherapy and oncology : journal of the European Society for Therapeutic Radiology and Oncology.* 2010;97(2):189-193.

21. Schinagl DAX, Hoffmann AL, Vogel WV, et al. Can FDG-PET assist in radiotherapy target volume definition of metastatic lymph nodes in head-and-neck cancer? *Radiotherapy and oncology : journal of the European Society for Therapeutic Radiology and Oncology.* 2009;91(1):95-100.

22. Kim CK, Gupta NC, Chandramouli B, Alavi A. Standardized uptake values of FDG: body surface area correction is preferable to body weight correction. *Journal of nuclear medicine : official publication, Society of Nuclear Medicine.* 1994;35(1):164-167.

23. Avril N, Bense S, Ziegler SI, et al. Breast imaging with fluorine-18-FDG PET: quantitative image analysis. *Journal of nuclear medicine : official publication, Society of Nuclear Medicine.* 1997;38(8):1186-1191.

24. Lucignani G. SUV and segmentation: pressing challenges in tumour assessment and treatment. *European Journal of Nuclear Medicine and Molecular Imaging.* 2009;36(4):715-720.

25. Benz MR, Evilevitch V, Allen-Auerbach MS, et al. Treatment Monitoring by 18F-FDG PET/CT in Patients with Sarcomas: Interobserver Variability of Quantitative Parameters in Treatment-Induced Changes in Histopathologically Responding and Nonresponding Tumors. *Journal of Nuclear Medicine.* July 2008 2008;49(7):1038-1046.

26. Boellaard R, Krak NC, Hoekstra OS, Lammertsma AA. Effects of Noise, Image Resolution, and ROI Definition on the Accuracy of Standard Uptake Values: A Simulation Study. *Journal of Nuclear Medicine.* September 1, 2004 2004;45(9):1519-1527.

27. Adams MC, Turkington TG, Wilson JM, Wong TZ. A Systematic Review of the Factors Affecting Accuracy of SUV Measurements. *American Journal of Roentgenology.* August 1, 2010;195(2):310-320.

28. Weber WA, Ziegler SI, Thodtmann R, Hanauske AR, Schwaiger M. Reproducibility of metabolic measurements in malignant tumors using FDG PET. *Journal of nuclear medicine : official publication, Society of Nuclear Medicine.* 1999;40(11):1771-1777.

29. Patlak CS, Blasberg RG, Fenstermacher JD. Graphical Evaluation of Blood-to-Brain Transfer Constants from Multiple-Time Uptake Data. *J Cereb Blood Flow Metab.* 1983;3(1):1-7.

30. Patlak CS, Blasberg RG. Graphical Evaluation of Blood-to-Brain Transfer Constants from Multiple-Time Uptake Data. Generalizations. *J Cereb Blood Flow Metab.* 1985;5(4):584-590.

31. Minn H, Zasadny KR, Quint LE, Wahl RL. Lung cancer: reproducibility of quantitative measurements for evaluating 2-[F-18]-fluoro-2-deoxy-D-glucose uptake at PET. *Radiology.* July 1, 1995 1995;196(1):167-173.

32. Phelps ME, Huang SC, Hoffman EJ, Selin C, Sokoloff L, Kuhl DE. Tomographic measurement of local cerebral glucose metabolic rate in humans with (F-18)2-fluoro-2-deoxy-D-glucose: Validation of method. *Annals of Neurology.* 1979;6(5):371-388.

33. Carson RE, Bailey DL, Townsend DW, Valk PE, Maisey MN. Tracer Kinetic Modeling in PET. *Positron Emission Tomography*: Springer London; 2005:127-159.

34. Sanabria-Boh 贸 rquez SM, Maes A, Dupont P, et al. Image-Derived Input Function for [11C]Flumazenil Kinetic Analysis in Human Brain. *Molecular Imaging & Biology.* 2003/4// 2003;5(2):72-78.

35. Kim J, Herrero P, Sharp T, et al. Minimally Invasive Method of Determining Blood Input Function from PET Images in Rodents. *Journal of Nuclear Medicine.* February 2006 2006;47(2):330-336.

36. Ferl GZ, Zhang X, Wu H-M, Huang S-C. Estimation of the 18F-FDG Input Function in Mice by Use of Dynamic Small-Animal PET and Minimal Blood Sample Data. *Journal of Nuclear Medicine.* 2007;48(12):2037-2045.

37. Carson RE. Precision and Accuracy Considerations of Physiological Quantitation in PET. *J Cereb Blood Flow Metab.* 1991;11(S1):A45-A50.

38. Weber W, Wieder H. Monitoring chemotherapy and radiotherapy of solid tumors. *European Journal of Nuclear Medicine and Molecular Imaging.* 2006;33(0):27-37.

39. Zasadny KR, Wahl RL. Standardized uptake values of normal tissues at PET with 2-[fluorine-18]-fluoro-2-deoxy-D-glucose: variations with body weight and a method for correction. *Radiology.* December 1, 1993 1993;189(3):847-850.

40. Graham MM, Peterson LM, Hayward RM. Comparison of simplified quantitative analyses of FDG uptake. *Nuclear medicine and biology.* 2000;27(7):647-655.

41. Wong K-P, Sha W, Zhang X, Huang S-C. Effects of Administration Route, Dietary Condition, and Blood Glucose Level on Kinetics and Uptake of 18F-FDG in Mice. *Journal of Nuclear Medicine.* May 1, 2011;52(5):800-807.

42. Kubota K, Watanabe H, Murata Y, et al. Effects of blood glucose level on FDG uptake by liver: a FDG-PET/CT study. *Nuclear medicine and biology*.38(3):347-351.

43. Zhao S, Kuge Y, Tsukamoto E, et al. Effects of insulin and glucose loading on FDG uptake in experimental malignant tumours and inflammatory lesions. *European Journal of Nuclear Medicine and Molecular Imaging.* 2001;28(6):730-735.

44. Allen LA, Gerritsen ME. Regulation of hexose transport in cultured bovine retinal microvessel endothelium by insulin. *Experimental Eye Research.* 1986;43(4):679-686.

45. Obata T, Kashiwagi A, Maegawa H, et al. Insulin signaling and its regulation of system A amino acid uptake in cultured rat vascular smooth muscle cells. *Circulation research.* 1996;79(6):1167-1176.

46. G Zeng MJQ. Insulin-stimulated production of nitric oxide is inhibited by wortmannin. Direct measurement in vascular endothelial cells. *J Clin Invest.* 1996;98(4): 894–898.

47. Haney PM, Slot JW, Piper RC, James DE, Mueckler M. Intracellular targeting of the insulin-regulatable glucose transporter (GLUT4) is isoform specific and independent of cell type. *The Journal of Cell Biology.* August 15, 1991 1991;114(4):689-699.

48. Torizuka T, Fisher SJ, Wahl RL. Insulin-induced hypoglycemia decreases uptake of 2-[F-18] fluoro-2-deoxy-D-glucose to experimental mammary carcinoma. *Radiology.* 1997;203(1):169-172.

49. Lee K-H, Ko B-H, Paik J-Y, et al. Effects of anesthetic agents and fasting duration on ^{18}F-FDG biodistribution and insulin levels in tumor-bearing mice. *J Nucl Med.* 2005;46:1531-1536.

50. Minn H, Lindholm P, Nuutila P, et al. In vivo effects of insulin on tumor and skeletal muscle glucose metabolism in patients with lymphoma. *Cancer.* 1994;73(5):1490-1498.

51. Hoffman EJ, Huang S-C, Phelps ME. Quantitation in Positron Emission Computed Tomography: 1. Effect of Object Size. *Journal of Computer Assisted Tomography.* 1979;3(3):299-308.

52. Hatt M, Le Pogam A, Visvikis D, Pradier O, Cheze Le Rest C. Impact of Partial-Volume Effect Correction on the Predictive and Prognostic Value of Baseline 18F-FDG PET Images in Esophageal Cancer. *Journal of Nuclear Medicine.* January 1, 2012;53(1):12-20.

53. Scheuermann JS, Saffer JR, Karp JS, Levering AM, Siegel BA. Qualification of PET Scanners for Use in Multicenter Cancer Clinical Trials: The American College of Radiology Imaging Network Experience. *Journal of Nuclear Medicine.* July 2009 2009;50(7):1187-1193.

54. Boellaard R. Standards for PET Image Acquisition and Quantitative Data Analysis. *Journal of Nuclear Medicine.* May 2009 2009;50(Suppl 1):11S-20S.

55. Jacene HA, Leboulleux S, Baba S, et al. Assessment of Interobserver Reproducibility in Quantitative 18F-FDG PET and CT Measurements of Tumor Response to Therapy. *Journal of Nuclear Medicine.* November 2009 2009;50(11):1760-1769.

56. Boellaard R. Standards for PET Image Acquisition and Quantitative Data Analysis. *J Nucl Med.* May 1, 2009 2009;50(Suppl_1):11S-20.

57. Higashi K, Clavo AC, Wahl RL. In Vitro Assessment of 2-Fluoro-2-Deoxy-D Glucose, L-Methionine and Thymidine as Agents to Monitor the Early Response of a Human Adenocarcinoma Cell Line to Radiotherapy. *J Nucl Med.* May 1, 1993 1993;34(5):773-779.

58. Dittrich PS, Manz A. Lab-on-a-chip: microfluidics in drug discovery. *Nat Rev Drug Discov.* Mar 2006;5(3):210-218.

59. Vu. NT. Performance of an integrated microfluidic chip and position sensitive APD for the detection of beta emitting probes in cell cultures. *IEEE Medical Imaging Conference*; 2007.

60. Yu. ZTF. Design and characterization of a biomedical device capable

of pico-Ci level beta detection for the study of cell metabolism. *Proc. of IEEE*

International Conference on Micro Electro Mechanical Systems; 2008.

61. Vu NT, Yu ZTF, Silverman RW, et al. Performance of an integrated microfluidic chip and position sensitive APD for the detection of beta emitting probes in cell cultures. Paper presented at: Nuclear Science Symposium Conference Record, 2007. NSS '07. IEEE, 2007.

62. Richard EC. PET physiological measurements using constant infusion. *Nuclear medicine and biology*. 2000;27(7):657-660.

63. Mazoyer BM, Huesman RH, Budinger TF, Knittel BL. Dynamic PET data analysis. *Journal of computer assisted tomography.* 1986;10(4):645-653.

64. Huang SC. Automated experimental design of scanning sequences for dynamic PET/SPECT studies. *J Nucl Med.* 1994;35.

65. Chen XLDFK. Optimal image sampling schedule: a new effective way to reduce dynamic image storage space and functional image processing time. *Medical Imaging, IEEE Transactions.* 1996;15(5):710 - 719

66. Liao W-HL, K.; Huang, S.-C.; Bergsneider, M. Optimal design in PET data acquisition: a new approach using simulated annealing and component-wise Metropolis updating. *Nuclear Science Symposium Conference Record, 2001 IEEE*; 2001:1979 - 1983.

67. Jiao J, Wang S, Qiao R, et al. Murine Cell Lines Derived from Pten Null Prostate Cancer Show the Critical Role of PTEN in Hormone Refractory Prostate Cancer Development. *Cancer Res.* July 1, 2007 2007;67(13):6083-6091.

68. DiStefano JJ. Optimized blood sampling protocols and sequential design of kinetic experiments. *American Journal of Physiology - Regulatory, Integrative and Comparative Physiology.* May 1, 1981 1981;240(5):R259-R265.

69. Kirkpatrick S. Optimization by simulated annealing: Quantitative studies. *Journal of Statistical Physics.* 1984;34(5):975-986.

70. Fang C, Wang Y, Vu NT, et al. Integrated Microfluidic and Imaging Platform for a Kinase Activity Radioassay to Analyze Minute Patient Cancer Samples. *Cancer Research.* November 1, 2010;70(21):8299-8308.

71. Chen K, Sung CH, Dan CY. The effects of measurement errors in the plasma radioactivity curve on parameter estimation in positron emission tomography. *Physics in Medicine and Biology.* 1991;36(9):1183.

72. Marquardt DW. An algorithm for least squares estimation of nonlinear parameters. *J Soc Ind Appl Math.* 1963;11:431-441.

73. Jin Zhang; Foudray AMKO, P.D.; Levin, C.S.; PerkinElmer Optoelectron. Performance characterization of a novel thin position-sensitive avalanche photodiode-based detector for high resolution PET. *Nuclear Science Symposium Conference Record, 2005 IEEE* 2006(23-29 Oct. 2005):2478 - 2482.

74. Fang C, Wang Y, Vu NT, et al. Integrated Microfluidic and Imaging Platform for a Kinase Activity Radioassay to Analyze Minute Patient Cancer Samples. *Cancer Research.* 2010.

75. Dimitrakopoulou-Strauss A, Strauss LG, Burger C, et al. Prognostic Aspects of 18F-FDG PET Kinetics in Patients with Metastatic Colorectal Carcinoma Receiving FOLFOX Chemotherapy. *Journal of Nuclear Medicine.* September 1, 2004 2004;45(9):1480-1487.

76. Dimitrakopoulou-Strauss A, Strauss LG, Heichel T, et al. The Role of Quantitative 18F-FDG PET Studies for the Differentiation of Malignant and Benign Bone Lesions. *Journal of Nuclear Medicine.* April 1, 2002 2002;43(4):510-518.

77. Dimitrakopoulou-Strauss A, Strauss LG, Schwarzbach M, et al. Dynamic PET 18F-FDG Studies in Patients with Primary and Recurrent Soft-Tissue Sarcomas: Impact on Diagnosis and Correlation with Grading. *Journal of Nuclear Medicine.* May 1, 2001 2001;42(5):713-720.

78. GZ Ferl XZ, HM Wu, SC Huang Estimation of the 18F-FDG Input Function in Mice by Use of Dynamic Small-Animal PET and Minimal Blood Sample Data. *Journal of Nuclear Medicine.* 2007.

79. Strauss LG, Dimitrakopoulou-Strauss A, Koczan D, et al. 18F-FDG Kinetics and Gene Expression in Giant Cell Tumors. *Journal of Nuclear Medicine.* September 1, 2004 2004;45(9):1528-1535.

80. Hosokawa K, Fujii T, Endo I. Handling of Picoliter Liquid Samples in a Poly(dimethylsiloxane)-Based Microfluidic Device. *Analytical Chemistry.* 2012/02/20 1999;71(20):4781-4785.

81. Lu H KL, Wang WM, Lauffenburger DA, Griffith LG, Jensen KF. . Microfluidic Shear Devices for Quantitative Analysis of Cell Adhesion. *Analytical Chemistry.* 08/17 2004;76(18):5257-5264.

82. Craig SL, Edward JH. Calculation of positron range and its effect on the fundamental limit of positron emission tomography system spatial resolution. *Physics in Medicine and Biology.* 1999;44(3):781.

83. Dresner A, Laurent D, Marcucci M, et al. Effects of free fatty acids on glucose transport and IRS-1 associated phosphatidylinositol 3-kinase activity. *The Journal of Clinical Investigation.* 1999;103(2):253-259.

84. Wolfe BM, Klein S, Peters EJ, Schmidt BF, Wolfe RR. Effect of elevated free fatty acids on glucose oxidation in normal humans. *Metabolism.* 1988;37(4):323-329.

85. Kroemer G, Pouyssegur J. Tumor Cell Metabolism: Cancer's Achilles' Heel. *Cancer Cell.* 2008;13(6):472-482.

86. Boden G, Chen X, Ruiz J, White JV, Rossetti L. Mechanisms of fatty acid-induced inhibition of glucose uptake. *The Journal of Clinical Investigation.* 1994;93(6):2438-2446.

87. Been LB, Suurmeijer AJH, Cobben DCP, Jager PL, Hoekstra HJ, Elsinga PH. [18F]-3'-fluoro-3'-deoxy-L-thymidine FLT-PET in oncology: current status and opportunities. *European Journal of Nuclear Medicine and Molecular Imaging.* 2004;31(12):1659-1672.

88. Toyohara J, Waki A, Takamatsu S, Yonekura Y, Magata Y, Fujibayashi Y. Basis of FLT as a cell proliferation marker: comparative uptake studies with [3H]thymidine and [3H]arabinothymidine, and cell-analysis in 22 asynchronously growing tumor cell lines. *Nuclear medicine and biology.* 2002;29(3):281-287.

89. Lee TS, Ahn SH, Moon BS, et al. Comparison of 18F-FDG, 18F-FET and 18F-FLT for differentiation between tumor and inflammation in rats. *Nuclear medicine and biology.* 2009;36(6):681-686.

90. Hoshikawa H, Nishiyama Y, Kishino T, Yamamoto Y, Haba R, Mori N. Comparison of FLT-PET and FDG-PET for Visualization of Head and Neck Squamous Cell Cancers. *Molecular Imaging and Biology.*13(1):172-177.

91. van Westreenen HL, Cobben DCP, Jager PL, et al. Comparison of 18F-FLT PET and 18F-FDG PET in Esophageal Cancer. *Journal of Nuclear Medicine.* March 1, 2005 2005;46(3):400-404.

92. Reivich M, Alavi A, Wolf A, et al. Glucose Metabolic Rate Kinetic Model Parameter Determination in Humans: The Lumped Constants and Rate Constants for [18F]Fluorodeoxyglucose and [11C]Deoxyglucose. *J Cereb Blood Flow Metab.* 1985;5(2):179-192.

93. Sokoroff L. [14-C]deoxyglucose method for the measurement of local cerebral glucose utilization: theory, procedure, and normal values in the conscious and anesthetized albino rat. *J Neurochem.* 1977;28:897-916.

94. Wong C-yO, Thie J, Parling-Lynch KJ, et al. Glucose-Normalized Standardized Uptake Value from 18F-FDG PET in Classifying Lymphomas. *Journal of Nuclear Medicine.* 2005;46(10):1659-1663.

95. Wahl RL, Henry CA, Ethier SP. Serum glucose: effects on tumor and normal tissue accumulation of 2-[F-18]-fluoro-2-deoxy-D-glucose in rodents with mammary carcinoma. *Radiology.* June 1, 1992 1992;183(3):643-647.

96. Torizuka T. FSJaWRL. Insulin-induced hypoglycemia decreases uptake of 2-[F-18]fluoro-2-deoxy-D-glucose into experimental mammary carcinoma. . *Radiology.* 1997;203:169–172.

97. Sokoloff L, Reivich M, Kennedy C, et al. The [^{14}C]deoxyglucose method for the measurement of local cerebral glucose utilization: Theory, procedure and normal values in the conscious and anesthetized albino rat. *J Neurochem.* 1977;28:897-916.

98. Schuier F, Oriz F, Suda S, Lucignani G, Kennedy C, Sokoloff L. Influence of plasma glucose concentration on lumped constant of the deoxyglucose method: Effects of hyperglycemia in the rat. *J Cereb Blood Flow Metab.* 1990;10:765-773.

99. Spence AM, Muzi M, Graham MM, et al. Glucose Metabolism in Human Malignant Gliomas Measured Quantitatively with PET, l-[C-ll]Glucose and FDG: Analysis of the FDG Lumped Constant. *Journal of Nuclear Medicine.* 1998;39(3):440-448.

100. Schwartz JL, Tamura Y, Jordan R, Grierson JR, Krohn KA. Monitoring Tumor Cell Proliferation by Targeting DNA Synthetic Processes with Thymidine and Thymidine Analogs. *Journal of Nuclear Medicine.* December 1, 2003 2003;44(12):2027-2032.

101. Weber G. Enzymology of Cancer Cells. *New England Journal of Medicine.* 1977;296(10):541-551.

102. Brown RS, Wahl RL. Overexpression of glut-1 glucose transporter in human breast cancer an immunohistochemical study. *Cancer.* 1993;72(10):2979-2985.

103. Kawamura T, Kusakabe T, Sugino T, et al. Expression of glucose transporter-1 in human gastric carcinoma. *Cancer.* 2001;92(3):634-641.

104. Nishioka T, Oda Y, Seino Y, et al. Distribution of the Glucose Transporters in Human Brain Tumors. *Cancer Research.* July 15, 1992 1992;52(14):3972-3979.

105. Aliaga A, Rousseau J, Cadorette J, et al. A Small Animal Positron Emission Tomography Study of the Effect of Chemotherapy and Hormonal Therapy on the Uptake of 2-Deoxy-2-[F-18]fluoro-glucose in Murine Models of Breast Cancer. *Molecular Imaging and Biology.* 2007;9(3):144-150.

106. Su H, Bodenstein C, Dumont RA, et al. Monitoring Tumor Glucose Utilization by Positron Emission Tomography for the Prediction of Treatment Response to Epidermal Growth Factor Receptor Kinase Inhibitors. *Clinical Cancer Research.* 2006;12(19):5659-5667.

107. Murayama C, Harada N, Kakiuchi T, et al. Evaluation of d-18F-FMT, 18F-FDG, l-11C-MET, and 18F-FLT for Monitoring the Response of Tumors to Radiotherapy in Mice. *Journal of Nuclear Medicine.* 2009;50(2):290-295.

108. Huang S-C. Anatomy of SUV. *Nuclear medicine and biology.* 2000;27(7):643-646.

109. Stahl A, Ott K, Schwaiger M, Weber WA. Comparison of different SUV-based methods for monitoring cytotoxic therapy with FDG PET. *European Journal of Nuclear Medicine and Molecular Imaging.* 2004;31(11):1471-1478.

110. Hadi M, Bacharach SL, Whatley M, et al. Glucose and insulin variations in patients during the time course of a FDG-PET study and implications for the â€œglucose-correctedâ€• SUV. *Nuclear Medicine and Biology.* 2008;35(4):441-445.

111. Suckow C, Kuntner C, Chow P, Silverman R, Chatziioannou A, Stout D. Multimodality rodent imaging chambers for use under barrier conditions with gas anesthesia. *Mol Imaging Biol.* 2009;11:100-106.

112. Chow PL, Rannou FR, Chatziioannou AF. Attenuation correction for small animal PET tomographs. *Phys Med Biol.* 2005;50:1837-1850.

113. Patlak CS, Blasberg RG, Fenstermacher J. Graphical evaluation of blood-to-brain transfer constants from multiple-time uptake data. *J Cereb Blood Flow Metab.* 1983;3:1-7.

114. Huang S-C, Phelps ME, Hoffman EJ, Sideris K, Selin CJ, Kuhl DE. Noninvasive determination of local cerebral metabolic rate of glucose in man. *Am J Physiol.* 1980;238:E69-E82.

115. Shao J. Linear Model Selection by Cross-Validation. *Journal of the American Statistical Association.* 1993;88(422):486-494.

116. Fueger BJ, Czernin J, Hildebrandt I, et al. Impact of Animal Handling on the Results of 18F-FDG PET Studies in Mice. *Journal of Nuclear Medicine.* 2006;47(6):999-1006.

117. Aide N, Poulain L, Briand M, et al. Early evaluation of the effects of chemotherapy with longitudinal FDG small-animal PET in human testicular cancer xenografts: early flare response does not reflect refractory disease. *European Journal of Nuclear Medicine and Molecular Imaging.* 2009;36(3):396-405.

118. Mudd S, Holich K, Voorbach M, et al. Pharmacodynamic Evaluation of Irinotecan Therapy by FDG and FLT PET/CT Imaging in a Colorectal Cancer Xenograft Model. *Molecular Imaging and Biology.* 2011:1-8.

119. Fueger BJ, Czernin J, Hildebrandt I, et al. Impact of Animal Handling on the Results of 18F-FDG PET Studies in Mice. *J Nucl Med.* June 1, 2006 2006;47(6):999-1006.

120. Hardwick M, Rone J, Han Z, Haddad B, Papadopoulos V. Peripheral-type benzodiazepine receptor levels correlate with the ability of human breast cancer MDA-MB-231 cell line to grow in scid mice. *International Journal of Cancer.* 2001;94(3):322-327.

121. Huang P, Allam A, Taghian A, Freeman J, Duffy M, Suit HD. Growth and metastatic behavior of five human glioblastomas compared with nine other histological types of human tumor xenografts in SCID mice. *Journal of Neurosurgery.* 1995;83(2):308-315.

122. Holdsworth CH, Badawi RD, Manola JB, et al. CT and PET: Early Prognostic Indicators of Response to Imatinib Mesylate in Patients with Gastrointestinal Stromal Tumor. *American Journal of Roentgenology.* December 1, 2007 2007;189(6):W324-W330.

123. Zander T, Scheffler M, Nogova L, et al. Early Prediction of Nonprogression in Advanced Non-small-Cell Lung Cancer Treated With Erlotinib By Using [18F]Fluorodeoxyglucose and [18F]Fluorothymidine Positron Emission Tomography. *Journal of Clinical Oncology.* 2011;29(13):1701-1708.

124. Soret M, Bacharach SL, Buvat I. Partial-Volume Effect in PET Tumor Imaging. *Journal of Nuclear Medicine.* 2007;48(6):932-945.

125. Shreve PD, Anzai Y, Wahl RL. Pitfalls in Oncologic Diagnosis with FDG PET Imaging: Physiologic and Benign Variants. *Radiographics.* January 1, 1999 1999;19(1):61-77.